

EUROPEAN ORGANISATION FOR NUCLEAR RESEARCH (CERN)



Submitted to: EPJC

CERN-PH-EP-2015-154
8th September 2022

Search for an additional, heavy Higgs boson in the $H \rightarrow ZZ$ decay channel at $\sqrt{s} = 8$ TeV in pp collision data with the ATLAS detector

The ATLAS Collaboration

Abstract

A search is presented for a high-mass Higgs boson in the $H \rightarrow ZZ \rightarrow \ell^+ \ell^- \ell^+ \ell^-$, $H \rightarrow ZZ \rightarrow \ell^+ \ell^- \nu \bar{\nu}$, $H \rightarrow ZZ \rightarrow \ell^+ \ell^- q \bar{q}$, and $H \rightarrow ZZ \rightarrow \nu \bar{\nu} q \bar{q}$ decay modes using the ATLAS detector at the CERN Large Hadron Collider. The search uses proton–proton collision data at a centre-of-mass energy of 8 TeV corresponding to an integrated luminosity of 20.3 fb^{-1} . The results of the search are interpreted in the scenario of a heavy Higgs boson with a width that is small compared with the experimental mass resolution. The Higgs boson mass range considered extends up to 1 TeV for all four decay modes and down to as low as 140 GeV, depending on the decay mode. No significant excess of events over the Standard Model prediction is found. A simultaneous fit to the four decay modes yields upper limits on the production cross-section of a heavy Higgs boson times the branching ratio to Z boson pairs. 95% confidence level upper limits range from 0.53 pb at $m_H = 195$ GeV to 0.008 pb at $m_H = 950$ GeV for the gluon-fusion production mode and from 0.31 pb at $m_H = 195$ GeV to 0.009 pb at $m_H = 950$ GeV for the vector-boson-fusion production mode. The results are also interpreted in the context of Type-I and Type-II two-Higgs-doublet models.

Contents

1	Introduction	3
2	ATLAS detector	4
3	Data and Monte Carlo samples	4
3.1	Data sample	4
3.2	Signal samples and modelling	5
3.3	Background samples	6
3.4	Detector simulation	7
4	Object reconstruction and common event selection	7
5	$H \rightarrow ZZ \rightarrow \ell^+ \ell^- \ell^+ \ell^-$ event selection and background estimation	10
5.1	Event selection	10
5.2	Background estimation	11
6	$H \rightarrow ZZ \rightarrow \ell^+ \ell^- \nu \bar{\nu}$ event selection and background estimation	13
6.1	Event selection	13
6.2	Background estimation	14
7	$H \rightarrow ZZ \rightarrow \ell^+ \ell^- q \bar{q}$ event selection and background estimation	15
7.1	Event selection	15
7.1.1	Resolved ggF channel	17
7.1.2	Merged-jet ggF channel	17
7.1.3	VBF channel	18
7.2	Background estimation	19
8	$H \rightarrow ZZ \rightarrow \nu \bar{\nu} q \bar{q}$ event selection and background estimation	24
8.1	Event selection	24
8.2	Background estimation	24
9	Systematic uncertainties	26
9.1	Experimental uncertainties	28
9.2	Signal acceptance uncertainty	29
9.3	$ZZ^{(*)}$ background uncertainties	29
10	Combination and statistical interpretation	30
11	Results	31
12	Summary	35
A	Flavour tagging in the $\ell\ell qq$ and $\nu\nu qq$ searches	36
B	Corrections to MC simulation for the $\ell\ell qq$ search	37

1. Introduction

In 2012, a Higgs boson h with a mass of 125 GeV was discovered by the ATLAS and CMS collaborations at the LHC [1, 2]. One of the most important remaining questions is whether the newly discovered particle is part of an extended scalar sector as postulated by various extensions to the Standard Model (SM) such as the two-Higgs-doublet model (2HDM) [3] and the electroweak-singlet (EWS) model [4]. These predict additional Higgs bosons, motivating searches at masses other than 125 GeV.

This paper reports four separate searches with the ATLAS detector for a heavy neutral scalar H decaying into two SM Z bosons, encompassing the decay modes $ZZ \rightarrow \ell^+ \ell^- \ell^+ \ell^-$, $ZZ \rightarrow \ell^+ \ell^- \nu \bar{\nu}$, $ZZ \rightarrow \ell^+ \ell^- q \bar{q}$, and $ZZ \rightarrow \nu \bar{\nu} q \bar{q}$, where ℓ stands for either an electron or a muon. These modes are referred to, respectively, as $\ell\ell\ell\ell$, $\ell\ell\nu\nu$, $\ell\ell qq$, and $\nu\nu qq$.

It is assumed that additional Higgs bosons would be produced predominantly via the gluon fusion (ggF) and vector-boson fusion (VBF) processes but that the ratio of the two production mechanisms is unknown in the absence of a specific model. For this reason, results are interpreted separately for ggF and VBF production modes. For Higgs boson masses below 200 GeV, associated production (VH , where V stands for either a W or a Z boson) is important as well. In this mass range, only the $\ell\ell\ell\ell$ decay mode is considered. Due to its excellent mass resolution and high signal-to-background ratio, the $\ell\ell\ell\ell$ decay mode is well-suited for a search for a narrow resonance in the range $140 < m_H < 500$ GeV; thus, this search covers the m_H range down to 140 GeV. The $\ell\ell\ell\ell$ search includes channels sensitive to VH production as well as to the VBF and ggF production modes. The $\ell\ell qq$ and $\ell\ell\nu\nu$ searches, covering m_H ranges down to 200 GeV and 240 GeV respectively, consider ggF and VBF channels only. The $\nu\nu qq$ search covers the m_H range down to 400 GeV and does not distinguish between ggF and VBF production. Due to their higher branching ratios, the $\ell\ell qq$, $\ell\ell\nu\nu$, and $\nu\nu qq$ decay modes dominate at higher masses, and contribute to the overall sensitivity of the combined result. The m_H range for all four searches extends up to 1000 GeV.

The ggF production mode for the $\ell\ell\ell\ell$ search is further divided into four channels based on lepton flavour, while the $\ell\ell\nu\nu$ search includes four channels, corresponding to two lepton flavours for each of the ggF and VBF production modes. For the $\ell\ell qq$ and $\nu\nu qq$ searches, the ggF production modes are divided into two subchannels each based on the number of b -tagged jets in the event. For Higgs boson masses above 700 GeV, jets from Z boson decay are boosted and tend to be reconstructed as a single jet; the ggF $\ell\ell qq$ search includes an additional channel sensitive to such final states.

For each channel, a discriminating variable sensitive to m_H is identified and used in a likelihood fit. The $\ell\ell\ell\ell$ and $\ell\ell qq$ searches use the invariant mass of the four-fermion system as the final discriminant, while the $\ell\ell\nu\nu$ and $\nu\nu qq$ searches use a transverse mass distribution. Distributions of these discriminants for each channel are combined in a simultaneous likelihood fit which estimates the rate of heavy Higgs boson production and simultaneously the nuisance parameters corresponding to systematic uncertainties. Additional distributions from background-dominated control regions also enter the fit in order to constrain nuisance parameters. Unless otherwise stated, all figures show shapes and normalizations determined from this fit. All results are interpreted in the scenario of a new Higgs boson with a narrow width, as well as in Type-I and Type-II 2HDMs.

The ATLAS collaboration has published results of searches for a Standard Model Higgs boson decaying in the $\ell\ell\ell\ell$, $\ell\ell qq$, and $\ell\ell\nu\nu$ modes with 4.7–4.8 fb⁻¹ of data collected at $\sqrt{s} = 7$ TeV [5–7]. A heavy Higgs boson with the width and branching fractions predicted by the SM was excluded at the 95% confidence level in the ranges $182 < m_H < 233$ GeV, $256 < m_H < 265$ GeV, and $268 < m_H < 415$ GeV by the $\ell\ell\ell\ell$ mode; in the ranges $300 < m_H < 322$ GeV and $353 < m_H < 410$ GeV by the $\ell\ell qq$ mode; and

in the range $319 < m_H < 558$ GeV by the $\ell\ell\nu\nu$ mode. The searches in this paper improve on the earlier results by using a larger data set of 20.3 fb^{-1} of pp collision data collected at a higher centre-of-mass energy of $\sqrt{s} = 8$ TeV, by adding the $\nu\nu qq$ decay mode, by further optimizing the event selection and other aspects of the analysis, and by combining results of all four searches. The CMS Collaboration has also recently published a search for a heavy Higgs boson in $H \rightarrow ZZ$ decays [8].

This paper is organized as follows. After a brief description of the ATLAS detector in Section 2, the simulation of the background and signal processes used in this analysis is outlined in Section 3. Section 4 summarizes the reconstruction of the final-state objects used by these searches. The event selection and background estimation for the four searches are presented in Sections 5 to 8, and Section 9 discusses the systematic uncertainties common to all searches. Section 10 details the statistical combination of all the searches into a single limit, which is given in Section 11. Finally, Section 12 gives the conclusions.

2. ATLAS detector

ATLAS is a multi-purpose detector [9] which provides nearly full solid-angle coverage around the interaction point.¹ It consists of a tracking system (inner detector or ID) surrounded by a thin superconducting solenoid providing a 2 T magnetic field, electromagnetic and hadronic calorimeters, and a muon spectrometer (MS). The ID consists of pixel and silicon microstrip detectors covering the pseudorapidity region $|\eta| < 2.5$, surrounded by a transition radiation tracker (TRT), which improves electron identification in the region $|\eta| < 2.0$. The sampling calorimeters cover the region $|\eta| < 4.9$. The forward region ($3.2 < |\eta| < 4.9$) is instrumented with a liquid-argon (LAr) calorimeter for electromagnetic and hadronic measurements. In the central region, a high-granularity lead/LAr electromagnetic calorimeter covers $|\eta| < 3.2$. Hadron calorimetry is based on either steel absorbers with scintillator tiles ($|\eta| < 1.7$) or copper absorbers in LAr ($1.5 < |\eta| < 3.2$). The MS consists of three large superconducting toroids arranged with an eight-fold azimuthal coil symmetry around the calorimeters, and a system of three layers of precision gas chambers providing tracking coverage in the range $|\eta| < 2.7$, while dedicated chambers allow triggering on muons in the region $|\eta| < 2.4$. The ATLAS trigger system [10] consists of three levels; the first (L1) is a hardware-based system, while the second and third levels are software-based systems.

3. Data and Monte Carlo samples

3.1. Data sample

The data used in these searches were collected by ATLAS at a centre-of-mass energy of 8 TeV during 2012 and correspond to an integrated luminosity of 20.3 fb^{-1} .

Collision events are recorded only if they are selected by the online trigger system. For the $\nu\nu qq$ search this selection requires that the magnitude E_T^{miss} of the missing transverse momentum vector (see Section 4)

¹ ATLAS uses a right-handed coordinate system with its origin at the nominal interaction point (IP) in the centre of the detector and the z -axis coinciding with the axis of the beam pipe. The x -axis points from the IP towards the centre of the LHC ring, and the y -axis points upward. Cylindrical coordinates (r, ϕ) are used in the transverse plane, ϕ being the azimuthal angle around the z -axis. The pseudorapidity is defined in terms of the polar angle θ as $\eta = -\ln \tan(\theta/2)$. The distance in (η, ϕ) coordinates, $\Delta R = \sqrt{(\Delta\phi)^2 + (\Delta\eta)^2}$, is also used to define cone sizes. Transverse momentum and energy are defined as $p_T = p \sin \theta$ and $E_T = E \sin \theta$, respectively.

is above 80 GeV. Searches with leptonic final states use a combination of single-lepton and dilepton triggers in order to maximize acceptance. The main single-lepton triggers have a minimum p_T (muons) or E_T (electrons) threshold of 24 GeV and require that the leptons are isolated. They are complemented with triggers with higher thresholds (60 GeV for electrons and 36 GeV for muons) and no isolation requirement in order to increase acceptance at high p_T and E_T . The dilepton triggers require two same-flavour leptons with a threshold of 12 GeV for electrons and 13 GeV for muons. The acceptance in the $\ell\ell\ell\ell$ search is increased further with an additional asymmetric dimuon trigger selecting one muon with $p_T > 18$ GeV and another one with $p_T > 8$ GeV and an electron–muon trigger with thresholds of $E_T^e > 12$ GeV and $p_T^\mu > 8$ GeV.

3.2. Signal samples and modelling

The acceptance and resolution for the signal of a narrow-width heavy Higgs boson decaying to a Z boson pair are modelled using Monte Carlo (MC) simulation. Signal samples are generated using POWHEG r1508 [11, 12], which calculates separately the gluon and vector-boson-fusion Higgs boson production processes up to next-to-leading order (NLO) in α_S . The generated signal events are hadronized with PYTHIA 8.165 using the AU2 set of tunable parameters for the underlying event [13, 14]; PYTHIA also decays the Z bosons into all modes considered in this search. The contribution from Z boson decay to τ leptons is also included. The NLO CT10 [15] parton distribution function (PDF) is used. The associated production of Higgs bosons with a W or Z boson (WH and ZH) is significant for $m_H < 200$ GeV. It is therefore included as a signal process for the $\ell\ell\ell\ell$ search for $m_H < 400$ GeV and simulated using PYTHIA 8 with the LO CTEQ6L1 PDF set [16] and the AU2 parameter set. These samples are summarized in Table 1.

Besides model-independent results, a search in the context of a CP-conserving 2HDM [3] is also presented. This model has five physical Higgs bosons after electroweak symmetry breaking: two CP-even, h and H ; one CP-odd, A ; and two charged, H^\pm . The model considered here has seven free parameters: the Higgs boson masses (m_h, m_H, m_A, m_{H^\pm}), the ratio of the vacuum expectation values of the two doublets ($\tan\beta$), the mixing angle between the CP-even Higgs bosons (α), and the potential parameter m_{12}^2 that mixes the two Higgs doublets. The two Higgs doublets Φ_1 and Φ_2 can couple to leptons and up- and down-type quarks in several ways. In the Type-I model, Φ_2 couples to all quarks and leptons, whereas for Type-II, Φ_1 couples to down-type quarks and leptons and Φ_2 couples to up-type quarks. The ‘lepton-specific’ model is similar to Type-I except for the fact that the leptons couple to Φ_1 , instead of Φ_2 ; the ‘flipped’ model is similar to Type-II except that the leptons couple to Φ_2 , instead of Φ_1 . In all these models, the coupling of the H boson to vector bosons is proportional to $\cos(\beta - \alpha)$. In the limit $\cos(\beta - \alpha) \rightarrow 0$ the light CP-even Higgs boson, h , is indistinguishable from a SM Higgs boson with the same mass. In the context of $H \rightarrow ZZ$ decays there is no direct coupling of the Higgs boson to leptons, and so only the Type-I and -II interpretations are presented.

The production cross-sections for both the ggF and VBF processes are calculated using SusHi 1.3.0 [17–22], while the branching ratios are calculated with 2HDMC 1.6.4 [23]. For the branching ratio calculations it is assumed that $m_A = m_H = m_{H^\pm}$, $m_h = 125$ GeV, and $m_{12}^2 = m_A^2 \tan\beta/(1 + \tan\beta^2)$. In the 2HDM parameter space considered in this analysis, the cross-section times branching ratio for $H \rightarrow ZZ$ with $m_H = 200$ GeV varies from 2.4 fb to 10 pb for Type-I and from 0.5 fb to 9.4 pb for Type-II.

The width of the heavy Higgs boson varies over the parameter space of the 2HDM model, and may be significant compared with the experimental resolution. Since this analysis assumes a narrow-width signal,

the 2HDM interpretation is limited to regions of parameter space where the width is less than 0.5% of m_H (significantly smaller than the detector resolution). In addition, the off-shell contribution from the light Higgs boson and its interference with the non-resonant ZZ background vary over the 2HDM parameter space as the light Higgs boson couplings are modified from their SM values. Therefore the interpretation is further limited to regions of the parameter space where the light Higgs boson couplings are enhanced by less than a factor of three from their SM values; in these regions the variation is found to have a negligible effect.

3.3. Background samples

Monte Carlo simulations are also used to model the shapes of distributions from many of the sources of SM background to these searches. Table 1 summarizes the simulated event samples along with the PDF sets and underlying-event tunes used. Additional samples are also used to compute systematic uncertainties as detailed in Section 9.

SHERPA 1.4.1 [24] includes the effects of heavy-quark masses in its modelling of the production of W and Z bosons along with additional jets ($V + \text{jets}$). For this reason it is used to model these backgrounds in the hadronic $\ell\ell qq$ and $\nu\nu qq$ searches, which are subdivided based on whether the Z boson decays into b -quarks or light-flavour quarks. The ALPGEN 2.14 $W + \text{jets}$ and $Z/\gamma^* + \text{jets}$ samples are generated with up to five hard partons and with the partons matched to final-state particle jets [25, 26]. They are used to describe these backgrounds in the other decay modes and also in the VBF channel of the $\ell\ell qq$ search² since the additional partons in the matrix element give a better description of the VBF topology. The SHERPA (ALPGEN) $Z/\gamma^* + \text{jets}$ samples have a dilepton invariant mass requirement of $m_{\ell\ell} > 40$ GeV (60 GeV) at the generator level.

The background from the associated production of the 125 GeV h boson along with a Z boson is non-negligible in the $\ell\ell qq$ and $\nu\nu qq$ searches and is taken into account. Contributions to Zh from both $q\bar{q}$ annihilation and gluon fusion are included. The $q\bar{q} \rightarrow Zh$ samples take into account NLO electroweak corrections, including differential corrections as a function of Z boson p_T [27, 28]. The Higgs boson branching ratio is calculated using HDECAY [29]. Further details can be found in Ref. [30].

Continuum $ZZ^{(*)}$ events form the dominant background for the $\ell\ell\ell\ell$ and $\ell\ell\nu\nu$ decay modes; this is modelled with a dedicated $q\bar{q} \rightarrow ZZ^{(*)}$ sample. This sample is corrected to match the calculation described in Ref. [31], which is next-to-next-to-leading order (NNLO) in α_S , with a K -factor that is differential in m_{ZZ} . Higher-order electroweak effects are included following the calculation reported in Refs. [32, 33] by applying a K -factor based on the kinematics of the diboson system and the initial-state quarks, using a procedure similar to that described in Ref. [34]. The off-shell SM ggF Higgs boson process, the $gg \rightarrow ZZ$ continuum, and their interference are considered as backgrounds. These samples are generated at leading order (LO) in α_S using MCFM 6.1 [35] ($\ell\ell\ell\ell$) or gg2vv 3.1.3 [36, 37] ($\ell\ell\nu\nu$) but corrected to NNLO as a function of m_{ZZ} [38] using the same procedure as described in Ref. [6]. For the $\ell\ell qq$ and $\nu\nu qq$ searches, the continuum $ZZ^{(*)}$ background is smaller so the $q\bar{q} \rightarrow ZZ^{(*)}$ sample is used alone. It is scaled to include the contribution from $gg \rightarrow ZZ^{(*)}$ using the $gg \rightarrow ZZ^{(*)}$ cross-section calculated by MCFM 6.1 [35].

For samples in which the hard process is generated with ALPGEN or MC@NLO 4.03 [39], HERWIG 6.520 [40] is used to simulate parton showering and fragmentation, with JIMMY [41] used for the underlying-event simulation. PYTHIA 6.426 [42] is used for samples generated with MADGRAPH [43] and ACERMC [44],

² The VBF channel is inclusive in quark flavour and hence dominated by the $Z + \text{light-quark jet}$ background.

while PYTHIA 8.165 [45] is used for the gg2vv 3.1.3 [36, 37], MCFM 6.1 [46], and POWHEG samples. SHERPA implements its own parton showering and fragmentation model.

In the $\ell\ell qq$ and $\nu\nu qq$ searches, which have jets in the final state, the principal background is V +jets, where V stands for either a W or a Z boson. In simulations of these backgrounds, jets are labelled according to which generated hadrons with $p_T > 5$ GeV are found within a cone of size $\Delta R = 0.4$ around the reconstructed jet axis. If a b -hadron is found, the jet is labelled as a b -jet; if not and a charmed hadron is found, the jet is labelled as a c -jet; if neither is found, the jet is labelled as a light (i.e., u -, d -, or s -quark, or gluon) jet, denoted by ‘ j ’. For V +jets events that pass the selections for these searches, two of the additional jets are reconstructed as the hadronically-decaying Z boson candidate. Simulated V +jets events are then categorized based on the labels of these jets. If one jet is labelled as a b -jet, the event belongs to the $V+b$ category; if not, and one of the jets is labelled as a c -jet, the event belongs to the $V+c$ category; otherwise, the event belongs to the $V+j$ category. Further subdivisions are defined according to the flavour of the other jet from the pair, using the same precedence order: $V+bb$, $V+bc$, $V+bj$, $V+cc$, $V+cj$, and $V+jj$; the combination of $V+bb$, $V+bc$, and $V+cc$ is denoted by $V+hf$.

3.4. Detector simulation

The simulation of the detector is performed with either a full ATLAS detector simulation [66] based on GEANT 4 9.6 [67] or a fast simulation³ based on a parameterization of the performance of the ATLAS electromagnetic and hadronic calorimeters [68] and on GEANT 4 elsewhere. All simulated samples are generated with a variable number of minimum-bias interactions (simulated using PYTHIA 8 with the MSTW2008LO PDF [69] and the A2 tune [48]), overlaid on the hard-scattering event to account for additional pp interactions in either the same or a neighbouring bunch crossing (pile-up).

Corrections are applied to the simulated samples to account for differences between data and simulation for the lepton trigger and reconstruction efficiencies, and for the efficiency and misidentification rate of the algorithm used to identify jets containing b -hadrons (b -tagging).

4. Object reconstruction and common event selection

The exact requirements used to identify physics objects vary between the different searches. This section outlines features that are common to all of the searches; search-specific requirements are given in the sections below.

Event vertices are formed from tracks with $p_T > 400$ MeV. Each event must have an identified primary vertex, which is chosen from among the vertices with at least three tracks as the one with the largest $\sum p_T^2$ of associated tracks.

Muon candidates (‘muons’) [70] generally consist of a track in the ID matched with one in the MS. However, in the forward region ($2.5 < |\eta| < 2.7$), MS tracks may be used with no matching ID tracks; further, around $|\eta| = 0$, where there is a gap in MS coverage, ID tracks with no matching MS track

³ The background samples that use the parameterized fast simulation are: SHERPA W/Z +jets production with $p_T^{W/Z} < 280$ GeV (for higher $p_T^{W/Z}$ the full simulation is used since it improves the description of the jet mass in the merged $\ell\ell qq$ search described in Section 7.1.2); POWHEG-Box $t\bar{t}$, single top, and diboson production; and SM PYTHIA $q\bar{q} \rightarrow Zh$ and POWHEG-Box $gg \rightarrow Zh$ production with $h \rightarrow bb$. The remaining background samples and the signal samples, with the exception of those used for the $\nu\nu qq$ search, use the full GEANT 4 simulation.

Physics process	$H \rightarrow ZZ$ search final state	Generator	Cross-section normalization	PDF set	Tune
W/Z boson + jets					
$Z/\gamma^* \rightarrow \ell^+ \ell^- / \nu \bar{\nu}$	$\ell \ell \ell \ell / \ell \ell \nu \nu$	ALPGEN 2.14 [25]	NNLO [47]	CTEQ6L1 [16]	AUET2 [14, 48]
	$\ell \ell q q^* / \nu \nu q q$	SHERPA 1.4.1 [24]	NNLO [49, 50]	NLO CT10	SHERPA default
$W \rightarrow \ell \nu$	$\ell \ell \nu \nu$	ALPGEN 2.14	NNLO [47]	CTEQ6L1	AUET2
	$\nu \nu q q$	SHERPA 1.4.1	NNLO [49, 50]	NLO CT10	SHERPA default
Top quark					
$t \bar{t}$	$\ell \ell \ell \ell / \ell \ell q q / \nu \nu q q$	POWHEG-Box r2129 [51–53]	NNLO+NNLL [55, 56]	NLO CT10	PERUGIA2011C [54]
	$\ell \ell \nu \nu$	MC@NLO 4.03 [39]			AUET2
s -channel and $W t$	$\ell \ell \ell \ell / \ell \ell q q / \nu \nu q q$	POWHEG-Box r1556	NNLO+NNLL [57, 58]	NLO CT10	PERUGIA2011C
	$\ell \ell \nu \nu$	MC@NLO 4.03			AUET2
t -channel	all	ACERMC 3.8 [44]	NNLO+NNLL [59]	CTEQ6L1	AUET2
Dibosons					
$q \bar{q} \rightarrow ZZ(*)$	$\ell \ell q q / \nu \nu q q$	POWHEG-Box r1508 [60]	NLO [35, 61]	NLO CT10	AUET2
	$\ell \ell \ell \ell / \ell \ell \nu \nu$	POWHEG-Box r1508 [60]	NNLO QCD [31] NLO EW [32, 33]	NLO CT10	AUET2
EW $q \bar{q} (\rightarrow h) \rightarrow ZZ(*) + 2j$	$\ell \ell \ell \ell$	MADGRAPH 5 1.3.28 [43]		CTEQ6L1	AUET2
$gg (\rightarrow h^*) \rightarrow ZZ$	$\ell \ell \ell \ell$	MCFM 6.1 [46]	NNLO [38]	NLO CT10	AU2
	$\ell \ell \nu \nu$	GG2VV 3.1.3 [36, 37]	(for $h \rightarrow ZZ$)	NLO CT10	AU2
$q \bar{q} \rightarrow WZ$	$\ell \ell \nu \nu / \ell \ell q q / \nu \nu q q$	POWHEG-Box r1508	NLO [35, 61]	NLO CT10	AUET2
	$\ell \ell \ell \ell$	SHERPA 1.4.1			SHERPA default
$q \bar{q} \rightarrow WW$	all	POWHEG-Box r1508	NLO [35, 61]	NLO CT10	AUET2
$m_h = 125$ GeV SM Higgs boson (background) [‡]					
$q \bar{q} \rightarrow Zh \rightarrow \ell^+ \ell^- b \bar{b} / \nu \bar{\nu} b \bar{b}$	$\ell \ell q q / \nu \nu q q$	PYTHIA 8.165	NNLO [62–64]	CTEQ6L	AU2
$gg \rightarrow Zh \rightarrow \ell^+ \ell^- b \bar{b} / \nu \bar{\nu} b \bar{b}$	$\ell \ell q q / \nu \nu q q$	POWHEG-Box r1508	NLO [65]	CT10	AU2
Signal					
$gg \rightarrow H \rightarrow ZZ(*)$	all	POWHEG-Box r1508	—	NLO CT10	AU2
$q \bar{q} \rightarrow H + 2j$; $H \rightarrow ZZ(*)$	all	POWHEG-Box r1508	—	NLO CT10	AU2
$q \bar{q} \rightarrow (W/Z)H$; $H \rightarrow ZZ(*)$	$\ell \ell \ell \ell$	PYTHIA 8.163	—	CTEQ6L1	AU2

Table 1: Details of the generation of simulated signal and background event samples. For each physics process, the table gives the final states generated, the $H \rightarrow ZZ$ final states(s) for which they are used, the generator, the PDF set, and the underlying-event tune. For the background samples, the order in α_s used to normalize the event yield is also given; for the signal, the normalization is the parameter of interest in the fit. More details can be found in the text.

[†]The $H \rightarrow ZZ \rightarrow \ell^+ \ell^- q \bar{q}$ VBF search uses ALPGEN instead.

[‡]For the $H \rightarrow ZZ \rightarrow \ell^+ \ell^- \ell^+ \ell^-$ and $H \rightarrow ZZ \rightarrow \ell^+ \ell^- \nu \bar{\nu}$ searches, the SM $h \rightarrow ZZ$ boson contribution, along with its interference with the continuum ZZ background, is included in the diboson samples.

may be used if they match an energy deposit in the calorimeter consistent with a muon. In addition to quality requirements, muon tracks are required to pass close to the reconstructed primary event vertex. The longitudinal impact parameter, z_0 , is required to be less than 10 mm, while the transverse impact parameter, d_0 , is required to be less than 1 mm to reject non-collision backgrounds. This requirement is not applied in the case of muons with no ID track.

Electron candidates (‘electrons’) [71–73] consist of an energy cluster in the EM calorimeter with $|\eta| < 2.47$ matched to a track reconstructed in the inner detector. The energy of the electron is measured from the energy of the calorimeter cluster, while the direction is taken from the matching track. Electron candidates are selected using variables sensitive to the shape of the EM cluster, the quality of the track, and the goodness of the match between the cluster and the track. Depending on the search, either a selection is made on each variable sequentially or all the variables are combined into a likelihood discriminant.

Electron and muon energies are calibrated from measurements of $Z \rightarrow ee/\mu\mu$ decays [70, 72]. Electrons and muons must be isolated from other tracks, using $p_T^{\ell, \text{isol}}/p_T^\ell < 0.1$, where $p_T^{\ell, \text{isol}}$ is the scalar sum of the transverse momenta of tracks within a $\Delta R = 0.2$ cone around the electron or muon (excluding the electron or muon track itself), and p_T^ℓ is the transverse momentum of the electron or muon candidate. The isolation requirement is not applied in the case of muons with no ID track. For searches with electrons or muons in the final state, the reconstructed lepton candidates must match the trigger lepton candidates that resulted in the events being recorded by the online selection.

Jets are reconstructed [74] using the anti- k_t algorithm [75] with a radius parameter $R = 0.4$ operating on massless calorimeter energy clusters constructed using a nearest-neighbour algorithm. Jet energies and directions are calibrated using energy- and η -dependent correction factors derived using MC simulations, with an additional calibration applied to data samples derived from in situ measurements [76]. A correction is also made for effects of energy from pile-up. For jets with $p_T < 50$ GeV within the acceptance of the ID ($|\eta| < 2.4$), the fraction of the summed scalar p_T of the tracks associated with the jet (within a $\Delta R = 0.4$ cone around the jet axis) contributed by those tracks originating from the primary vertex must be at least 50%. This ratio is called the jet vertex fraction (JVF), and this requirement reduces the number of jet candidates originating from pile-up vertices [77, 78].

In the $\ell\ell qq$ search at large Higgs boson masses, the decay products of the boosted Z boson may be reconstructed as a single anti- k_t jet with a radius of $R = 0.4$. Such configurations are identified using the jet invariant mass, obtained by summing the momenta of the jet constituents. After the energy calibration, the jet masses are calibrated, based on Monte Carlo simulations, as a function of jet p_T , η , and mass.

The missing transverse momentum, with magnitude E_T^{miss} , is the negative vectorial sum of the transverse momenta of all clusters in the calorimeters with $|\eta| < 4.5$, calibrated appropriately based on their identification as contributing to electrons, photons, hadronic decays of τ leptons, jets, or unassociated calorimeter clusters, and all selected muons in the event [79]. Calorimeter deposits associated with muons are subtracted from E_T^{miss} to avoid double counting.

Jets containing b -hadrons (b -jets) can be discriminated from other jets (‘tagged’) based on the relatively long lifetime of b -hadrons. Several methods are used to tag jets originating from the fragmentation of a b -quark, including looking for tracks with a large impact parameter with respect to the primary event vertex, looking for a secondary decay vertex, and reconstructing a b -hadron $\rightarrow c$ hadron decay chain. For the $\ell\ell qq$ and $\nu\nu qq$ searches, this information is combined into a single neural-network discriminant (‘MV1c’). This is a continuous variable that is larger for jets that are more like b -jets. A selection is then applied that gives an efficiency of about 70%, on average, for identifying true b -jets, while the efficiencies for accepting c -jets or light-quark jets are 1/5 and 1/140 respectively [30, 80–83]. The $\ell\ell\nu\nu$ search uses

an alternative version of this discriminant, ‘MV1’ [80], to reject background due to top-quark production; compared with MV1c it has a smaller c -jet rejection. Tag efficiencies and mistag rates are calibrated using data. For the purpose of forming the invariant mass of the b -jets, m_{bb} , the energies of b -tagged jets are corrected to account for muons within the jets and an additional p_T -dependent correction is applied to account for biases in the response due to resolution effects.

In channels which require two b -tagged jets in the final state, the efficiency for simulated events of the dominant Z + jets background to pass the b -tagging selection is low. To effectively increase the sizes of simulated samples, jets are ‘truth tagged’: each event is weighted by the flavour-dependent probability of the jets to actually pass the b -tagging selection.

5. $H \rightarrow ZZ \rightarrow \ell^+ \ell^- \ell^+ \ell^-$ event selection and background estimation

5.1. Event selection

The event selection and background estimation for the $H \rightarrow ZZ \rightarrow \ell^+ \ell^- \ell^+ \ell^-$ ($\ell\ell\ell\ell$) search is very similar to the analysis described in Ref. [84]. More details may be found there; a summary is given here.

Higgs boson candidates in the $\ell\ell\ell\ell$ search must have two same-flavour, opposite-charge lepton pairs. Muons must satisfy $p_T > 6$ GeV and $|\eta| < 2.7$, while electrons are identified using the likelihood discriminant corresponding to the ‘loose LH’ selection from Ref. [73] and must satisfy $p_T > 7$ GeV. The impact parameter requirements that are made for muons are also applied to electrons, and electrons (muons) must also satisfy a requirement on the transverse impact parameter significance, $|d_0|/\sigma_{d_0} < 6.5$ (3.5). For this search, the track-based isolation requirement is relaxed to $p_T^{\ell, \text{isol}}/p_T^\ell < 0.15$ for both the electrons and muons. In addition, lepton candidates must also be isolated in $E_T^{\ell, \text{isol}}$, the sum of the transverse energies in calorimeter cells within a $\Delta R = 0.2$ cone around the candidate (excluding the deposit from the candidate itself). The requirement is $E_T^{\ell, \text{isol}}/p_T^\ell < 0.2$ for electrons, < 0.3 for muons with a matching ID track, and < 0.15 for other muons. The three highest- p_T leptons in the event must satisfy, in order, $p_T > 20, 15$, and 10 GeV. To ensure well-measured leptons, and reduce backgrounds containing electrons from bremsstrahlung, same-flavour leptons must be separated from each other by $\Delta R > 0.1$, and different-flavour leptons by $\Delta R > 0.2$. Jets that are $\Delta R < 0.2$ from electrons are removed. Final states in this search are classified depending on the flavours of the leptons present: 4μ , $2e2\mu$, $2\mu2e$, and $4e$. The selection of lepton pairs is made separately for each of these flavour combinations; the pair with invariant mass closest to the Z boson mass is called the leading pair and its invariant mass, m_{12} , must be in the range $50\text{--}106$ GeV. For the $2e2\mu$ channel, the electrons form the leading pair, while for the $2\mu2e$ channel the muons are leading. The second, subleading, pair of each combination is the pair from the remaining leptons with invariant mass m_{34} closest to that of the Z boson in the range $m_{\min} < m_{34} < 115$ GeV. Here m_{\min} is 12 GeV for $m_{\ell\ell\ell\ell} < 140$ GeV, rises linearly to 50 GeV at $m_{\ell\ell\ell\ell} = 190$ GeV, and remains at 50 GeV for $m_{\ell\ell\ell\ell} > 190$ GeV. Finally, if more than one flavour combination passes the selection, which could happen for events with more than four leptons, the flavour combination with the highest expected signal acceptance is kept; i.e., in the order: 4μ , $2e2\mu$, $2\mu2e$, and $4e$. For 4μ and $4e$ events, if an opposite-charge same-flavour dilepton pair is found with $m_{\ell\ell}$ below 5 GeV, the event is vetoed in order to reject backgrounds from J/ψ decays.

To improve the mass resolution, the four-momentum of any reconstructed photon consistent with having been radiated from one of the leptons in the leading pair is added to the final state. Also, the four-momenta

of the leptons in the leading pair are adjusted by means of a kinematic fit assuming a $Z \rightarrow \ell\ell$ decay; this improves the $m_{\ell\ell\ell}$ resolution by up to 15%, depending on m_H . This is not applied to the subleading pair in order to retain sensitivity at lower m_H where one of the Z boson decays may be off-shell. For 4μ events, the resulting mass resolution varies from 1.5% at $m_H = 200$ GeV to 3.5% at $m_H = 1$ TeV, while for $4e$ events it ranges from 2% at $m_H = 200$ GeV to below 1% at 1 TeV.

Signal events can be produced via ggF or VBF, or associated production (VH , where V stands for either a W or a Z boson). In order to measure the rates for these processes separately, events passing the event selection described above are classified into channels, either ggF, VBF, or VH . Events containing at least two jets with $p_T > 25$ GeV and $|\eta| < 2.5$ or $p_T > 30$ GeV and $2.5 < |\eta| < 4.5$ and with the leading two such jets having $m_{jj} > 130$ GeV are classified as VBF events. Otherwise, if a jet pair satisfying the same p_T and η requirements is present but with $40 < m_{jj} < 130$ GeV, the event is classified as VH , providing it also passes a selection on a multivariate discriminant used to separate the VH and ggF signal. The multivariate discriminant makes use of m_{jj} , $\Delta\eta_{jj}$, the p_T of the two jets, and the η of the leading jet. In order to account for leptonic decays of the V (W or Z) boson, events failing this selection may still be classified as VH if an additional lepton with $p_T > 8$ GeV is present. All remaining events are classified as ggF. Due to the differing background compositions and signal resolutions, events in the ggF channel are further classified into subchannels according to their final state: $4e$, $2e2\mu$, $2\mu2e$, or 4μ . The selection for VBF is looser than that used in the other searches; however, the effect on the final results is small. The $m_{\ell\ell\ell}$ distributions for the three channels are shown in Fig. 1.

5.2. Background estimation

The dominant background in this channel is continuum $ZZ^{(*)}$ production. Its contribution to the yield is determined from simulation using the samples described in Section 3.3. Other background components are small and consist mainly of $t\bar{t}$ and Z + jets events. These are difficult to estimate from MC simulations due to the small rate at which such events pass the event selection, and also because they depend on details of jet fragmentation, which are difficult to model reliably in simulations. Therefore, both the rate and composition of these backgrounds are estimated from data. Since the composition of these backgrounds depends on the flavour of the subleading dilepton pair, different approaches are taken for the $\ell\ell\mu\mu$ and the $\ell\ell ee$ final states.

The $\ell\ell\mu\mu$ non- ZZ background comprises mostly $t\bar{t}$ and $Z + b\bar{b}$ events, where in the latter the muons arise mostly from heavy-flavour semileptonic decays, and to a lesser extent from π/K in-flight decays. The contribution from single-top production is negligible. The normalization of each component is estimated by a simultaneous fit to the m_{12} distribution in four control regions, defined by inverting the impact parameter significance or isolation requirements on the subleading muon, or by selecting a subleading $e\mu$ or same-charge pair. A small contribution from WZ decays is estimated using simulation. The electron background contributing to the $\ell\ell ee$ final states comes mainly from jets misidentified as electrons, arising in three ways: light-flavour hadrons misidentified as electrons, photon conversions reconstructed as electrons, and non-isolated electrons from heavy-flavour hadronic decays. This background is estimated in a control region in which the three highest- p_T leptons must satisfy the full selection, with the third lepton being an electron. For the lowest- p_T lepton, which must also be an electron, the impact parameter and isolation requirements are removed and the likelihood requirement is relaxed. In addition, it must have the same charge as the other subleading electron in order to minimize the contribution from the $ZZ^{(*)}$ background. The yields of the background components of the lowest- p_T lepton are extracted with a fit

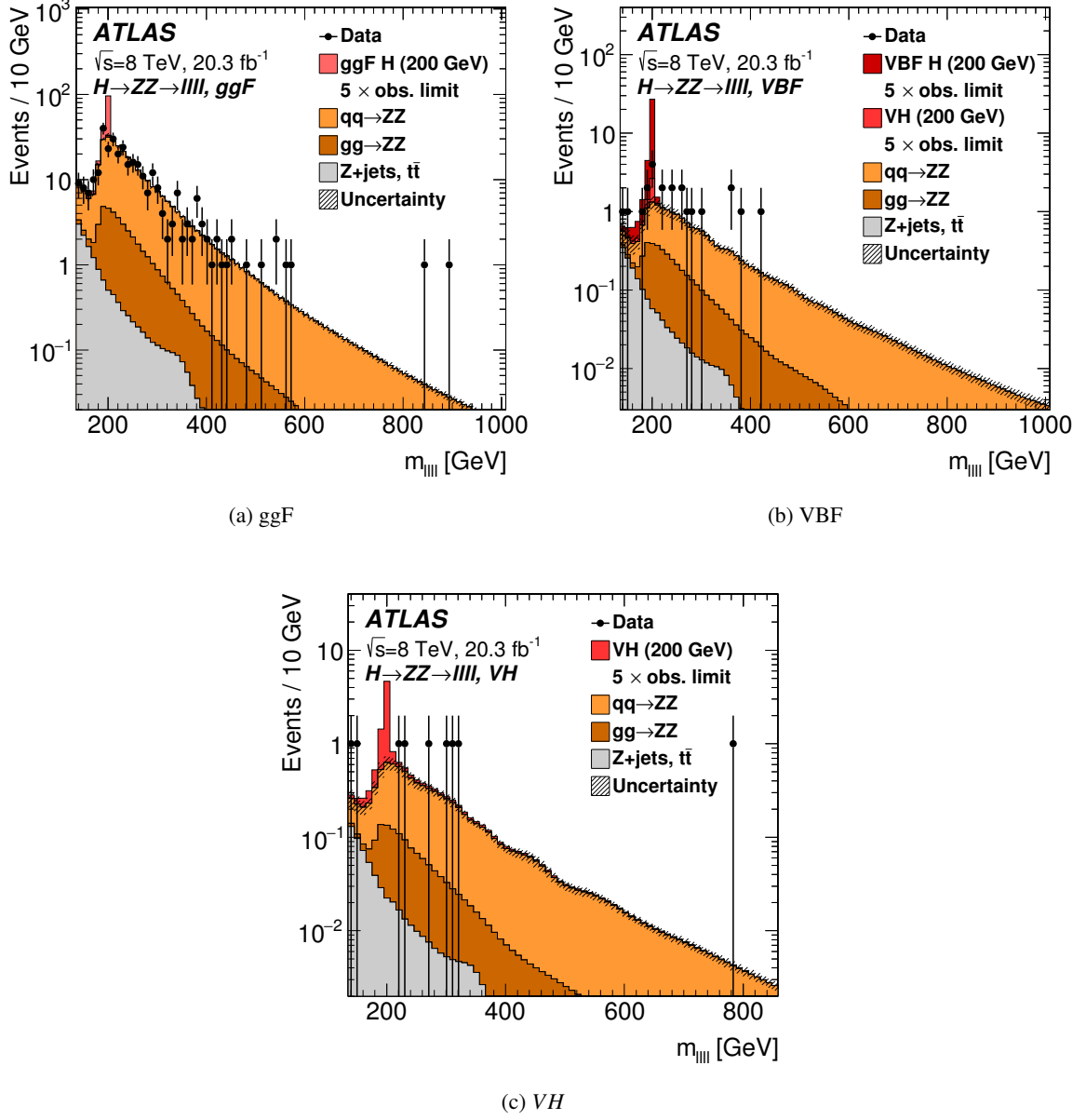


Figure 1: The distributions used in the likelihood fit of the four-lepton invariant mass $m_{\ell\ell\ell\ell}$ for the $H \rightarrow ZZ \rightarrow \ell^+ \ell^- \ell^+ \ell^-$ search in the (a) ggF, (b) VBF, and (c) VH channels. The ‘Z+jets, $t\bar{t}$ ’ entry includes all backgrounds other than ZZ, as measured from data. No events are observed beyond the upper limit of the plots. The simulated $m_H = 200$ GeV signal is normalized to a cross-section corresponding to five times the observed limit given in Section 11. Both the VBF and VH signal modes are shown in (b) as there is significant contamination of VH events in the VBF category.

to the number of hits in the innermost pixel layer and the ratio of the number of high-threshold to low-threshold TRT hits (which provides discrimination between electrons and pions). For both backgrounds, the fitted yields in the control regions are extrapolated to the signal region using efficiencies obtained from simulation.

For the non-ZZ components of the background, the $m_{\ell\ell\ell\ell}$ shape is evaluated for the $\ell\ell\mu\mu$ final states using simulated events, and from data for the $\ell\ell ee$ final states by extrapolating the shape from the $\ell\ell ee$ control region described above. The fraction of this background in each channel (ggF, VBF, VH) is evaluated using simulation. The non-ZZ background contribution for $m_{\ell\ell\ell\ell} > 140$ GeV is found to be approximately 4% of the total background.

Major sources of uncertainty in the estimate of the non-ZZ backgrounds include differences in the results when alternative methods are used to estimate the background [84], uncertainties in the transfer factors used to extrapolate from the control region to the signal region, and the limited statistical precision in the control regions. For the $\ell\ell\mu\mu$ ($\ell\ell ee$) background, the uncertainty is 21% (27%) in the ggF channel, 100% (117%) in the VBF channel, and 62% (79%) in the VH channel. The larger uncertainty in the VBF channel arises due to large statistical uncertainties on the fraction of Z + jets events falling in this channel. Uncertainties in the expected $m_{\ell\ell\ell\ell}$ shape are estimated from differences in the shapes obtained using different methods for estimating the background.

6. $H \rightarrow ZZ \rightarrow \ell^+ \ell^- \nu \bar{\nu}$ event selection and background estimation

6.1. Event selection

The event selection for the $H \rightarrow ZZ \rightarrow \ell^+ \ell^- \nu \bar{\nu}$ ($\ell\ell\nu\nu$) search starts with the reconstruction of either a $Z \rightarrow e^+ e^-$ or $Z \rightarrow \mu^+ \mu^-$ lepton pair; the leptons must be of opposite charge and must have invariant mass $76 < m_{\ell\ell} < 106$ GeV. The charged lepton selection is tighter than that described in Section 4. Muons must have matching tracks in the ID and MS and lie in the region $|\eta| < 2.5$. Electrons are identified using a series of sequential requirements on the discriminating variables, corresponding to the ‘medium’ selection from Ref. [73]. Candidate leptons for the $Z \rightarrow \ell^+ \ell^-$ decay must have $p_T > 20$ GeV, and leptons within a cone of $\Delta R = 0.4$ around jets are removed. Jets that lie $\Delta R < 0.2$ of electrons are also removed. Events containing a third lepton or muon with $p_T > 7$ GeV are rejected; for the purpose of this requirement, the ‘loose’ electron selection from Ref. [73] is used. To select events with neutrinos in the final state, the magnitude of the missing transverse momentum must satisfy $E_T^{\text{miss}} > 70$ GeV.

As in the $\ell\ell\ell\ell$ search, samples enriched in either ggF or VBF production are selected. An event is classified as VBF if it has at least two jets with $p_T > 30$ GeV and $|\eta| < 4.5$ with $m_{jj} > 550$ GeV and $\Delta\eta_{jj} > 4.4$. Events failing to satisfy the VBF criteria and having no more than one jet with $p_T > 30$ GeV and $|\eta| < 2.5$ are classified as ggF. Events not satisfying either set of criteria are rejected.

To suppress the Drell–Yan background, the azimuthal angle between the combined dilepton system and the missing transverse momentum vector $\Delta\phi(p_T^{\ell\ell}, E_T^{\text{miss}})$ must be greater than 2.8 (2.7) for the ggF (VBF) channel (optimized for signal significance in each channel), and the fractional p_T difference, defined as $|p_T^{\text{miss,jet}} - p_T^{\ell\ell}|/p_T^{\ell\ell}$, must be less than 20%, where $p_T^{\text{miss,jet}} = |\vec{E}_T^{\text{miss}} + \sum_{\text{jet}} \vec{p}_T^{\text{jet}}|$. Z bosons originating from the decay of a high-mass state are boosted; thus, the azimuthal angle between the two leptons $\Delta\phi_{\ell\ell}$ must be less than 1.4. Events containing a b -tagged jet with $p_T > 20$ GeV and $|\eta| < 2.5$ are rejected in order

to reduce the background from top-quark production. All jets in the event must have an azimuthal angle greater than 0.3 relative to the missing transverse momentum.

The discriminating variable used is the transverse mass m_T^{ZZ} reconstructed from the momentum of the dilepton system and the missing transverse momentum, defined by:

$$(m_T^{ZZ})^2 \equiv \left(\sqrt{m_Z^2 + |\vec{p}_T^{\ell\ell}|^2} + \sqrt{m_Z^2 + |\vec{E}_T^{\text{miss}}|^2} \right)^2 - \left| \vec{p}_T^{\ell\ell} + \vec{E}_T^{\text{miss}} \right|^2. \quad (1)$$

The resulting resolution in m_T^{ZZ} ranges from 7% at $m_H = 240$ GeV to 15% at $m_H = 1$ TeV.

Figure 2 shows the m_T^{ZZ} distribution in the ggF channel. The event yields in the VBF channel are very small (see Table 2).

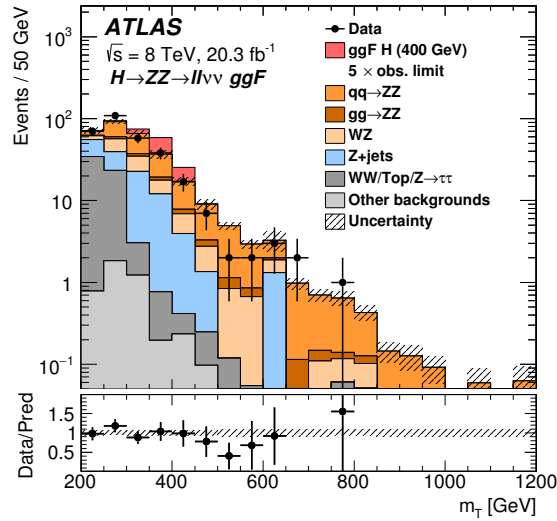


Figure 2: The distribution used in the likelihood fit of the transverse mass m_T^{ZZ} reconstructed from the momentum of the dilepton system and the missing transverse momentum for the $H \rightarrow ZZ \rightarrow \ell^+ \ell^- \nu \bar{\nu}$ search in the ggF channel. The simulated signal is normalized to a cross-section corresponding to five times the observed limit given in Section 11. The contribution labelled as ‘Top’ includes both the $t\bar{t}$ and single-top processes. The bottom pane shows the ratio of the observed data to the predicted background.

6.2. Background estimation

The dominant background is ZZ production, followed by WZ production. Other important backgrounds to this search include the WW , $t\bar{t}$, Wt , and $Z \rightarrow \tau^+ \tau^-$ processes, and also the $Z + \text{jets}$ process with poorly reconstructed E_T^{miss} , but these processes tend to yield final states with low m_T . Backgrounds from $W + \text{jets}$, $t\bar{t}$, single top quark (s - and t -channel), and multijet processes with at least one jet misidentified as an electron or muon are very small.

The POWHEG simulation is used to estimate the ZZ background in the same way as for the $\ell\ell\ell\ell$ search. The WZ background is also estimated with POWHEG and validated with data using a sample of events that pass the signal selection and that contain an extra electron or muon in addition to the $Z \rightarrow \ell^+ \ell^-$ candidate.

The WW , $t\bar{t}$, Wt , and $Z \rightarrow \tau^+\tau^-$ processes give rise to both same-flavour as well as different-flavour lepton final states. The total background from these processes in the same-flavour final state can be estimated from control samples that contain an electron–muon pair rather than a same-flavour lepton pair by

$$\begin{aligned} N_{ee}^{\text{bkg}} &= \frac{1}{2} \times N_{e\mu}^{\text{data,sub}} \times \alpha, \\ N_{\mu\mu}^{\text{bkg}} &= \frac{1}{2} \times N_{e\mu}^{\text{data,sub}} \times \frac{1}{\alpha}, \end{aligned} \quad (2)$$

where N_{ee}^{bkg} and $N_{\mu\mu}^{\text{bkg}}$ are the number of electron and muon pair events in the signal region and $N_{e\mu}^{\text{data,sub}}$ is the number of events in the $e\mu$ control sample with WZ , ZZ , and other small backgrounds (W + jets, $t\bar{t}W/Z$, and triboson) subtracted using simulation. The factor of two arises because the branching ratio to final states containing electrons and muons is twice that of either ee or $\mu\mu$. The factor α takes into account the different efficiencies for electrons and muons and is measured from data as $\alpha^2 = N_{ee}^{\text{data}}/N_{\mu\mu}^{\text{data}}$, the ratio of the number of electron pair to muon pair events in the data after the Z boson mass requirement ($76 < m_{\ell\ell} < 106$ GeV). The measured value of α is 0.94 with a systematic uncertainty of 0.04 and a negligible statistical uncertainty. There is also a systematic uncertainty from the background subtraction in the control sample; this is less than 1%. For the VBF channel, no events remain in the $e\mu$ control sample after applying the full selection. In this case, the background estimate is calculated after only the requirements on E_T^{miss} and the number of jets; the efficiencies of the remaining selections for this background are estimated using simulation.

The Z + jets background is estimated from data by comparing the signal region (A) with regions in which one (B, C) or both (D) of the $\Delta\phi_{\ell\ell}$ and $\Delta\phi(p_T^{\ell\ell}, E_T^{\text{miss}})$ requirements are reversed. An estimate of the number of background events in the signal region is then $N_A^{\text{est}} = N_C^{\text{obs}} \times (N_B^{\text{obs}}/N_D^{\text{obs}})$, where N_X^{obs} is the number of events observed in region X after subtracting non- Z boson backgrounds. The shape is estimated by taking N_C^{obs} (the region with the $\Delta\phi_{\ell\ell}$ requirement reversed) bin-by-bin and applying a correction derived from MC simulations to account for shape differences between regions A and C. Systematic uncertainties arise from differences in the shape of the E_T^{miss} and m_T^{ZZ} distributions among the four regions, the small correlation between the two variables, and the subtraction of non- Z boson backgrounds.

The W + jets and multijet backgrounds are estimated from data using the fake-factor method [85]. This uses a control sample derived from data using a loosened requirement on E_T^{miss} and several kinematic selections. The background in the signal region is then derived using an efficiency factor from simulation to correct for the acceptance. Both of these backgrounds are found to be negligible.

Table 2 shows the expected yields of the backgrounds and signal, and observed counts of data events. The expected yields of the backgrounds in the table are after applying the combined likelihood fit to the data, as explained in Section 10.

7. $H \rightarrow ZZ \rightarrow \ell^+\ell^-q\bar{q}$ event selection and background estimation

7.1. Event selection

As in the previous search, the event selection starts with the reconstruction of a $Z \rightarrow \ell\ell$ decay. For the purpose of this search, leptons are classified as either ‘loose’, with $p_T > 7$ GeV, or ‘tight’, with

Process	ggF channel			VBF channel		
$q\bar{q} \rightarrow ZZ$	110	± 1	± 10	$0.13 \pm 0.04 \pm 0.02$		
$gg \rightarrow ZZ$	11	± 0.1	± 5	$0.12 \pm 0.01 \pm 0.05$		
WZ	47	± 1	± 5	$0.10 \pm 0.05 \pm 0.1$		
$WW/t\bar{t}/Wt/Z \rightarrow \tau^+\tau^-$	58	± 6	± 5	$0.41 \pm 0.01 \pm 0.08$		
$Z(\rightarrow e^+e^-, \mu^+\mu^-)+\text{jets}$	74	± 7	± 20	$0.8 \pm 0.3 \pm 0.3$		
Other backgrounds	4.5	± 0.7	± 0.5	—		
Total background	310	± 9	± 40	$1.6 \pm 0.3 \pm 0.5$		
Observed	309			4		
ggF signal ($m_H = 400$ GeV)	45	± 1	± 3	—		
VBF signal ($m_H = 400$ GeV)	1	$\pm < 0.1$	± 2	10	± 0.5	± 1

Table 2: Expected background yields and observed counts of data events after all selections for the ggF and VBF channels of the $H \rightarrow ZZ \rightarrow \ell^+\ell^-\nu\bar{\nu}$ search. The first and second uncertainties correspond to the statistical and systematic uncertainties, respectively.

$p_T > 25$ GeV. Loose muons extend to $|\eta| < 2.7$, while tight muons are restricted to $|\eta| < 2.5$ and must have tracks in both the ID and the MS. The transverse impact parameter requirement for muons is tightened for this search to $|d_0| < 0.1$ mm. Electrons are identified using a likelihood discriminant very similar to that used for the $\ell\ell\ell\ell$ search, except that it was tuned for a higher signal efficiency. This selection is denoted ‘very loose LH’ [73]. To avoid double counting, the following procedure is applied to loose leptons and jets. First, any jets that lie $\Delta R < 0.4$ of an electron are removed. Next, if a jet is within a cone of $\Delta R = 0.4$ of a muon, the jet is discarded if it has less than two matched tracks or if the JVF recalculated without muons (see Section 4) is less than 0.5, since in this case it is likely to originate from a muon having showered in the calorimeter; otherwise the muon is discarded. (Such muons are nevertheless included in the computation of the E_T^{miss} and in the jet energy corrections described in Section 4.) Finally, if an electron is within a cone of $\Delta R = 0.2$ of a muon, the muon is kept unless it has no track in the MS, in which case the electron is kept.

Events must contain a same-flavour lepton pair with invariant mass satisfying $83 < m_{\ell\ell} < 99$ GeV. At least one of the leptons must be tight, while the other may be either tight or loose. Events containing any additional loose leptons are rejected. The two muons in a pair are required to have opposite charge, but this requirement is not imposed for electrons because larger energy losses from showering in material in the inner tracking detector lead to higher charge misidentification probabilities.

Jets used in this search to reconstruct the $Z \rightarrow q\bar{q}$ decay, referred to as ‘signal’ jets, must have $|\eta| < 2.5$ and $p_T > 20$ GeV; the leading signal jet must also have $p_T > 45$ GeV. The search for forward jets in the VBF production mode uses an alternative, ‘loose’, jet definition, which includes both signal jets and any additional jets satisfying $2.5 < |\eta| < 4.5$ and $p_T > 30$ GeV. Since no high- p_T neutrinos are expected in this search, the significance of the missing transverse momentum, $E_T^{\text{miss}}/\sqrt{H_T}$ (all quantities in GeV), where H_T is the scalar sum of the transverse momenta of the leptons and loose jets, must be less than 3.5. This requirement is loosened to 6.0 for the case of the resolved channel (see Section 7.1.1) with two b -tagged jets due to the presence of neutrinos from heavy-flavour decay. The E_T^{miss} significance requirement rejects mainly top-quark background.

Following the selection of the $Z \rightarrow \ell\ell$ decay, the search is divided into several channels: resolved ggF,

merged-jet ggF, and VBF, as discussed below.

7.1.1. Resolved ggF channel

Over most of the mass range considered in this search ($m_H \lesssim 700$ GeV), the $Z \rightarrow q\bar{q}$ decay results in two well-separated jets that can be individually resolved. Events in this channel should thus contain at least two signal jets. Since b -jets occur much more often in the signal ($\sim 21\%$ of the time) than in the dominant Z + jets background ($\sim 2\%$ of the time), the sensitivity of this search is optimized by dividing it into ‘tagged’ and ‘untagged’ subchannels, containing events with exactly two and fewer than two b -tagged jets, respectively. Events with more than two b -tagged jets are rejected.

In the tagged subchannel, the two b -tagged jets form the candidate $Z \rightarrow q\bar{q}$ decay. In the untagged subchannel, if there are no b -tagged jets, the two jets with largest transverse momenta are used. Otherwise, the b -tagged jet is paired with the non- b -tagged jet with the largest transverse momentum. The invariant mass of the chosen jet pair m_{jj} must be in the range 70–105 GeV in order to be consistent with $Z \rightarrow q\bar{q}$ decay. To maintain orthogonality, any events containing a VBF-jet pair as defined by the VBF channel (see Section 7.1.3) are excluded from the resolved selection.

The discriminating variable in this search is the invariant mass of the $\ell\ell jj$ system, $m_{\ell\ell jj}$; a signal should appear as a peak in this distribution. To improve the mass resolution, the energies of the jets forming the dijet pair are scaled event-by-event by a single multiplicative factor to set the dijet invariant mass m_{jj} to the mass of the Z boson (m_Z). This improves the resolution by a factor of 2.4 at $m_H = 200$ GeV. The resulting $m_{\ell\ell jj}$ resolution is 2–3%, approximately independent of m_H , for both the untagged and tagged channels.

Following the selection of the candidate $\ell\ell qq$ decay, further requirements are applied in order to optimize the sensitivity of the search. For the untagged subchannel, the first requirement is on the transverse momentum of the leading jet, p_T^j , which tends to be higher for the signal than for the background. The optimal value for this requirement increases with increasing m_H . In order to avoid having distinct selections for different m_H regions, p_T^j is normalized by the reconstructed final-state mass $m_{\ell\ell jj}$; the actual selection is $p_T^j > 0.1 \times m_{\ell\ell jj}$. Studies have shown that the optimal requirement on $p_T^j/m_{\ell\ell jj}$ is nearly independent of the assumed value of m_H . Second, the total transverse momentum of the dilepton pair also increases with increasing m_H . Following a similar strategy, the selection is $p_T^{\ell\ell} > \min[-54 \text{ GeV} + 0.46 \times m_{\ell\ell jj}, 275 \text{ GeV}]$. Finally, the azimuthal angle between the two leptons decreases with increasing m_H ; it must satisfy $\Delta\phi_{\ell\ell} < (270 \text{ GeV}/m_{\ell\ell jj})^{3.5} + 1$. For the tagged channel, only one additional requirement is applied: $p_T^{\ell\ell} > \min[-79 \text{ GeV} + 0.44 \times m_{\ell\ell jj}, 275 \text{ GeV}]$; the different selection for $p_T^{\ell\ell}$ increases the sensitivity of the tagged channel at low m_H . Figures 3(a) and 3(b) show the $m_{\ell\ell jj}$ distributions of the two subchannels after the final selection.

7.1.2. Merged-jet ggF channel

For very large Higgs boson masses, $m_H \gtrsim 700$ GeV, the Z bosons become highly boosted and the jets from $Z \rightarrow q\bar{q}$ decay start to overlap, causing the resolved channel to lose efficiency. The merged-jet channel recovers some of this loss by looking for a $Z \rightarrow q\bar{q}$ decay that is reconstructed as a single jet.

Events are considered for the merged-jet channel if they have exactly one signal jet, or if the selected jet pair has an invariant mass outside the range 50–150 GeV (encompassing both the signal region and the

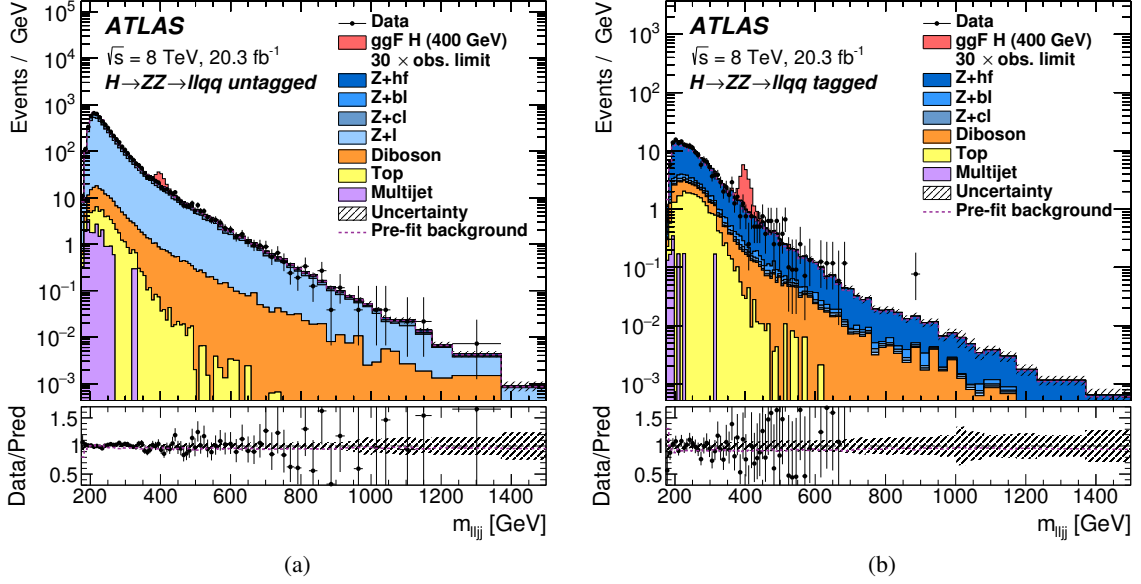


Figure 3: The distributions used in the likelihood fit of the invariant mass of dilepton+dijet system $m_{\ell\ell jj}$ for the $H \rightarrow ZZ \rightarrow \ell^+ \ell^- q \bar{q}$ search in the (a) untagged and (b) tagged resolved ggF subchannels. The dashed line shows the total background used as input to the fit. The simulated signal is normalized to a cross-section corresponding to thirty times the observed limit given in Section 11. The contribution labelled as ‘Top’ includes both the $t\bar{t}$ and single-top processes. The bottom panes show the ratio of the observed data to the predicted background.

control regions used for studying the background). Thus, the merged-jet channel is explicitly orthogonal to the resolved channel.

To be considered for the merged-jet channel, the dilepton pair must have $p_T^{\ell\ell} > 280$ GeV. The leading jet must also satisfy $p_T > 200$ GeV and $m/p_T > 0.05$, where m is the jet mass, in order to restrict the jet to the kinematic range in which the mass calibration has been studied. Finally, the invariant mass of the leading jet must be within the range 70–105 GeV. The merged-jet channel is not split into subchannels based on the number of b -tagged jets; as the sample size is small, this would not improve the expected significance.

Including this channel increases the overall efficiency for the $\ell\ell q\bar{q}$ signal at $m_H = 900$ GeV by about a factor of two. Figure 4(a) shows the distribution of the invariant mass of the leading jet after all selections except for that on the jet invariant mass; it can be seen that the simulated signal has a peak at the mass of the Z boson, with a tail at lower masses due to events where the decay products of the Z boson are not fully contained in the jet cone. The discriminating variable for this channel is the invariant mass of the two leptons plus the leading jet, $m_{\ell\ell j}$, which has a resolution of 2.5% for a signal with $m_H = 900$ GeV and is shown in Fig. 4(b).

7.1.3. VBF channel

Events produced via the VBF process contain two forward jets in addition to the reconstructed leptons and signal jets from $ZZ \rightarrow \ell^+ \ell^- q \bar{q}$ decay. These forward jets are called ‘VBF jets’. The search in the VBF channel starts by identifying a candidate VBF-jet pair. Events must have at least four loose jets, two

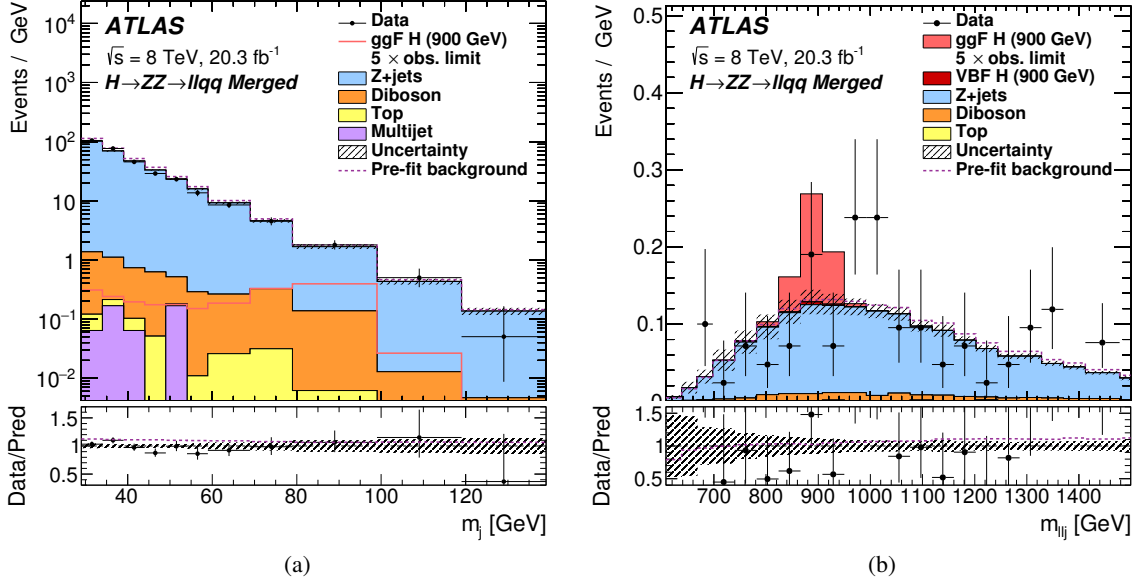


Figure 4: Distributions for the merged-jet channel of the $H \rightarrow ZZ \rightarrow \ell^+ \ell^- q \bar{q}$ search after the mass calibration. (a) The invariant mass of the leading jet, m_j , after the kinematic selection for the $\ell\ell qq$ merged-jet channel. (b) The distribution used in the likelihood fit of the invariant mass of the two leptons and the leading jet $m_{\ell\ell j}$ in the signal region. It is obtained requiring $70 < m_j < 105$ GeV. The dashed line shows the total background used as input to the fit. The simulated signal is normalized to a cross-section corresponding to five times the observed limit given in Section 11. The contribution labelled as ‘Top’ includes both the $t\bar{t}$ and single-top processes. The bottom panes show the ratio of the observed data to the predicted background. The signal contribution is shown added on top of the background in (b) but not in (a).

of them being non- b -tagged and pointing in opposite directions in z (that is, $\eta_1 \cdot \eta_2 < 0$). If more than one such pair is found, the one with the largest invariant mass, $m_{jj,\text{VBF}}$, is selected. The pair must further satisfy $m_{jj,\text{VBF}} > 500$ GeV and have a pseudorapidity gap of $|\Delta\eta_{jj,\text{VBF}}| > 4$. The distributions of these two variables are shown in Fig. 5.

Once a VBF-jet pair has been identified, the $ZZ \rightarrow \ell^+ \ell^- q \bar{q}$ decay is reconstructed in exactly the same way as in the resolved channel, except that the jets used for the VBF-jet pair are excluded and no b -tagging categories are created due to the small sample size. The final $m_{\ell\ell jj}$ discriminant is shown in Fig. 6. Again, the resolution is improved by constraining the dijet mass to m_Z as described in Section 7.1.1, resulting in a similar overall resolution of 2–3%.

7.2. Background estimation

The main background in the $\ell\ell qq$ search is Z + jets production, with significant contributions from both top-quark and diboson production in the resolved ggF channel, as well as a small contribution from multijet production in all channels. For the multijet background, the shape and normalization is taken purely from data, as described below. For the other background processes, the input is taken from simulation, with data-driven corrections for Z + jets and $t\bar{t}$ production. The normalizations of the Z + jets and top-quark backgrounds are left free to float and are determined in the final likelihood fit as described below and in Section 10.

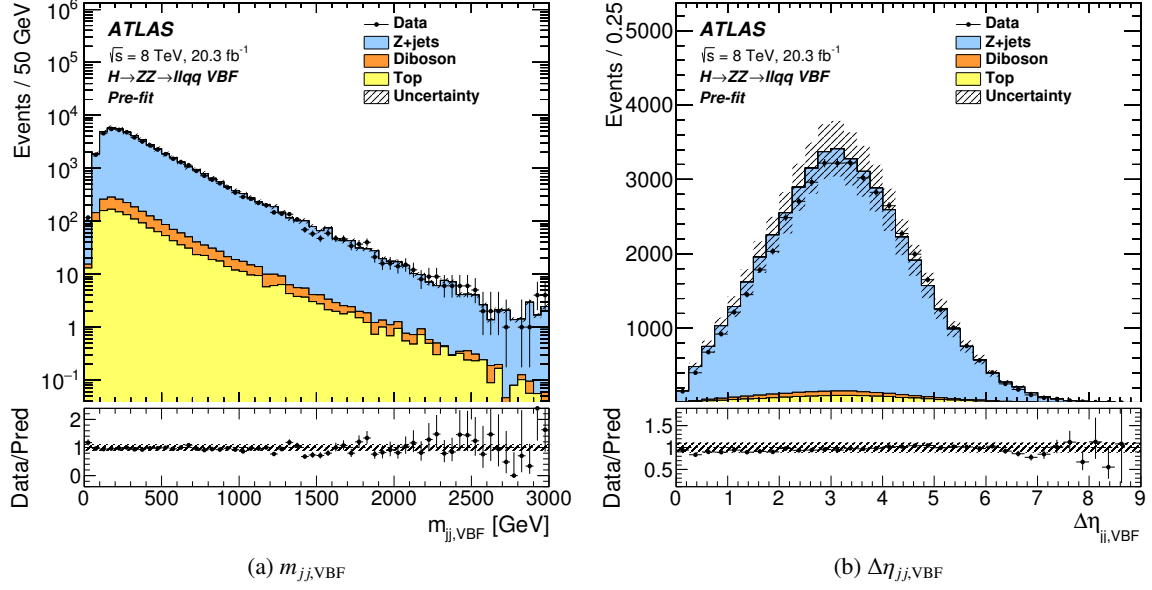


Figure 5: Distribution of (a) invariant mass and (b) pseudorapidity gap for the VBF-jet pair in the VBF channel of the $H \rightarrow ZZ \rightarrow \ell^+ \ell^- q \bar{q}$ search before applying the requirements on these variables (and prior to the combined fit described in Section 10). The contribution labelled as ‘Top’ includes both the $t\bar{t}$ and single-top processes. The bottom panes show the ratio of the observed data to the predicted background.

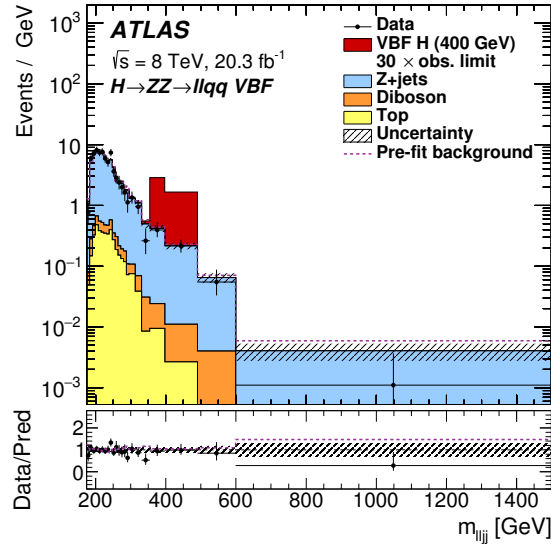


Figure 6: The distribution of $m_{\ell\ell jj}$ used in the likelihood fit for the $H \rightarrow ZZ \rightarrow \ell^+ \ell^- q \bar{q}$ search in the VBF channel. The dashed line shows the total background used as input to the fit. The simulated signal is normalized to a cross-section corresponding to thirty times the observed limit given in Section 11. The contribution labelled as ‘Top’ includes both the $t\bar{t}$ and single-top processes. The bottom pane shows the ratio of the observed data to the predicted background.

The $Z + \text{jets}$ MC sample is constrained using control regions that have the same selection as the signal regions except that m_{jj} (m_j in the case of the merged-jet channel) lies in a region just outside of that selected by the signal Z boson requirement. For the resolved channels, the requirement for the control region is $50 < m_{jj} < 70$ GeV or $105 < m_{jj} < 150$ GeV; for the merged-jet channel, it is $30 < m_j < 70$ GeV. In the resolved ggF channel, which is split into untagged and tagged subchannels as described in Section 7.1.1, the $Z + \text{jets}$ control region is further subdivided into 0-tag, 1-tag, and 2-tag subchannels based on the number of b -tagged jets. The sum of the 0-tag and 1-tag subchannels is referred to as the untagged control region, while the 2-tag subchannel is referred to as the tagged control region.

The normalization of the $Z + \text{jets}$ background is determined by the final profile-likelihood fit as described in Section 10. In the resolved ggF channel, the simulated $Z + \text{jets}$ sample is split into several different components according to the true flavour of the jets as described in Section 3.3: $Z + jj$, $Z + cj$, $Z + bj$, and $Z + \text{hf}$. The individual normalizations for each of these four components are free to float in the fit and are constrained by providing as input to the fit the distribution of the “ b -tagging category” in the untagged and tagged $Z + \text{jets}$ control regions. The b -tagging category is defined by the combination of the MV1c b -tagging discriminants of the two signal jets as described in Appendix A. In the VBF and merged-jet ggF channels, which are not divided into b -tag subchannels, the background is dominated by $Z + \text{light-jets}$. Thus, only the inclusive $Z + \text{jets}$ normalization is varied in the fit for these channels. Since these two channels probe very different regions of phase space, each has a separate normalization factor in the fit; these are constrained by providing to the fit the distributions of $m_{\ell\ell jj}$ or $m_{\ell\ell j}$ for the corresponding $Z + \text{jets}$ control regions.

Differences are observed between data and MC simulation for the distributions of the azimuthal angle between the two signal jets, $\Delta\phi_{jj}$, and the transverse momentum of the leptonically-decaying Z boson, $p_T^{\ell\ell}$, for the resolved region, and for the $m_{\ell\ell jj}$ distribution in the VBF channel. To correct for these differences, corrections are applied to the SHERPA $Z + \text{jets}$ simulation (prior to the likelihood fit) as described in Appendix B. The distributions of $m_{\ell\ell jj}$ or $m_{\ell\ell j}$ in the various $Z + \text{jets}$ control regions are shown in Fig. 7; it can be seen that after the corrections (and after normalizing to the results of the likelihood fit), the simulation provides a good description of the data.

The simulation models the m_{jj} distribution well in the resolved ggF and VBF channels. An uncertainty is assigned by weighting each event of the $Z + \text{jets}$ MC simulation by a linear function of m_{jj} in order to cover the residual difference between data and MC events in the control regions.

Top-quark production is a significant background in the tagged subchannel of the resolved ggF channel. This background is predominantly ($> 97\%$) $t\bar{t}$ production with only a small contribution from single-top processes, mainly Wt production. Corrections to the simulation to account for discrepancies in the $p_T^{t\bar{t}}$ distributions are described in Appendix B. The description of the top-quark background is cross-checked and normalized using a control region with a selection identical to that of the tagged ggF channel except that instead of two same-flavour leptons, events must contain an electron and a muon with opposite charge. The $m_{\ell\ell jj}$ distribution in this control region is used as an input to the final profile-likelihood fit, in which the normalization of the top-quark background is left free to float (see Section 10). There are few events in the control region for the VBF and merged-jet ggF channels, so the normalization is assumed to be the same across all channels, in which the top-quark contribution to the background is very small. Figure 8 shows that the data in the control region are well-described by the simulation after the normalization.

Further uncertainties in the top-quark background arising from the parton showering and hadronization models are estimated by varying the amount of parton showering in ACERMC and also by comparing with POWHEG+HERWIG. Uncertainties in the $t\bar{t}$ production matrix element are estimated by comparing the

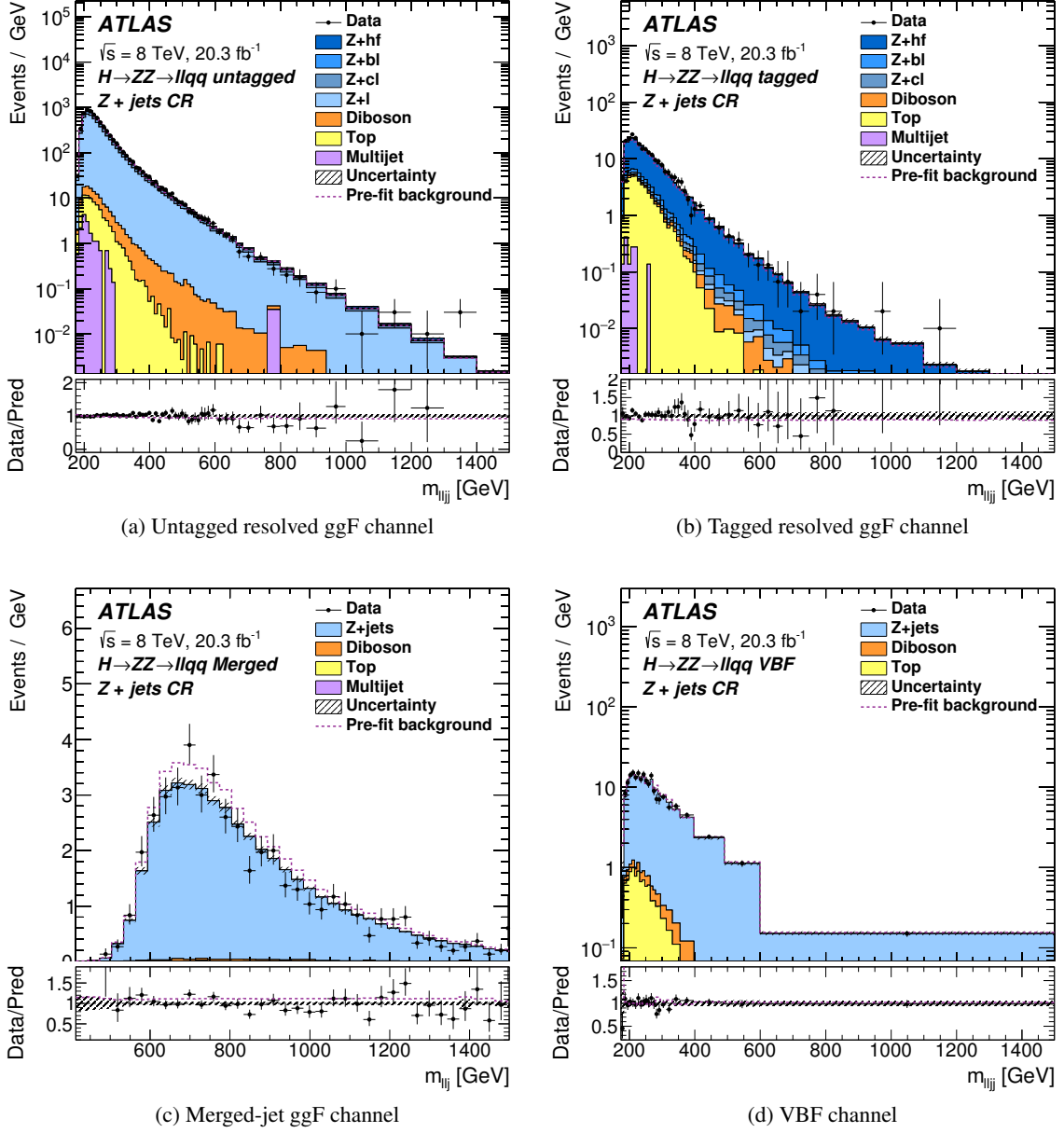


Figure 7: The distributions of $m_{\ell\ell jj}$ or $m_{\ell\ell j}$ in the Z + jets control region of the $H \rightarrow ZZ \rightarrow \ell^+ \ell^- q \bar{q}$ search in the (a) untagged ggF, (b) tagged ggF, (c) merged-jet ggF, and (d) VBF channels. The dashed line shows the total background used as input to the fit. The contribution labelled as ‘Top’ includes both the $t\bar{t}$ and single-top processes. The bottom panes show the ratio of the observed data to the predicted background.

leading-order MC generator ALPGEN with the NLO generator aMC@NLO. Comparisons are also made with alternate PDF sets. A similar procedure is used for single-top production. In addition, for the dominant Wt single-top channel, uncertainties in the shapes of the m_{jj} and leading-jet p_T distributions are evaluated by comparing results from HERWIG to those from ACERMC.

The small multijet background in the $H \rightarrow ZZ \rightarrow ee q \bar{q}$ decay mode is estimated from data by selecting

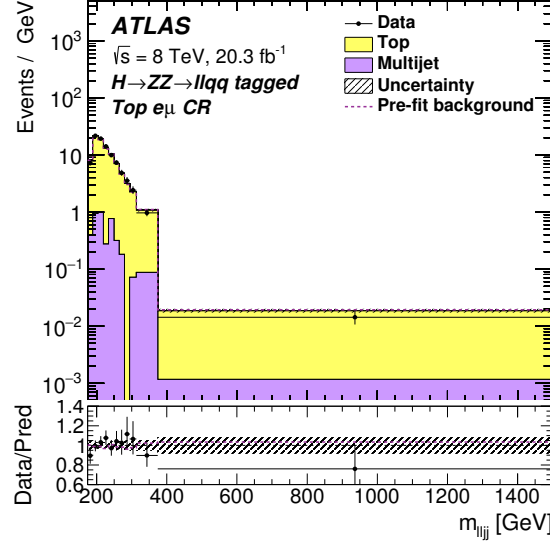


Figure 8: The distribution of $m_{\ell\ell jj}$ in the $e\mu$ top-quark control region of the $H \rightarrow ZZ \rightarrow \ell^+ \ell^- q\bar{q}$ search in the tagged ggF channel. The dashed line shows the total background used as input to the fit. The contribution labelled as ‘Top’ includes both the $t\bar{t}$ and single-top processes. The bottom pane shows the ratio of the observed data to the predicted background.

a sample of events with the electron isolation requirement inverted, which is then normalized by fitting the m_{ee} distribution in each channel. In the $H \rightarrow ZZ \rightarrow \mu\mu q\bar{q}$ decay mode, the multijet background is found to be negligible. The residual multijet background in the top-quark control region is taken from the opposite-charge $e\mu$ data events, which also accounts for the small W + jets background in that region. An uncertainty of 50% is assigned to these two normalizations, which are taken to be uncorrelated.

The diboson background, composed mainly of ZZ and $WZ \rightarrow \ell\ell jj$ production, and the SM $Zh \rightarrow \ell\ell b\bar{b}$ background are taken directly from Monte Carlo simulation, as described in Section 3.3. The uncertainty in the diboson background is estimated by varying the factorization and renormalization scales in an MCFM calculation [35]. The method described in Refs. [86, 87] is used to avoid underestimating the uncertainty due to cancellations. Differences due to the choice of alternate PDF sets and variations in the value of α_S are included in the normalization uncertainty. Additional shape uncertainties in the m_{jj} distribution are obtained by comparing results from HERWIG, an LO simulation, with those from POWHEG+PYTHIA, an NLO simulation.

The rate of the SM $Vh(V = W/Z, h \rightarrow b\bar{b})$ process, relative to the SM expectation, has been measured by ATLAS as $\mu = \sigma/\sigma_{SM} = 0.52 \pm 0.32$ (stat.) ± 0.24 (syst.) [30]. Since this is compatible with the SM expectation, the small $Zh(h \rightarrow b\bar{b})$ background in this channel is normalized to the SM cross-section and a 50% uncertainty is assigned to cover the difference between the prediction and the measured mean value.

8. $H \rightarrow ZZ \rightarrow \nu\bar{\nu}q\bar{q}$ event selection and background estimation

8.1. Event selection

Events selected for this search must contain no electrons or muons as defined by the ‘loose’ lepton selection of the $\ell\ell q\bar{q}$ search. To select events with neutrinos in the final state, the magnitude of the missing transverse momentum vector must satisfy $E_T^{\text{miss}} > 160$ GeV; the trigger is 100% efficient in this range. Events must have at least two jets with $p_T > 20$ GeV and $|\eta| < 2.5$; the leading jet must further satisfy $p_T > 45$ GeV. To select a candidate $Z \rightarrow q\bar{q}$ decay, the invariant mass of the leading two jets must satisfy $70 < m_{jj} < 105$ GeV.

The multijet background, due mainly to the mismeasurement of jet energies, is suppressed using a track-based missing transverse momentum, \vec{p}_T^{miss} , defined as the negative vectorial sum of the transverse momenta of all good-quality inner detector tracks. The requirements are $p_T^{\text{miss}} > 30$ GeV, the azimuthal angle between the directions of \vec{E}_T^{miss} and \vec{p}_T^{miss} satisfy $\Delta\phi(\vec{E}_T^{\text{miss}}, \vec{p}_T^{\text{miss}}) < \pi/2$, and the azimuthal angle between the directions of \vec{E}_T^{miss} and the nearest jet satisfy $\Delta\phi(\vec{E}_T^{\text{miss}}, j) > 0.6$.

As in the resolved ggF channel of the $\ell\ell q\bar{q}$ search, this search is divided into ‘tagged’ (exactly two b -tagged jets) and ‘untagged’ (fewer than two b -tagged jets) subchannels. Events with more than two b -tags are rejected.

The sensitivity of this search is improved by adding a requirement on the jet transverse momenta. As in the $\ell\ell q\bar{q}$ search, the optimal threshold depends on m_H . However, due to the neutrinos in the final state, this decay mode does not provide a good event-by-event measurement of the mass of the diboson system, m_{ZZ} . So, rather than having a single requirement on the jet transverse energy which is a function of the measured m_{ZZ} , instead there is a set of requirements, based on the generated m_H , with the background estimated separately for each of these separate jet requirements. The specific requirement is found by rounding the generated m_H to the nearest 100 GeV; this is called m_H^{bin} . Then the subleading jet must satisfy $p_T^{j2} > 0.1 \times m_H^{\text{bin}}$ in events with no b -tagged jets, and $p_T^{j2} > 0.1 \times m_H^{\text{bin}} - 10$ GeV in events with at least one b -tagged jet.

The discriminating variable for this search is the transverse mass of the $\nu\nu q\bar{q}$ system, shown in Fig. 9, defined as in Eq. (1) with p_T^{jj} replacing $p_T^{\ell\ell}$. To improve the transverse mass resolution, the energies of the leading two jets are scaled event-by-event by a multiplicative factor to set the dijet invariant mass m_{jj} to the Z boson mass, in the same manner as in the $\ell\ell q\bar{q}$ search. This improves the transverse mass resolution by approximately 20% at $m_H = 400$ GeV and by approximately 10% at $m_H = 1$ TeV. The resulting resolution in m_T ranges from about 9% at $m_H = 400$ GeV to 14% at $m_H = 1$ TeV.

8.2. Background estimation

The dominant backgrounds for this search are Z + jets, W + jets, and $t\bar{t}$ production. The normalization of the Z + jets background is determined using the Z + jets control region from the $\ell\ell q\bar{q}$ channel in the final profile-likelihood fit as described in Section 10. To check how well this background is modelled after the $\nu\nu q\bar{q}$ selection, an alternative Z + jets control region is defined in the same way as the signal sample for $m_H^{\text{bin}} = 400$ GeV except that events must contain exactly two loose muons. The E_T^{miss} is calculated without including the muons and must satisfy the same requirement as for the signal: $E_T^{\text{miss no } \mu} > 160$ GeV. The

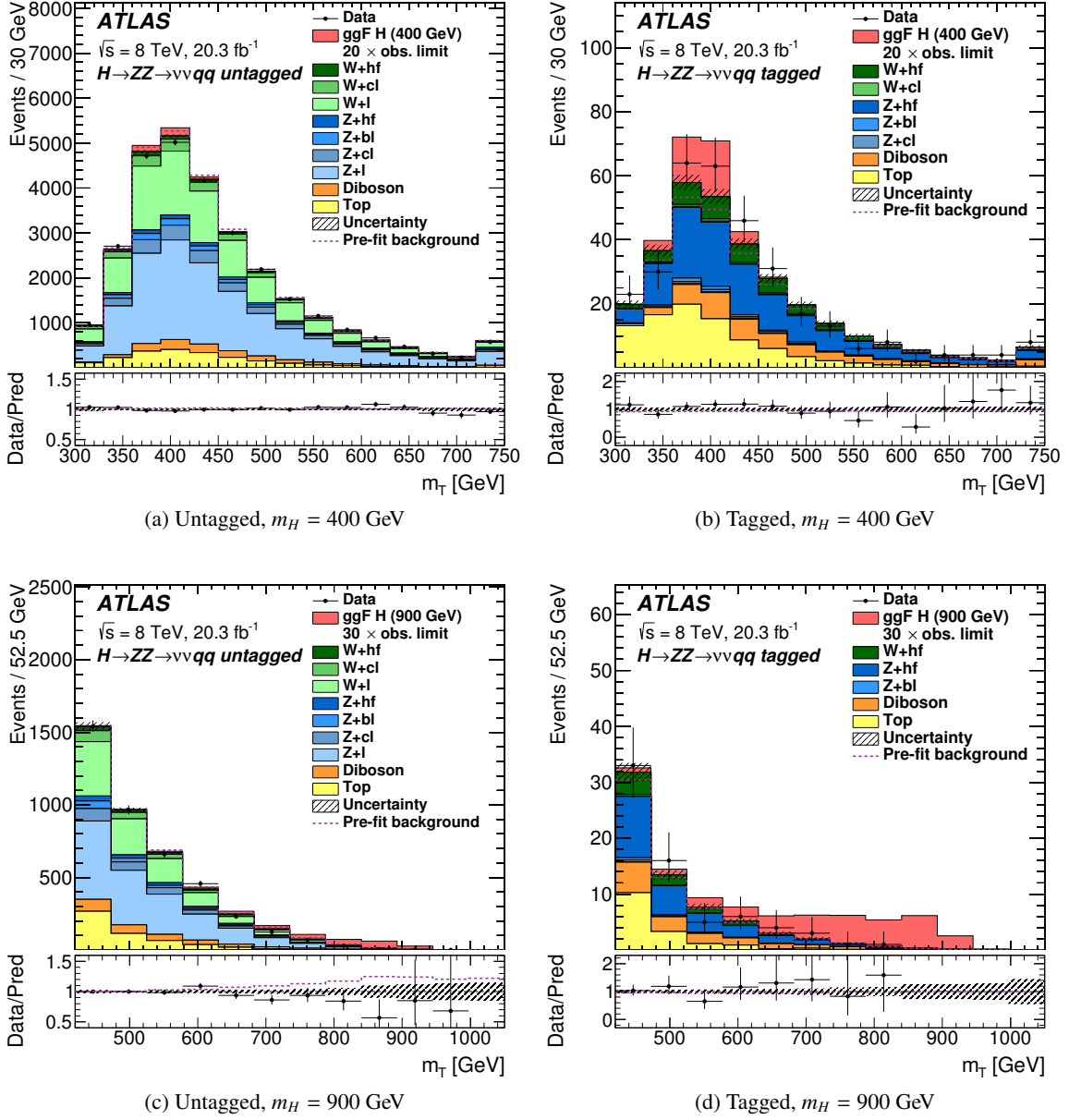


Figure 9: The distributions of m_T , the transverse mass of the $Z(\nu\nu)Z(jj)$ system, used in the likelihood fit for the $H \rightarrow ZZ \rightarrow \nu\nu qq$ search in the (a, c) untagged and (b, d) tagged channels, for Higgs boson mass hypotheses of (a, b) $m_H = 400$ GeV and (c, d) $m_H = 900$ GeV. The dashed line shows the total background used as input to the fit. For the $m_H = 400$ GeV hypothesis (a, b) the simulated signal is normalized to a cross-section corresponding to twenty times the observed limit given in Section 11, while for the $m_H = 900$ GeV hypothesis (c, d) it is normalized to thirty times the observed limit. The contribution labelled as ‘Top’ includes both the $t\bar{t}$ and single-top processes. The bottom panes show the ratio of the observed data to the predicted background.

Z + jets MC simulation is corrected as a function of $\Delta\phi_{jj}$ and $p_T^{\ell\ell}$ in the same manner as in the resolved ggF channel of the $\ell\ell qq$ search, as described in Section 7.2 and Appendix B.

The W + jets background estimate similarly uses a control sample with the same selection as the signal

sample for $m_H^{\text{bin}} = 400$ GeV except that there must be exactly one loose muon and the E_T^{miss} requirement is again on $E_T^{\text{miss no } \mu}$. The simulated $W + \text{jets}$ sample is also split into several different flavour components, as in the case of $Z + \text{jets}$. The normalization of the $W + jj$ and $W + cj$ components are free to float in the final profile-likelihood fit, and are constrained by providing as input to the fit the distribution of the MV1c b -tagging category, described in Appendix A, in the 0- b -tag and 1- b -tag control regions. Unlike the $Z + \text{jets}$ case, the 2- b -tag control region is not used in the final profile-likelihood fit to constrain the $W + bj$ and $W + \text{hf}$ background components since it is highly dominated by $t\bar{t}$ production. Their normalizations are instead taken from the NNLO cross section predictions with an uncertainty of 50%. The uncertainty is determined by comparing the nominal fit value from the profile-likelihood fit with the value when including the 2- b -tag control region, where $W + bj$ and $W + \text{hf}$ are free to float; this uncertainty also covers the normalization determined in Ref. [30]. Following Ref. [30], the agreement between simulation and data for this background is improved by applying a correction to $\Delta\phi_{jj}$ for $W + jj$ and $W + cj$, with half the correction assigned as a systematic uncertainty; in the case of $W + bj$ and $W + \text{hf}$, no correction is applied, but a dedicated systematic uncertainty is assigned.

Even after these corrections, the simulation does not accurately describe the data in the $Z + \text{jets}$ and $W + \text{jets}$ control sample with no b -tagged jets (which is dominated by $Z/W + jj$) for important kinematic distributions such as E_T^{miss} and jet transverse momenta. Moreover, because the resolution of the transverse mass of the $ZZ \rightarrow \nu\bar{\nu}q\bar{q}$ system is worse than that of $m_{\ell\ell jj}$, the $\nu\bar{\nu}q\bar{q}$ search is more sensitive to E_T^{miss} (i.e. Z/W boson p_T) than the $\ell\ell q\bar{q}$ search. Therefore, a further correction is applied, as a linear function of E_T^{miss} , derived from measuring the ratio of the E_T^{miss} distributions from simulation and data in the control sample with no b -tagged jets after non- $Z/W + jj$ backgrounds have been subtracted. An uncertainty of 50% is assigned to this correction. Following this correction, there is good agreement between simulation and data, as shown in Figs. 10 and 11. For higher m_H^{bin} signal samples, which have tighter selections on kinematic variables than the control sample, the E_T^{miss} correction is somewhat underestimated, leading to some remaining difference between data and pre-fit simulation at high m_T , as can be seen in Fig. 9(c). However, the profile-likelihood-ratio fit (Section 10) is able to correct this residual mismodelling, leading to reasonable agreement between the data and simulation.

The $t\bar{t}$ background is treated in the same manner as in the $\ell\ell q\bar{q}$ search; in particular, $p_T^{\ell\bar{\ell}}$ is corrected in the same way and the normalization is determined by $t\bar{t}$ control region from $\ell\ell q\bar{q}$ channel in the final profile-likelihood fit.

Backgrounds from diboson and single-top production are estimated directly from MC simulations, both for shapes and normalization. The multijet background is estimated using a method similar to that used for the $Z + \text{jets}$ background in the $\ell\ell\nu\nu$ search (Section 6.2), except that the variables used are $\Delta\phi(\vec{E}_T^{\text{miss}}, \vec{p}_T^{\text{miss}})$ and $\Delta\phi(\vec{E}_T^{\text{miss}}, j)$ [30]. It is found to be negligible.

9. Systematic uncertainties

The systematic uncertainties can be divided into three categories: experimental uncertainties, related to the detector or to the reconstruction algorithms, uncertainties in the modelling of the signal, and uncertainties in the estimation of the backgrounds. The first two are largely common to all the searches and are treated as fully correlated. The uncertainties in the estimates of most backgrounds vary from search to search, and are summarized in the background estimation sections above. The estimation of the uncertainty of the $ZZ^{(*)}$ background is outlined in Section 9.3.

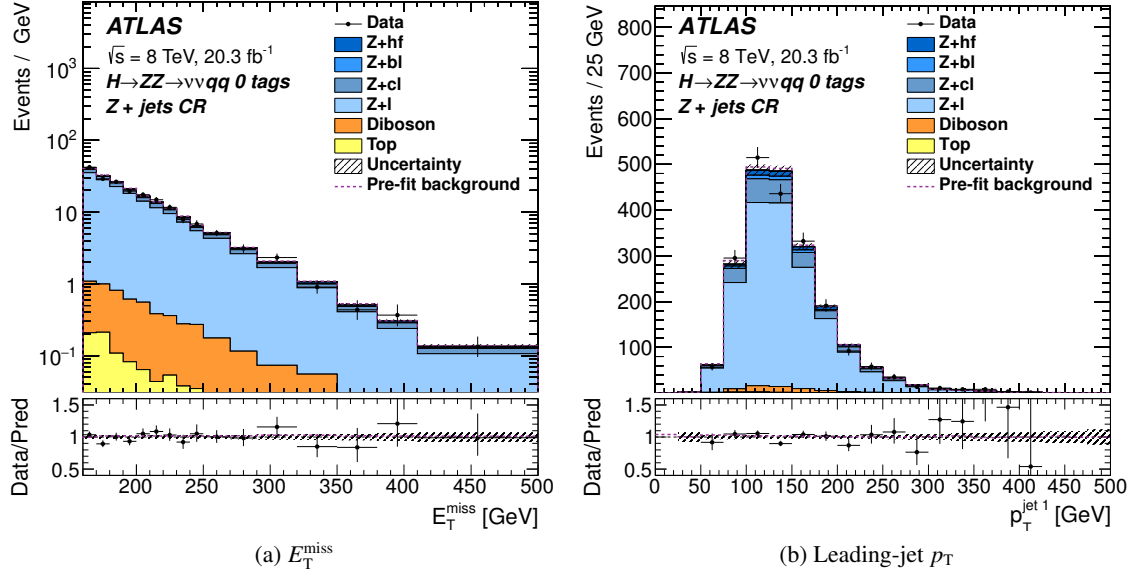


Figure 10: The distributions of (a) missing transverse momentum E_T^{miss} and (b) leading-jet p_T from the untagged ($Z \rightarrow \mu\mu$) + jets control sample of the $H \rightarrow ZZ \rightarrow \nu\bar{\nu}q\bar{q}$ search. The dashed line shows the total background used as input to the fit. The contribution labelled as ‘Top’ includes both the $t\bar{t}$ and single-top processes. The bottom panes show the ratio of the observed data to the predicted background.

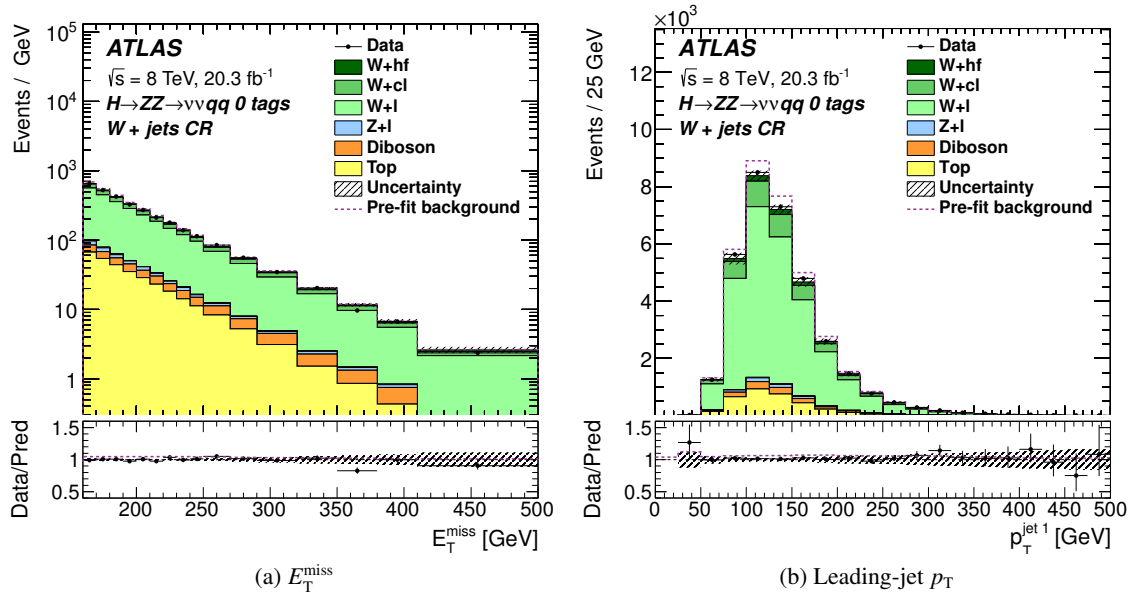


Figure 11: The distributions of (a) E_T^{miss} and (b) leading-jet p_T from the untagged ($W \rightarrow \mu\nu$) + jets control sample of the $H \rightarrow ZZ \rightarrow \nu\bar{\nu}q\bar{q}$ search. The dashed line shows the total background used as input to the fit. The contribution labelled as ‘Top’ includes both the $t\bar{t}$ and single-top processes. The bottom panes show the ratio of the observed data to the predicted background.

9.1. Experimental uncertainties

The following detector-related systematic uncertainties are common to all the searches unless otherwise stated.

The uncertainty in the integrated luminosity is determined to be 2.8% in a calibration following the methodology detailed in Ref. [88] using beam-separation scans performed in November 2012. This uncertainty is applied to the normalization of the signal and also to backgrounds for which the normalization is derived from MC calculations, and is correlated between all of the searches. There is also an uncertainty of 4% in the average number of interactions per bunch crossing, which leads to an uncertainty on distributions sensitive to pile-up.

There are small systematic uncertainties of $O(1\%)$ in the reconstruction and identification efficiencies for electrons and muons [70–73]. For the $\nu\nu qq$ search, the uncertainty is instead in the efficiency of the lepton veto, and is also $O(1\%)$. Uncertainties in the lepton energy scale and resolution are also taken into account. These uncertainties are treated as uncorrelated between all of the searches due to differences in lepton selections optimized for each search.

The uncertainty in the jet energy scale has several sources, including uncertainties in the in situ calibration analysis, corrections for pile-up, and the flavour composition of the sample [76, 89]. These uncertainties are decomposed into independent components. For central jets, the total relative uncertainty on the jet energy scale ranges from about 3% for jets with a p_T of 20 GeV to about 1% for a p_T of 1 TeV. The calibration of the b -jet transverse energy has an additional uncertainty of 1–2%. There is also an uncertainty in the jet energy resolution [90], which ranges from 10–20% for jets with a p_T of 20 GeV to less than 5% for jets with $p_T > 200$ GeV. The uncertainty associated with the pile-up rejection requirement (Section 4) is evaluated by varying the nominal value of 50% between 47% and 53% [78]. The jet energy scale uncertainties are correlated between the $\ell\ell qq$ and $\nu\nu qq$ searches, and separately between the $\ell\ell\ell\ell$ and $\ell\ell\nu\nu$ searches. They are not correlated between the two pairs of searches because although the $\ell\ell qq$ and $\nu\nu qq$ control regions have the power to constrain the jet energy scale uncertainties, these constraints do not necessarily apply to the $\ell\ell\ell\ell$ and $\ell\ell\nu\nu$ searches due to differences in the jet kinematics and composition.

Uncertainties on the lepton and jet energy scales are propagated into the uncertainty on E_T^{miss} . A contribution to E_T^{miss} also comes from energy deposits that are not associated with any identified physics object; uncertainties on the energy calibration (8%) and resolution (3%) of the sum of these deposits are also propagated to the uncertainty on E_T^{miss} [91].

Uncertainties in the efficiency for tagging b -jets and in the rejection factor for light jets are determined from $t\bar{t}$ and dijet control samples [81–83]. Additional uncertainties account for differences in b -tagging efficiency between simulated samples generated with SHERPA and PYTHIA and for differences observed between standard b -tagging and truth tagging (defined at the end of Section 4) for close-by jets [30].

The efficiencies for the lepton triggers in events with reconstructed leptons are nearly 100%, and hence the related uncertainties are negligible. For the selection used in the $\nu\nu qq$ search, the efficiency for the E_T^{miss} trigger is also close to 100% with negligible associated uncertainties.

The merged-jet channel of the $\ell\ell qq$ search relies on measuring single-jet masses. To estimate the uncertainty in this measurement, jets reconstructed as described in Section 4 are compared with jets constructed using the same clustering algorithm but using as input charged-particle tracks rather than calorimeter energy deposits. The uncertainty is found using a procedure similar to that described in Ref. [92] by

studying the double ratio of masses of jets found by both the calorimeter- and track-based algorithms: $R_{\text{trackcalo}}^m = r_{\text{trackcalo}}^{m,\text{data}} / r_{\text{trackcalo}}^{m,\text{MC}}$, where $r_{\text{trackcalo}}^{m,X} = m_{\text{calo}}^X / m_{\text{track}}^X$, $X = \text{data or MC simulation}$, and m is the jet mass. The uncertainty is taken as the deviation of this quantity from unity. Studies performed on dijet samples yield a constant value of 10% for this uncertainty. Applying the jet mass calibration derived from single jets in generic multijet samples to merged jets originating from boosted Z bosons results in a residual topology-dependent miscalibration. This effect can be bounded by an additional uncertainty of 10%. Adding these two effects in quadrature gives a total uncertainty on the jet mass scale of 14%. The uncertainty on the jet mass resolution has a negligible effect on the final result.

9.2. Signal acceptance uncertainty

The uncertainty in the experimental acceptance for the Higgs boson signal due to the modelling of Higgs boson production is estimated by varying parameters in the generator and re-applying the signal selection at generator level. The renormalization and factorization scales are varied up and down both independently and coherently by a factor of two; the amounts of initial- and final-state radiation (ISR/FSR) are increased and decreased separately; and the PDF set used is changed from the nominal CT10 to either MSTW2008 or NNPDF23.

9.3. $ZZ^{(*)}$ background uncertainties

Uncertainties on the $ZZ^{(*)}$ background are treated as correlated between the $\ell\ell\ell\ell$ and $\ell\ell\nu\nu$ searches.

Uncertainties in the PDF and in α_S are taken from Ref. [93] and are derived separately for the $q\bar{q} \rightarrow ZZ$ and $gg \rightarrow ZZ$ backgrounds, using the envelope of the CT10, MSTW, and NNPDF error sets following the PDF4LHC prescription given in Refs. [94, 95], giving an uncertainty parameterized in m_{ZZ} . These uncertainties amount to 3% for the $q\bar{q} \rightarrow ZZ$ process and 8% for the $gg \rightarrow ZZ$ process and are found to be anti-correlated between the two processes; this is taken into account in the fit. The QCD scale uncertainty for the $q\bar{q} \rightarrow ZZ$ process is also taken from Ref. [93] and is based on varying the factorization and renormalization scales up and down by a factor of two, giving an uncertainty parameterized in m_{ZZ} amounting to 4% on average.

The deviation of the NLO electroweak K -factor from unity is varied up and down by 100% in events with high QCD activity or with an off-shell Z boson, as described in Ref. [96]; this leads to an additional overall uncertainty of 1–3% for the $q\bar{q} \rightarrow ZZ$ process.

Full NLO and NNLO QCD calculations exist for the $gg \rightarrow h^* \rightarrow ZZ^{(*)}$ process, but not for the $gg \rightarrow ZZ$ continuum process. However, Ref. [97] showed that higher-order corrections affect $gg \rightarrow WW$ and $gg \rightarrow h^* \rightarrow WW$ similarly, within a 30% uncertainty on the interference term. This yields about a 60% uncertainty on the $gg \rightarrow WW$ process. Furthermore, Ref. [97] states that this conclusion also applies to the $ZZ^{(*)}$ final state, so the gg -induced part of the off-shell light Higgs boson K -factor from Ref. [38] is applied to the $gg \rightarrow ZZ$ background. The uncertainty on this K -factor depends on m_{ZZ} and is about 30%. An additional uncertainty of 100% is assigned to this procedure; this covers the 60% mentioned above. This uncertainty corresponds to the range considered for the $gg \rightarrow ZZ$ background K -factor in the ATLAS off-shell Higgs boson signal-strength measurement described in Ref. [96].

Acceptance uncertainties for the ggF and VBF (and VH for $\ell\ell\ell\ell$) channels due to the uncertainty on the ≤ 1 -jet and 2-jet cross-sections are estimated for the $q\bar{q} \rightarrow ZZ$ background by comparing the acceptance

upon varying the factorization and renormalization scales and changing the PDF set. For $\ell\ell\ell\ell$ this leads to uncertainties of 4%, 8%, and 3% on the ggF, VBF, and VH channels, respectively, where the uncertainty is fully anti-correlated between the ggF channel and the VBF and VH channels. For the $gg \rightarrow ZZ$ process where only LO generators are available, the VBF jets are simulated only in the parton shower, and so the acceptance uncertainty is estimated by taking the difference between the acceptances predicted by MCFM+PYTHIA8 and SHERPA, which have different parton shower simulations; this amounts to 90% for the VH channel.

10. Combination and statistical interpretation

The statistical treatment of the data is similar to that described in Refs. [98–102], and uses a simultaneous profile-likelihood-ratio fit to the data from all of the searches. The parameter of interest is the cross-section times branching ratio for heavy Higgs boson production, assumed to be correlated between all of the searches. It is assumed that an additional Higgs boson would be produced predominantly via the ggF and VBF processes but that the ratio of the two production mechanisms is unknown in the absence of a specific model. For this reason, fits for the ggF and VBF production processes are done separately, and in each case the other process is allowed to float in the fit as an additional nuisance parameter. The VH production mechanism is included in the fit for the $\ell\ell\ell\ell$ search and is assumed to scale with the VBF signal since both the VH and VBF production mechanisms depend on the coupling of the Higgs boson to vector bosons.

The simultaneous fit proceeds as follows. For each channel of each search, there is a distribution of the data with respect to some discriminating variable; these distributions are fitted to a sum of signal and backgrounds. The particular variables used are summarized in Table 3. The distributions for the $\ell\ell\ell\ell$ search are unbinned, since the resolution of $m_{\ell\ell\ell\ell}$ is very good, while other searches have binned distributions. For the VBF channels of the $\ell\ell\nu\nu$ search, only the overall event counts are used, rather than distributions, as the sample sizes are very small. The $\ell\ell qq$ and $\nu\nu qq$ searches include additional distributions in control regions in order to constrain the background, using either distributions of the mass variable or of the MV1c b -tagging category. The details of the specific variables used and the definitions of the signal and control regions are discussed in Sections 5 to 8.

As discussed in Section 9, the signal acceptance uncertainties, and many of the background theoretical and experimental uncertainties, are treated as fully correlated between the searches. A given correlated uncertainty is modelled in the fit by using a nuisance parameter common to all of the searches. The mass hypothesis for the heavy Higgs boson strongly affects which sources of systematic uncertainty have the greatest effect on the result. At lower masses, the $ZZ^{(*)}$ background theory uncertainties, the Z + jets modelling uncertainties, and the uncertainties on the jet energy scale dominate. At higher masses, uncertainties in the $\ell\ell\nu\nu$ non- ZZ background, the jet mass scale, and the Z + jets background in the merged-jet regime dominate. The contribution to the uncertainty on the best-fit signal cross-section from the dominant systematic uncertainties is shown in Table 4.

As no significant excess is observed, exclusion limits are calculated with a modified frequentist method [103], also known as CL_s , using the \tilde{q}_μ test statistic in the asymptotic approximation [104, 105]. The observed limits can be compared with expectations by generating ‘Asimov’ data sets, which are representative event samples that provide both the median expectation for an experimental result and its expected statistical variation in the asymptotic approximation, as described in Refs. [104, 105]. When producing the Asimov data set for the expected limits, the background-only hypothesis is assumed and the cross-sections for

Search	Channel	SR	Z CR	W CR	Top CR
$\ell\ell\ell\ell$	ggF	$m_{eeee}, m_{\mu\mu\mu\mu},$			
		$m_{ee\mu\mu}, m_{\mu\mu ee}$			
	VBF	$m_{\ell\ell\ell\ell}$			
	VH	$m_{\ell\ell\ell\ell}$			
$\ell\ell\nu\nu$	ggF	$m_{\text{T}}^{ee}, m_{\text{T}}^{\mu\mu}$			
	VBF	$N_{\text{evt}}^{ee}, N_{\text{evt}}^{\mu\mu}$			
$\ell\ell qq$	ggF	untagged	$m_{\ell\ell jj}$	MV1c cat.	
		tagged	$m_{\ell\ell jj}$	MV1c cat.	$m_{\ell\ell jj}$
		merged-jet	$m_{\ell\ell j}$	$m_{\ell\ell j}$	
	VBF		$m_{\ell\ell jj}$	$m_{\ell\ell jj}$	
$\nu\nu qq$	ggF	untagged	m_{T}		MV1c cat. (0 b -tags)
		tagged	m_{T}		MV1c cat. (1 b -tag)

Table 3: Summary of the distributions entering the likelihood fit for each channel of each search, both in the signal region (SR) and the various control regions (CR) used to constrain the background. Each entry represents one distribution; some channels have several distributions for different lepton flavours. MV1c cat. refers to the MV1c b -tagging event category. The distributions are unbinned for the $\ell\ell\ell\ell$ search and binned elsewhere. The VBF channels of the $\ell\ell\nu\nu$ search use only the overall event counts. See the text for the definitions of the specific variables used as well as for the definitions of the signal and control regions.

both ggF and VBF production of the heavy Higgs boson are set to zero. The remaining nuisance parameters are set to the value that maximizes the likelihood function for the observed data (profiled). When using the asymptotic procedure to calculate limits it is necessary to generate an Asimov data set both for the background-only hypothesis and for the signal hypothesis. When setting the observed limits, the cross-section for the other production mode not under consideration is profiled to data before generating the background-only Asimov data set.

11. Results

Limits on the cross-section times branching ratio from the combination of all of the searches are shown in Fig. 12. Also shown are expected limits from the $\ell\ell\ell\ell$, $\ell\ell\nu\nu$ and the combined $\ell\ell qq + \nu\nu qq$ searches (the latter two searches are only shown in combination as they share control regions). At low mass the $\ell\ell\ell\ell$ search has the best sensitivity while at high mass the sensitivity of the combined $\ell\ell qq + \nu\nu qq$ search is greatest, with the sensitivity of the $\ell\ell\nu\nu$ channel only slightly inferior. In the mass range considered for this search the 95% confidence level (CL) upper limits on the cross-section times branching ratio for heavy Higgs boson production vary between 0.53 pb at $m_H = 195$ GeV and 0.008 pb at $m_H = 950$ GeV in the ggF channel and between 0.31 pb at $m_H = 195$ GeV and 0.009 pb at $m_H = 950$ GeV in the VBF channel. The excursions into the 2σ band around the expected limit originate from local deviations in the input distributions. For example, the excess occurring around 200 GeV and the deficit occurring around 300 GeV arise from the $\ell\ell\ell\ell$ (see Fig. 1) search. Deficits at higher mass are driven by fluctuations in the

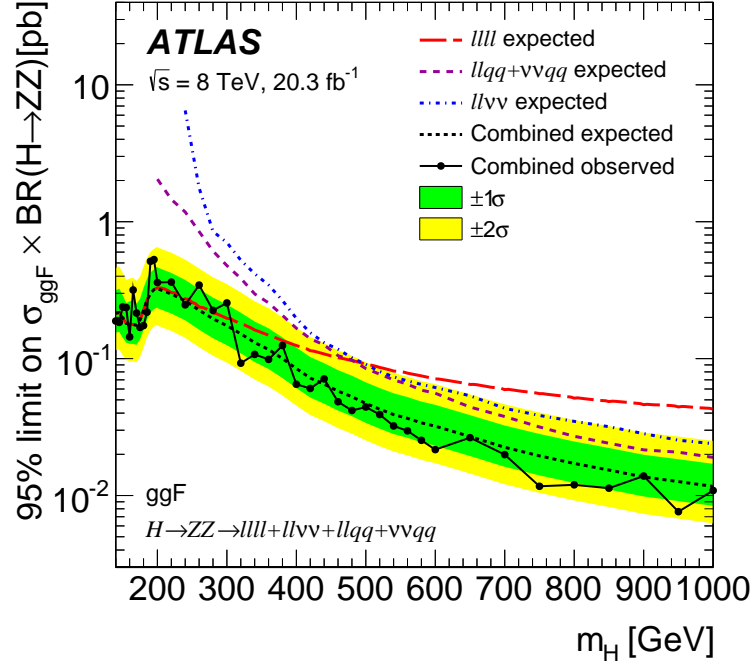
ggF mode		VBF mode	
Systematic source	Effect [%]	Systematic source	Effect [%]
$m_H = 200$ GeV			
$gg \rightarrow ZZ$ K -factor uncertainty	27	$gg \rightarrow ZZ$ acceptance	13
Z+hf $\Delta\phi$ reweighting	5.3	Jet vertex fraction ($\ell\ell qq/vvqq$)	13
Luminosity	5.2	$gg \rightarrow ZZ$ K -factor uncertainty	13
Jet energy resolution ($\ell\ell qq/vvqq$)	3.9	Z + jets $\Delta\phi$ reweighting	7.9
QCD scale $gg \rightarrow ZZ$	3.7	Jet energy scale η modelling ($\ell\ell qq/vvqq$)	5.3
$m_H = 400$ GeV			
$qq \rightarrow ZZ$ PDF	21	Z + jets estimate ($\ell\ell vv$)	34
QCD scale $qq \rightarrow ZZ$	13	Jet energy resolution ($\ell\ell\ell\ell/\ell\ell vv$)	6.5
Z + jets estimate ($\ell\ell vv$)	13	VBF Z + jets $m_{\ell\ell jj}$	5.5
Signal acceptance ISR/FSR ($\ell\ell\ell\ell/\ell\ell vv$)	7.8	Jet flavour composition ($\ell\ell\ell\ell/\ell\ell vv$)	5.3
Z + $b\bar{b}$, Z + $c\bar{c}$, $p_T^{\ell\ell}$	5.6	Jet vertex fraction ($\ell\ell qq/vvqq$)	4.8
$m_H = 900$ GeV			
Jet mass scale ($\ell\ell qq$)	7	Z + jets estimate ($\ell\ell vv$)	19
Z + jj p_T^Z shape ($vvqq$)	5.6	Jet mass scale ($\ell\ell qq$)	8.7
$qq \rightarrow ZZ$ PDF	4.3	Z + jj $p_T^{\ell\ell}$ shape	7.3
QCD scale $qq \rightarrow ZZ$	3.5	Jet energy resolution ($\ell\ell\ell\ell/\ell\ell vv$)	4.4
Luminosity	2.6	Jet flavour composition (VV/Signal)	2.6

Table 4: The effect of the leading systematic uncertainties on the best-fit signal cross-section uncertainty, expressed as a percentage of the total (systematic and statistical) uncertainty, for the ggF (left) and VBF (right) modes at $m_H = 200, 400$, and 900 GeV. The uncertainties are listed in decreasing order of their effect on the total uncertainty; additional uncertainties with smaller effects are not shown.

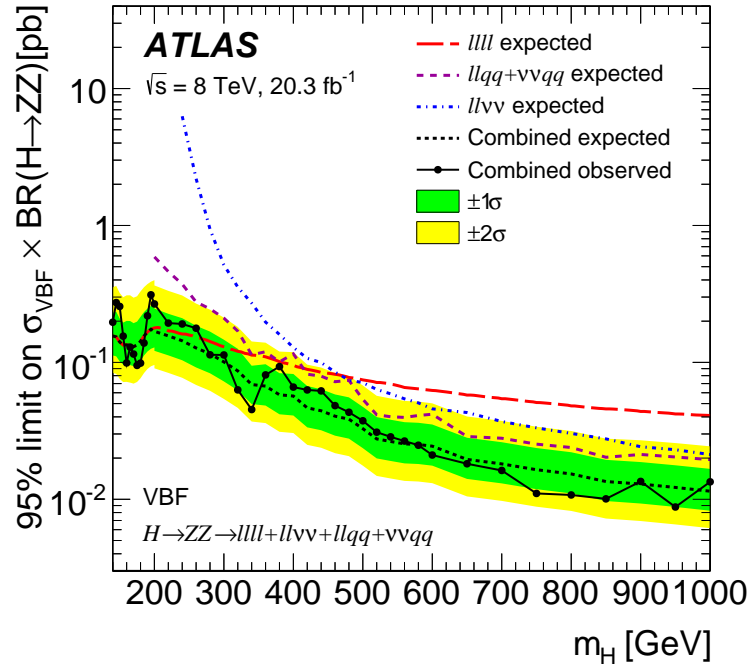
$\ell\ell qq$ search (see Figs. 3 and 6).

Figure 13 shows exclusion limits in the $\cos(\beta - \alpha)$ versus $\tan\beta$ plane for Type-I and Type-II 2HDMs, for a heavy Higgs boson with mass $m_H = 200$ GeV. This m_H value is chosen so the assumption of a narrow-width Higgs boson is valid over most of the parameter space, and the experimental sensitivity is at a maximum. As explained in Section 3.2, the range of $\cos(\beta - \alpha)$ and $\tan\beta$ explored is limited to the region where the assumption of a heavy narrow-width Higgs boson with negligible interference is valid. When calculating the limits at a given choice of $\cos(\beta - \alpha)$ and $\tan\beta$, the relative rate of ggF and VBF production in the fit is set according to the prediction of the 2HDM for that parameter choice. Figure 14 shows exclusion limits as a function of the heavy Higgs boson mass m_H and the parameter $\tan\beta$ for $\cos(\beta - \alpha) = -0.1$. The white regions in the exclusion plots indicate regions of parameter space not excluded by the present analysis; in these regions the cross-section predicted by the 2HDM is below the experimental sensitivity. Compared with recent studies of indirect limits [106], the exclusion presented here is considerably more stringent for Type-I with $\cos(\beta - \alpha) < 2$ and $0.5 < \tan\beta < 2$, and for Type-II with $0.5 < \tan\beta < 2$.

The previously published ATLAS results using data collected at $\sqrt{s} = 7$ TeV [5–7] assumed a SM Higgs boson with the relative rate of ggF and VBF production fixed to the SM prediction. Thus, they are not directly comparable with the current results, which assume that the heavy Higgs boson has a narrow width but also allow the rates of ggF and VBF production to vary independently. These results are



(a) ggF



(b) VBF

Figure 12: 95% CL upper limits on $\sigma \times \text{BR}(H \rightarrow ZZ)$ as a function of m_H , resulting from the combination of all of the searches in the (a) ggF and (b) VBF channels. The solid black line and points indicate the observed limit. The dashed black line indicates the expected limit and the bands the $1\text{-}\sigma$ and $2\text{-}\sigma$ uncertainty ranges about the expected limit. The dashed coloured lines indicate the expected limits obtained from the individual searches; for the $\ell\ell qq$ and $\nu\nu qq$ searches, only the combination of the two is shown as they share control regions.

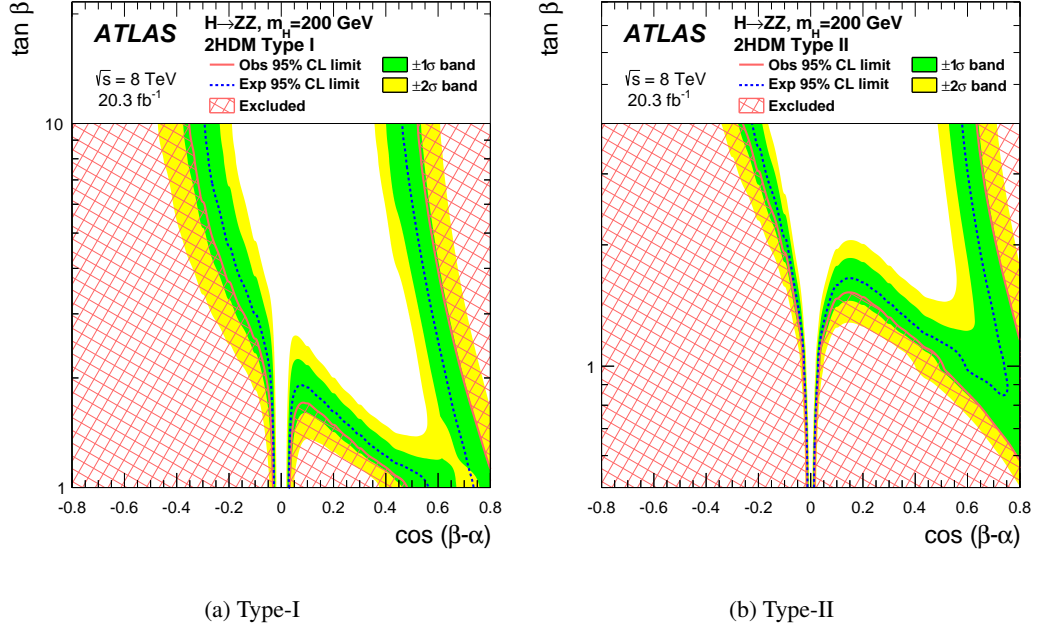


Figure 13: 95% CL exclusion contours in the 2HDM (a) Type-I and (b) Type-II models for $m_H = 200$ GeV, shown as a function of the parameters $\cos(\beta - \alpha)$ and $\tan \beta$. The red hashed area shows the observed exclusion, with the solid red line denoting the edge of the excluded region. The dashed blue line represents the expected exclusion contour and the shaded bands the $1\text{-}\sigma$ and $2\text{-}\sigma$ uncertainties on the expectation. The vertical axis range is set such that regions where the light Higgs couplings are enhanced by more than a factor of three from their SM values are avoided.

also not directly comparable with the recent results published by the CMS Collaboration [8] for similar reasons.

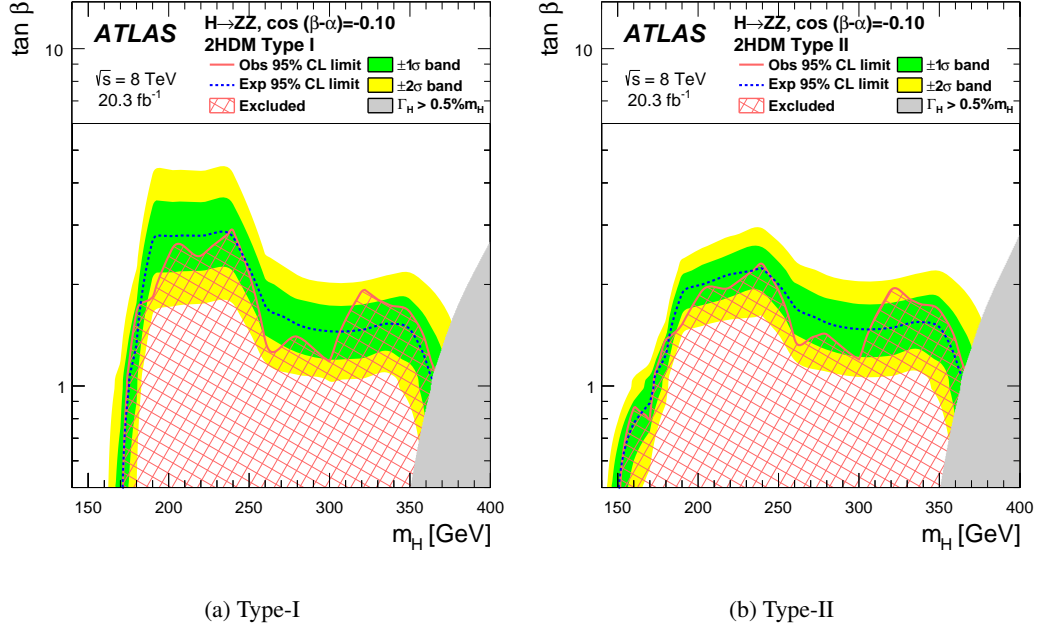


Figure 14: 95% CL exclusion contours in the 2HDM (a) Type-I and (b) Type-II models for $\cos(\beta - \alpha) = -0.1$, shown as a function of the heavy Higgs boson mass m_H and the parameter $\tan\beta$. The shaded area shows the observed exclusion, with the black line denoting the edge of the excluded region. The blue line represents the expected exclusion contour and the shaded bands the $1\text{-}\sigma$ and $2\text{-}\sigma$ uncertainties on the expectation. The grey area masks regions where the width of the boson is greater than 0.5% of m_H . For the choice of $\cos(\beta - \alpha) = -0.1$ the light Higgs couplings are not altered from their SM values by more than a factor of two.

12. Summary

A search is presented for a high-mass Higgs boson in the $H \rightarrow ZZ \rightarrow \ell^+ \ell^- \ell^+ \ell^-$, $H \rightarrow ZZ \rightarrow \ell^+ \ell^- \nu \bar{\nu}$, $H \rightarrow ZZ \rightarrow \ell^+ \ell^- q \bar{q}$, and $H \rightarrow ZZ \rightarrow \nu \bar{\nu} q \bar{q}$ decay modes using the ATLAS detector at the CERN Large Hadron Collider. The search uses proton–proton collision data at a centre-of-mass energy of 8 TeV corresponding to an integrated luminosity of 20.3 fb^{-1} . The results of the search are interpreted in the scenario of a heavy Higgs boson with a width that is small compared with the experimental mass resolution. The Higgs boson mass range considered extends up to 1 TeV for all four decay modes and down to as low as 140 GeV, depending on the decay mode. No significant excess of events over the Standard Model prediction is found. Limits on production and decay of a heavy Higgs boson to two Z bosons are set separately for gluon-fusion and vector-boson-fusion production modes. For the combination of all decay modes, 95% CL upper limits range from 0.53 pb at $m_H = 195 \text{ GeV}$ to 0.008 pb at $m_H = 950 \text{ GeV}$ for the gluon-fusion production mode and from 0.31 pb at $m_H = 195 \text{ GeV}$ to 0.009 pb at $m_H = 950 \text{ GeV}$ for the vector-boson-fusion production mode. The results are also interpreted in the context of Type-I and Type-II two-Higgs-doublet models, with exclusion contours given in the $\cos(\beta - \alpha)$ versus $\tan\beta$ and m_H versus $\tan\beta$ planes for $m_H = 200 \text{ GeV}$. This m_H value is chosen so that the assumption of a narrow-width Higgs boson is valid over most of the parameter space, and so that the experimental sensitivity is at a maximum. Compared with recent studies of indirect limits, the two-Higgs-doublet model exclusion presented here is considerably more stringent for Type-I with $\cos(\beta - \alpha) < 2$ and $0.5 < \tan\beta < 2$, and for Type-II with $0.5 < \tan\beta < 2$.

Acknowledgements

We thank CERN for the very successful operation of the LHC, as well as the support staff from our institutions without whom ATLAS could not be operated efficiently.

We acknowledge the support of ANPCyT, Argentina; YerPhI, Armenia; ARC, Australia; BMWFW and FWF, Austria; ANAS, Azerbaijan; SSTC, Belarus; CNPq and FAPESP, Brazil; NSERC, NRC and CFI, Canada; CERN; CONICYT, Chile; CAS, MOST and NSFC, China; COLCIENCIAS, Colombia; MSMT CR, MPO CR and VSC CR, Czech Republic; DNRF, DNSRC and Lundbeck Foundation, Denmark; EPLANET, ERC and NSRF, European Union; IN2P3-CNRS, CEA-DSM/IRFU, France; GNSF, Georgia; BMBF, DFG, HGF, MPG and AvH Foundation, Germany; GSRT and NSRF, Greece; RGC, Hong Kong SAR, China; ISF, MINERVA, GIF, I-CORE and Benoziyo Center, Israel; INFN, Italy; MEXT and JSPS, Japan; CNRST, Morocco; FOM and NWO, Netherlands; BRF and RCN, Norway; MNiSW and NCN, Poland; GRICES and FCT, Portugal; MNE/IFA, Romania; MES of Russia and NRC KI, Russian Federation; JINR; MSTB, Serbia; MSSR, Slovakia; ARRS and MIZŠ, Slovenia; DST/NRF, South Africa; MINECO, Spain; SRC and Wallenberg Foundation, Sweden; SER, SNSF and Cantons of Bern and Geneva, Switzerland; NSC, Taiwan; TAEK, Turkey; STFC, the Royal Society and Leverhulme Trust, United Kingdom; DOE and NSF, United States of America.

The crucial computing support from all WLCG partners is acknowledged gratefully, in particular from CERN and the ATLAS Tier-1 facilities at TRIUMF (Canada), NDGF (Denmark, Norway, Sweden), CC-IN2P3 (France), KIT/GridKA (Germany), INFN-CNAF (Italy), NL-T1 (Netherlands), PIC (Spain), ASGC (Taiwan), RAL (UK) and BNL (USA) and in the Tier-2 facilities worldwide.

A. Flavour tagging in the $\ell\ell qq$ and $\nu\nu qq$ searches

In order to constrain the normalizations of the various flavour components of the Z +jets ($Z + jj$, $Z + cj$, $Z + bj$, and $Z+hf$) and W + jets ($W + jj$ and $W + cj$) backgrounds in the $\ell\ell qq$ and $\nu\nu qq$ searches, it is necessary to distinguish the different combinations of jet flavour. This is achieved by combining the information from the MV1c b -tagging discriminant of the two signal jets in order to disentangle the different light- and heavy-flavour components.

Besides the MV1c selection criterion described in Section 4, which had an average efficiency of 70% for jets with $p_T > 20$ GeV containing b -hadrons (b -jets), additional criteria, or operating points, are defined with average efficiencies of 80%, 60%, and 50%. The efficiencies for accepting c -jets or light-quark jets for the 50% (80%) operating point are 1/29 (1/3) and 1/1400 (1/30), respectively. Based on these operating points, five bins in MV1c are defined:

Bin	b -tagging efficiency
Very loose (VL)	$> 80\%$
Loose (L)	$80 - 70\%$
Medium (M)	$70 - 60\%$
Tight (T)	$60 - 50\%$
Very tight (VT)	$< 50\%$

In this analysis, jets selected by the M, T, or VT operating points (i.e. $> 70\%$ efficiency for b -jets) are considered as b -tagged. Events are then categorized based on the combination of the binned MV1c

operating points for the two signal jets, as shown in Fig. 15, in order to obtain optimal separation of the flavour components.

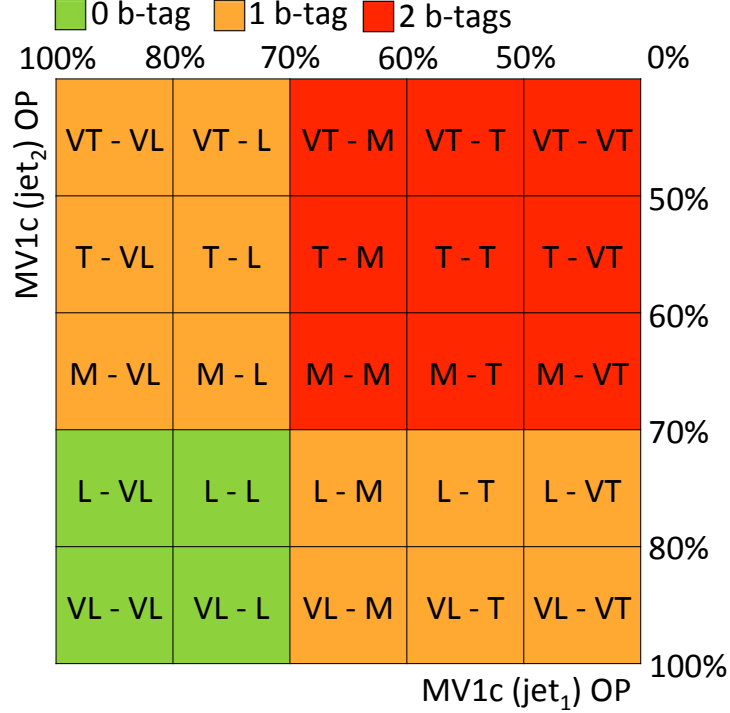


Figure 15: Event categorization as a function of the output of the MV1c b -tagging algorithm for the two signal jets. The bin boundaries correspond to the operating points (MV1c(jet) OP) giving b -tagging efficiencies of 100%, 80%, 70%, and 50%; i.e., the b -jet purity increases from left (bottom) to right (top). The event categories are labelled VL, L, M, T, and VT according to the definitions in the text, and the different colours correspond to events with 0, 1, and 2 identified b -jets.

Distributions of the resulting MV1c event categories are shown in Figs. 16 and 17 for the $\ell\ell qq$ Z + jets and $\nu\nu qq$ W + jets control regions, respectively. These distributions are provided as input to the simultaneous profile-likelihood-ratio fit described in Section 10 in order to determine the normalization of the background flavour components defined above. Following the fit, the data are well-described by the MC simulation.

B. Corrections to MC simulation for the $\ell\ell qq$ search

In order to improve the description of the data in the resolved ggF channel, corrections are applied to the SHERPA Z + jets simulation (prior to the likelihood fit) as a function of the azimuthal angle between the two signal jets, $\Delta\phi_{jj}$, and the transverse momentum of the leptonic Z boson, $p_T^{\ell\ell}$, following Ref. [30]. The simulation does not model well the observed $\Delta\phi_{jj}$ distribution in the untagged control regions for $p_T^{\ell\ell} < 120$ GeV; this is not seen at higher $p_T^{\ell\ell}$ or in the tagged control region. In order to improve the modelling, the Z + jj component of the background with $p_T^{\ell\ell} < 120$ GeV is scaled by a linear function derived from the control region with no b -tagged jets at low $p_T^{\ell\ell}$ with non- Z boson backgrounds subtracted. Half the value of the correction is taken as a systematic uncertainty where it is applied. In the Z +hf sample

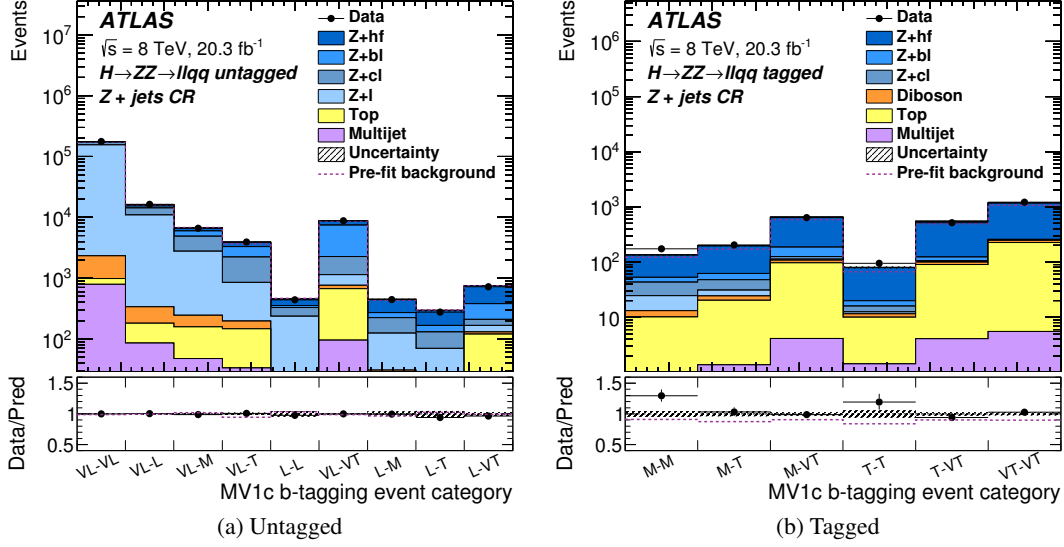


Figure 16: The distribution of the MV1c b -tagging event categories, based on the two signal jets, in the $Z + \text{jets}$ control region in the (a) untagged ggF and (b) tagged ggF channels of the $H \rightarrow ZZ \rightarrow \ell^+ \ell^- q \bar{q}$ search. The b -jet purity generally increases from left to right. The dashed line shows the total background used as input to the fit. The contribution labelled as ‘Top’ includes both the $t\bar{t}$ and single-top processes. The bottom panes show the ratio of the observed data to the predicted background.

with $p_T^{\ell\ell} < 120$ GeV, the full value of the correction is taken as an uncertainty. For $p_T^{\ell\ell} > 120$ GeV, no correction is applied for any sample. In this region, a linear fit is performed to the data/MC ratio of $\Delta\phi_{jj}$ in the untagged subchannel after subtracting the small non- Z background, and the uncertainty on the fitted slope taken as an uncertainty for all $Z + \text{jets}$ samples. Following this correction, the description of the $p_T^{\ell\ell}$ distribution in the control region with no b -tagged jets also improves, but there is still some residual discrepancy seen in the control regions that have b -tagged jets. Thus, the $Z+\text{hf}$ background component is scaled by a function logarithmic in $p_T^{\ell\ell}$, determined from the combination of the control regions with one or more b -tagged jets (after subtracting the $Z + jj$ and non- $Z + \text{jets}$ background components). An uncertainty of half this correction is applied for all $Z + \text{jets}$ channels. (All these uncertainties are taken to be uncorrelated between the $Z + \text{light-jet}$ and $Z+\text{hf}$ samples.) Following these corrections, the simulation models both the $\Delta\phi_{jj}$ and $p_T^{\ell\ell}$ distributions well in all $Z + \text{jets}$ control regions.

For the VBF channel, no significant differences are seen in the $\Delta\phi_{jj}$ and $p_T^{\ell\ell}$ distributions, but there is a small difference in the $m_{\ell\ell jj}$ distribution in the control region. The simulated $Z + \text{jets}$ background is corrected for this bin-by-bin and the full value of this correction is taken as an uncertainty, again uncorrelated between light- and heavy-flavour samples. No corrections are needed for the merged-jet ggF channel given the small sample size available.

It has been observed in an unfolded measurement of the p_T distribution of $t\bar{t}$ quark pairs that the simulation does not accurately describe the $p_T^{t\bar{t}}$ distribution [107]. To correct for this, $t\bar{t}$ MC events are weighed by a function of $p_T^{t\bar{t}}$ taken from 7 TeV data from Ref. [107] in order to make the simulation match the data. The correction is validated for 8 TeV data using the $e\mu$ top-quark control region, and the uncertainty in this correction is estimated by varying it from 50% to 150% of its nominal value.

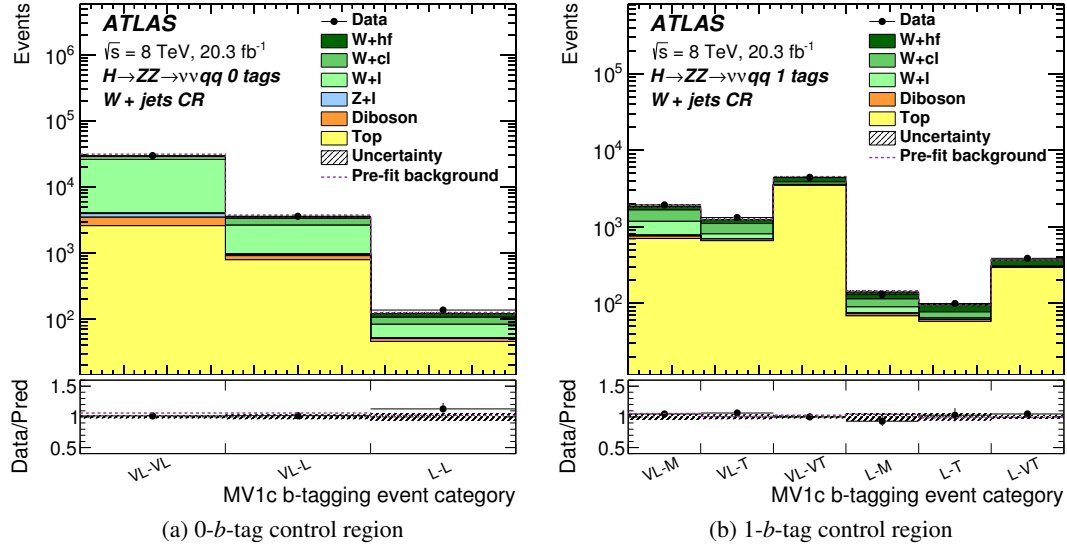


Figure 17: The distribution of the MV1c b -tagging event categories, based on the two signal jets, in the $W + \text{jets}$ (a) 0- b -tag and (b) 1- b -tag control regions of the $H \rightarrow ZZ \rightarrow \nu\bar{\nu}q\bar{q}$ search. The b -jet purity generally increases from left to right. The dashed line shows the total background used as input to the fit. The contribution labelled as ‘Top’ includes both the $t\bar{t}$ and single-top processes. The bottom panes show the ratio of the observed data to the predicted background.

References

- [1] ATLAS Collaboration, *Observation of a new particle in the search for the Standard Model Higgs boson with the ATLAS detector at the LHC*, *Phys. Lett. B* **716** (2012) 1, arXiv:1207.7214 [hep-ex].
- [2] CMS Collaboration, *Observation of a new boson at a mass of 125 GeV with the CMS experiment at the LHC*, *Phys. Lett. B* **716** (2012) 30, arXiv:1207.7235 [hep-ex].
- [3] G. Branco et al., *Theory and phenomenology of two-Higgs-doublet models*, *Phys. Rep.* **516** (2012) 1–102, arXiv:1106.0034 [hep-ph].
- [4] A. Hill and J. van der Bij, *Strongly interacting singlet-doublet Higgs model*, *Phys. Rev. D* **36** (1987) 3463–3473.
- [5] ATLAS Collaboration, *Search for the Standard Model Higgs boson in the decay channel $H \rightarrow ZZ^{(*)} \rightarrow 4\ell$ with 4.8 fb⁻¹ of pp collision data at $\sqrt{s} = 7$ TeV with ATLAS*, *Phys. Lett. B* **710** (2012) 383, arXiv:1202.1415 [hep-ex].
- [6] ATLAS Collaboration, *Search for a standard model Higgs boson in the mass range 200–600 GeV in the $H \rightarrow ZZ \rightarrow \ell^+\ell^-q\bar{q}$ decay channel with the ATLAS detector*, *Phys. Lett. B* **717** (2012) 70, arXiv:1206.2443 [hep-ex].

- [7] ATLAS Collaboration, *Search for a standard model Higgs boson in the $H \rightarrow ZZ \rightarrow \ell^+ \ell^- \nu \bar{\nu}$ decay channel using 4.7 fb^{-1} of $\sqrt{s} = 7 \text{ TeV}$ data with the ATLAS detector*, *Phys. Lett. B* **717** (2012) 29, arXiv:[1205.6744 \[hep-ex\]](#).
- [8] CMS Collaboration, *Search for a Higgs boson in the mass range from 145 to 1000 GeV decaying to a pair of W or Z bosons* (2015), submitted to JHEP, arXiv:[1504.00936 \[hep-ex\]](#).
- [9] ATLAS Collaboration, *The ATLAS Experiment at the CERN Large Hadron Collider*, *JINST* **3** (2008) S08003.
- [10] ATLAS Collaboration, *Performance of the ATLAS Trigger System in 2010*, *Eur. Phys. J. C* **72** (2012) 1849, arXiv:[1110.1530 \[hep-ex\]](#).
- [11] S. Alioli et al., *NLO Higgs boson production via gluon fusion matched with shower in POWHEG*, *JHEP* **0904** (2009) 002, arXiv:[0812.0578 \[hep-ph\]](#).
- [12] P. Nason and C. Oleari, *NLO Higgs boson production via vector-boson fusion matched with shower in POWHEG*, *JHEP* **1002** (2010) 037, arXiv:[0911.5299 \[hep-ph\]](#).
- [13] ATLAS Collaboration, *ATLAS tunes of PYTHIA 6 and Pythia 8 for MC11*, ATL-PHYS-PUB-2011-009, 2011, URL: <http://cds.cern.ch/record/1363300>.
- [14] ATLAS Collaboration, *New ATLAS event generator tunes to 2010 data*, ATL-PHYS-PUB-2011-008, 2011, URL: <http://cds.cern.ch/record/1345343>.
- [15] H.-L. Lai et al., *New parton distributions for collider physics*, *Phys. Rev. D* **82** (2010) 074024, arXiv:[1007.2241 \[hep-ph\]](#).
- [16] J. Pumplin et al., *New generation of parton distributions with uncertainties from global QCD analysis*, *JHEP* **0207** (2002) 012, arXiv:[hep-ph/0201195 \[hep-ph\]](#).
- [17] R. V. Harlander, S. Liebler and H. Mantler, *SusHi: A program for the calculation of Higgs production in gluon fusion and bottom-quark annihilation in the Standard Model and the MSSM*, *Comp. Phys. Comm.* **184** (2013) 1605–1617, arXiv:[1212.3249 \[hep-ph\]](#).
- [18] R. V. Harlander and W. B. Kilgore, *Next-to-next-to-leading order Higgs production at hadron colliders*, *Phys. Rev. Lett.* **88** (2002) 201801, arXiv:[hep-ph/0201206 \[hep-ph\]](#).
- [19] R. V. Harlander and W. B. Kilgore, *Higgs boson production in bottom quark fusion at next-to-next-to leading order*, *Phys. Rev. D* **68** (2003) 013001, arXiv:[hep-ph/0304035 \[hep-ph\]](#).
- [20] U. Aglietti et al., *Two-loop light fermion contribution to Higgs production and decays*, *Phys. Lett. B* **595** (2004) 432–441, arXiv:[hep-ph/0404071](#).
- [21] R. Bonciani, G. Degrossi and A. Vicini, *On the Generalized Harmonic Polylogarithms of One Complex Variable*, *Comp. Phys. Comm.* **182** (2011) 1253–1264, arXiv:[1007.1891 \[hep-ph\]](#).
- [22] R. Harlander and P. Kant, *Higgs production and decay: Analytic results at next-to-leading order QCD*, *JHEP* **0512** (2005) 015, arXiv:[hep-ph/0509189 \[hep-ph\]](#).

- [23] D. Eriksson, J. Rathsmann and O. Stal,
2HDMC: Two-Higgs-Doublet Model Calculator Physics and Manual,
Comp. Phys. Comm. **181** (2010) 189–205, arXiv:[0902.0851 \[hep-ph\]](#).
- [24] T. Gleisberg et al., *Event generation with SHERPA 1.1*, *JHEP* **0902** (2009) 007,
arXiv:[0811.4622 \[hep-ph\]](#).
- [25] M. L. Mangano et al.,
ALPGEN, a generator for hard multiparton processes in hadronic collisions,
JHEP **0307** (2003) 001, arXiv:[hep-ph/0206293](#).
- [26] M. L. Mangano et al.,
Matching matrix elements and shower evolution for top-quark production in hadronic collisions,
JHEP **0701** (2007) 013, arXiv:[hep-ph/0611129 \[hep-ph\]](#).
- [27] M. L. Ciccolini, S. Dittmaier and M. Kramer,
Electroweak radiative corrections to associated WH and ZH production at hadron colliders,
Phys. Rev. D **68** (2003) 073003, arXiv:[hep-ph/0306234](#).
- [28] A. Denner et al., *EW corrections to Higgs strahlung at the Tevatron and the LHC with HAWK*,
PoS **EPS-HEP2011** (2011) 235, arXiv:[1112.5258 \[hep-ph\]](#).
- [29] A. Djouadi, J. Kalinowski and M. Spira, *HDECAY: A program for Higgs boson decays in the
standard model and its supersymmetric extension*, *Comp. Phys. Comm.* **108** (1998) 56–74,
arXiv:[hep-ph/9704448](#).
- [30] ATLAS Collaboration, *Search for the $b\bar{b}$ decay of the Standard Model Higgs boson in associated
(W/Z)H production with the ATLAS detector*, *JHEP* **1501** (2015) 069,
arXiv:[1409.6212 \[hep-ex\]](#).
- [31] F. Cascioli et al., *ZZ production at hadron colliders in NNLO QCD*, *Phys. Lett. B* **735**
(2014) 311, extended by the authors to provide NNLO/NLO k -factors as a function of m_{ZZ} ,
arXiv:[1405.2219 \[hep-ph\]](#).
- [32] A. Bierweiler, T. Kasprzik and J. H. Kühn,
Vector-boson pair production at the LHC to $O(\alpha^3)$ accuracy, *JHEP* **1312** (2013) 071,
arXiv:[1305.5402 \[hep-ph\]](#).
- [33] J. Baglio, L. D. Ninh and M. M. Weber,
Massive gauge boson pair production at the LHC: a next-to-leading order story,
Phys. Rev. D **88** (2013) 113005, arXiv:[1307.4331](#).
- [34] S. Gieseke, T. Kasprzik and J. H. Kühn,
Vector-boson pair production and electroweak corrections in HERWIG++,
Eur. Phys. J. C **74** (2014) 2988.
- [35] J. M. Campbell, R. K. Ellis and C. Williams, *Vector boson pair production at the LHC*,
JHEP **1107** (2011) 018, arXiv:[1105.0020 \[hep-ph\]](#).
- [36] N. Kauer and G. Passarino,
Inadequacy of zero-width approximation for a light Higgs boson signal, *JHEP* **1208** (2012) 116,
arXiv:[1206.4803 \[hep-ph\]](#).
- [37] N. Kauer, *Interference effects for $H \rightarrow WW/ZZ \rightarrow \ell\bar{\nu}_\ell\bar{\ell}\nu_\ell$ searches in gluon fusion at the LHC*,
JHEP **1312** (2013) 082, arXiv:[1310.7011 \[hep-ph\]](#).
- [38] G. Passarino, *Higgs CAT*, *Eur. Phys. J. C* **74** (2014) 2866, arXiv:[1312.2397 \[hep-ph\]](#).

- [39] S. Frixione, P. Nason and B. R. Webber,
Matching NLO QCD and parton showers in heavy flavour production, **JHEP** **0308** (2003) 007,
arXiv:[hep-ph/0305252](#).
- [40] G. Corcella et al., *HERWIG 6.5: an event generator for Hadron Emission Reactions With Interfering Gluons (including supersymmetric processes)*, **JHEP** **0101** (2001) 010,
arXiv:[hep-ph/0011363](#).
- [41] J. Butterworth, J. R. Forshaw and M. Seymour,
Multiparton interactions in photoproduction at HERA, **Z. Phys. C** **72** (1996) 637–646,
arXiv:[hep-ph/9601371](#) [[hep-ph](#)].
- [42] T. Sjostrand, S. Mrenna and P. Z. Skands, *PYTHIA 6.4 Physics and Manual*,
JHEP **0605** (2006) 026, arXiv:[hep-ph/0603175](#).
- [43] J. Alwall et al., *MadGraph 5 : Going Beyond*, **JHEP** **1106** (2011) 128,
arXiv:[1106.0522](#) [[hep-ph](#)].
- [44] B. P. Kersevan and E. Richter-Was, *The Monte Carlo event generator AcerMC version 2.0 with interfaces to PYTHIA 6.2 and HERWIG 6.5*, **Comp. Phys. Comm.** **184** (2004) 919–985,
arXiv:[hep-ph/0405247](#) [[hep-ph](#)].
- [45] T. Sjostrand, S. Mrenna and P. Skands, *A Brief Introduction to PYTHIA 8.1*,
Comp. Phys. Comm. **178** (2008) 852, arXiv:[0710.3820](#) [[hep-ph](#)].
- [46] J. M. Campbell, R. K. Ellis and C. Williams,
Bounding the Higgs width at the LHC using full analytic results for $gg \rightarrow e^- e^+ \mu^- \mu^+$,
JHEP **1404** (2014) 060, arXiv:[1311.3589](#) [[hep-ph](#)].
- [47] K. Melnikov and F. Petriello,
Electroweak gauge boson production at hadron colliders through $O(\alpha_s^2)$,
Phys. Rev. D **74** (2006) 114017, arXiv:[hep-ph/0609070](#).
- [48] ATLAS Collaboration, *Further ATLAS tunes of PYTHIA 6 and Pythia 8*,
ATL-PHYS-PUB-2011-014, 2011, URL: <http://cds.cern.ch/record/1400677>.
- [49] S. Catani et al.,
Vector boson production at hadron colliders: a fully exclusive QCD calculation at NNLO,
Phys. Rev. Lett. **103** (2009) 082001, arXiv:[0903.2120](#) [[hep-ph](#)].
- [50] S. Catani and M. Grazzini, *An NNLO subtraction formalism in hadron collisions and its application to Higgs boson production at the LHC*, **Phys. Rev. Lett.** **98** (2007) 222002,
arXiv:[hep-ph/0703012](#) [[hep-ph](#)].
- [51] P. Nason, *A new method for combining NLO QCD with shower Monte Carlo algorithms*,
JHEP **0411** (2004) 040, arXiv:[hep-ph/0409146](#).
- [52] S. Frixione, P. Nason and C. Oleari,
Matching NLO QCD computations with Parton Shower simulations: the POWHEG method,
JHEP **0711** (2007) 070, arXiv:[0709.2092](#) [[hep-ph](#)].
- [53] S. Alioli et al., *A general framework for implementing NLO calculations in shower Monte Carlo programs: the POWHEG BOX*, **JHEP** **1006** (2010) 043, arXiv:[1002.2581](#) [[hep-ph](#)].
- [54] B. Cooper et al.,
Importance of a consistent choice of $\alpha(s)$ in the matching of AlpGen and Pythia,
Eur. Phys. J. C **72** (2012) 2078, arXiv:[1109.5295](#) [[hep-ph](#)].

- [55] M. Czakon, P. Fiedler and A. Mitov,
Total Top-Quark Pair-Production Cross Section at Hadron Colliders Through $O(\alpha_s^4)$,
Phys. Rev. Lett. **110** (2013) 252004, arXiv:1303.6524 [hep-ph].
- [56] M. Czakon and A. Mitov,
Top++: A Program for the Calculation of the Top-Pair Cross-Section at Hadron Colliders,
Comp. Phys. Comm. **185** (2014) 2930, arXiv:1112.5675 [hep-ph].
- [57] N. Kidonakis, *NNLL resummation for s-channel single top quark production,*
Phys. Rev. D **81** (2010) 054028, arXiv:1001.5034 [hep-ph].
- [58] N. Kidonakis,
Two-loop soft anomalous dimensions for single top quark associated production with a W- or H-,
Phys. Rev. D **82** (2010) 054018, arXiv:1005.4451 [hep-ph].
- [59] N. Kidonakis, *Next-to-next-to-leading-order collinear and soft gluon corrections for t-channel single top quark production,*
Phys. Rev. D **83** (2011) 091503, arXiv:1103.2792 [hep-ph].
- [60] P. Nason and G. Zanderighi, W^+W^- , WZ and ZZ production in the POWHEG-BOX-V2,
Eur. Phys. J. C **74** (2014) 2702, arXiv:1311.1365 [hep-ph].
- [61] J. M. Campbell and R. K. Ellis, *An update on vector boson pair production at hadron colliders,*
Phys. Rev. D **60** (1999) 113006, arXiv:hep-ph/9905386 [hep-ph].
- [62] J. Ohnemus and W. J. Stirling, *Order α_s corrections to the differential cross-section for the WH intermediate mass Higgs signal,*
Phys. Rev. D **47** (1993) 2722–2729.
- [63] H. Baer, B. Bailey and J. Owens, *$O(\alpha_s)$ Monte Carlo approach to $W + \text{Higgs}$ associated production at hadron supercolliders,*
Phys. Rev. D **47** (1993) 2730–2734.
- [64] O. Brein, A. Djouadi and R. Harlander,
NNLO QCD corrections to the Higgs-strahlung processes at hadron colliders,
Phys. Lett. B **579** (2004) 149–156, arXiv:hep-ph/0307206 [hep-ph].
- [65] L. Altenkamp et al., *Gluon-induced Higgs-strahlung at next-to-leading order QCD,*
JHEP **1302** (2013) 078, arXiv:1211.5015 [hep-ph].
- [66] ATLAS Collaboration, *The ATLAS Simulation Infrastructure,* *Eur. Phys. J. C* **70** (2010) 823,
arXiv:1005.4568 [hep-ex].
- [67] S. Agostinelli et al., *GEANT4: A Simulation toolkit,*
Nucl. Instrum. Meth. A **506** (2003) 250–303.
- [68] ATLAS Collaboration, *The simulation principle and performance of the ATLAS fast calorimeter simulation FastCaloSim,* ATL-PHYS-PUB-2010-013, 2010,
URL: <http://cds.cern.ch/record/1300517>.
- [69] A. Sherstnev and R. Thorne, *Parton Distributions for LO Generators,*
Eur. Phys. J. C **55** (2008) 553–575, arXiv:0711.2473 [hep-ph].
- [70] ATLAS Collaboration, *Measurement of the muon reconstruction performance of the ATLAS detector using 2011 and 2012 LHC proton–proton collision data,*
Eur. Phys. J. C **74** (2014) 3130, arXiv:1407.3935 [hep-ex].
- [71] ATLAS Collaboration, *Electron reconstruction and identification efficiency measurements with the ATLAS detector using the 2011 LHC proton–proton collision data,*
Eur. Phys. J. C **74** (2014) 2941, arXiv:1404.2240 [hep-ex].

- [72] ATLAS Collaboration, *Electron and photon energy calibration with the ATLAS detector using LHC Run 1 data*, *Eur. Phys. J. C* **74** (2014) 3071, arXiv:1407.5063 [hep-ex].
- [73] ATLAS Collaboration, *Electron efficiency measurements with the ATLAS detector using the 2012 LHC proton–proton collision data*, ATLAS-CONF-2014-032, 2014, URL: <http://cdsweb.cern.ch/record/1706245>.
- [74] M. Cacciari, G. P. Salam and G. Soyez, *FastJet User Manual*, *Eur. Phys. J. C* **72** (2012) 1896, arXiv:1111.6097 [hep-ph].
- [75] M. Cacciari, G. P. Salam and G. Soyez, *The anti- k_t jet clustering algorithm*, *JHEP* **0804** (2008) 063, arXiv:0802.1189 [hep-ph].
- [76] ATLAS Collaboration, *Jet energy measurement and its systematic uncertainty in proton–proton collisions at $\sqrt{s} = 7$ TeV with the ATLAS detector*, *Eur. Phys. J. C* **75** (2015) 17, arXiv:1406.0076 [hep-ex].
- [77] ATLAS Collaboration, *Pile-up corrections for jets from proton–proton collisions at $\sqrt{s} = 7$ TeV in ATLAS in 2011*, ATLAS-CONF-2012-064, 2012, URL: <http://cdsweb.cern.ch/record/1459529>.
- [78] ATLAS Collaboration, *Pile-up subtraction and suppression for jets in ATLAS*, ATLAS-CONF-2013-083, 2013, URL: <http://cdsweb.cern.ch/record/1570994>.
- [79] ATLAS Collaboration, *Performance of missing transverse momentum reconstruction in proton–proton collisions at $\sqrt{s} = 7$ TeV with ATLAS*, *Eur. Phys. J. C* **72** (2012) 1844, arXiv:1108.5602 [hep-ex].
- [80] ATLAS Collaboration, *Commissioning of the ATLAS high performance b -tagging algorithms in the 7 TeV collision data*, ATLAS-CONF-2011-102, 2011, URL: <http://cdsweb.cern.ch/record/1369219>.
- [81] ATLAS Collaboration, *Measurement of the b -tag Efficiency in a Sample of Jets Containing Muons with 5 fb^{-1} of data from the ATLAS detector*, ATLAS-CONF-2012-043, 2012, URL: <http://cdsweb.cern.ch/record/1435197>.
- [82] ATLAS Collaboration, *Calibration of b -tagging using dileptonic top pair events in a combinatorial likelihood approach with the ATLAS experiment*, ATLAS-CONF-2014-004, 2014, URL: <http://cdsweb.cern.ch/record/1664335>.
- [83] ATLAS Collaboration, *Measurement of the Mistag Rate of b -tagging algorithms with 5 fb^{-1} of Data Collected by the ATLAS Detector*, ATLAS-CONF-2012-040, 2012, URL: <http://cdsweb.cern.ch/record/1435194>.
- [84] ATLAS Collaboration, *Measurements of Higgs boson production and couplings in the four-lepton channel in pp collisions at center-of-mass energies of 7 and 8 TeV with the ATLAS detector*, *Phys. Rev. D* **91** (2015) 012006, arXiv:1408.5191 [hep-ex].
- [85] ATLAS Collaboration, *Search for Invisible Decays of a Higgs Boson Produced in Association with a Z Boson in ATLAS*, *Phys. Rev. Lett.* **112** (2014) 201802, arXiv:1402.3244 [hep-ex].

- [86] I. W. Stewart and F. J. Tackmann,
Theory uncertainties for Higgs mass and other searches using jet bins,
[Phys. Rev. D **85** \(2012\) 034011](#),
URL: <http://link.aps.org/doi/10.1103/PhysRevD.85.034011>.
- [87] S. Gangal and F. J. Tackmann,
Next-to-leading-order uncertainties in Higgs + jets from gluon fusion,
[Phys. Rev. D **87** \(2013\) 093008](#),
URL: <http://link.aps.org/doi/10.1103/PhysRevD.87.093008>.
- [88] ATLAS Collaboration, *Improved luminosity determination in pp collisions at $\sqrt{s} = 7$ TeV using the ATLAS detector at the LHC*, [Eur. Phys. J. C **73** \(2013\) 2518](#), arXiv:[1302.4393 \[hep-ex\]](#).
- [89] ATLAS Collaboration,
Jet energy measurement with the ATLAS detector in proton–proton collisions at $\sqrt{s} = 7$ TeV,
[Eur. Phys. J. C **73** \(2013\) 2304](#), arXiv:[1112.6426 \[hep-ex\]](#).
- [90] ATLAS Collaboration, *Jet energy resolution in proton–proton collisions at $\sqrt{s} = 7$ TeV recorded in 2010 with the ATLAS detector*, [Eur. Phys. J. C **73** \(2013\) 2306](#), arXiv:[1210.6210 \[hep-ex\]](#).
- [91] ATLAS Collaboration, *Performance of Missing Transverse Momentum Reconstruction in ATLAS studied in Proton–Proton Collisions recorded in 2012 at $\sqrt{s} = 8$ TeV*, ATLAS-CONF-2013-082, 2013, URL: <http://cdsweb.cern.ch/record/1570993>.
- [92] ATLAS Collaboration, *Performance of jet substructure techniques for large- R jets in proton–proton collisions at $\sqrt{s} = 7$ TeV using the ATLAS detector*, [JHEP **1309** \(2013\) 076](#), arXiv:[1306.4945 \[hep-ex\]](#).
- [93] LHC Higgs Cross Section Working Group,
Handbook of LHC Higgs Cross Sections: 2. Differential distributions, 2012,
arXiv:[1201.3084 \[hep-ph\]](#).
- [94] M. Botje et al., *The PDF4LHC working group interim recommendations*, 2011,
arXiv:[1101.0538 \[hep-ph\]](#).
- [95] S. Alekhin et al., *The PDF4LHC working group interim report*, 2011,
arXiv:[1101.0536 \[hep-ph\]](#).
- [96] ATLAS Collaboration, *Determination of the off-shell Higgs boson signal strength in the high-mass ZZ and WW final states with the ATLAS detector* (2015), submitted to Eur. Phys. J. C, arXiv:[1503.01060 \[hep-ex\]](#).
- [97] M. Bonvini et al.,
Signal-background interference effects for $gg \rightarrow H \rightarrow W^+W^-$ beyond leading order,
[Phys. Rev. D **88** \(2013\) 034032](#), arXiv:[1304.3053 \[hep-ph\]](#).
- [98] ATLAS Collaboration, *Combined search for the Standard Model Higgs boson in pp collisions at $\sqrt{s} = 7$ TeV with the ATLAS detector*, [Phys. Rev. D **86** \(2012\) 032003](#), arXiv:[1207.0319 \[hep-ex\]](#).
- [99] ATLAS Collaboration,
Procedure for the LHC Higgs boson search combination in summer 2011,
ATL-PHYS-PUB-2011-011, 2011, URL: <http://cds.cern.ch/record/1375842>.
- [100] L. Moneta et al., *The RooStats Project*, PoS **ACAT2010** (2010) 057,
arXiv:[1009.1003 \[physics.data-an\]](#).

- [101] K. Cranmer et al.,
HistFactory: A tool for creating statistical models for use with RooFit and RooStats,
CERN-OPEN-2012-016 (2012), URL: <http://cdsweb.cern.ch/record/1456844>.
- [102] W. Verkerke et al., *The RooFit Toolkit for Data Modelling*,
Available from <http://roofit.sourceforge.net> or with recent versions of the ROOT framework
available at <http://root.cern.ch>.
- [103] A. L. Read, *Presentation of search results: The CL(s) technique*,
J. Phys. G **28** (2002) 2693–2704.
- [104] G. Cowan et al., *Asymptotic formulae for likelihood-based tests of new physics*,
Eur. Phys. J. C **71** (2011) 1554, arXiv:[1007.1727 \[physics.data-an\]](#).
- [105] G. Cowan et al., *Erratum to: Asymptotic formulae for likelihood-based tests of new physics*,
Eur. Phys. J. C **73** (2013) 1434.
- [106] B. Dumont et al., *Addendum to "Constraints on and future prospects for Two-Higgs-Doublet Models in light of the LHC Higgs signal"* (2014), arXiv:[1409.4088 \[hep-ph\]](#).
- [107] ATLAS Collaboration, *Measurements of normalized differential cross-sections for $t\bar{t}$ production in pp collisions at $\sqrt{s} = 7$ TeV using the ATLAS detector*, *Phys. Rev. D* **90** (2014) 072004, arXiv:[1407.0371 \[hep-ex\]](#).

The ATLAS Collaboration

G. Aad⁸⁵, B. Abbott¹¹³, J. Abdallah¹⁵¹, O. Abdinov¹¹, R. Aben¹⁰⁷, M. Abolins⁹⁰, O.S. AbouZeid¹⁵⁸, H. Abramowicz¹⁵³, H. Abreu¹⁵², R. Abreu¹¹⁶, Y. Abulaiti^{146a,146b}, B.S. Acharya^{164a,164b,a}, L. Adamczyk^{38a}, D.L. Adams²⁵, J. Adelman¹⁰⁸, S. Adomeit¹⁰⁰, T. Adye¹³¹, A.A. Affolder⁷⁴, T. Agatonovic-Jovin¹³, J. Agricola⁵⁴, J.A. Aguilar-Saavedra^{126a,126f}, S.P. Ahlen²², F. Ahmadov^{65,b}, G. Aielli^{133a,133b}, H. Akerstedt^{146a,146b}, T.P.A. Åkesson⁸¹, A.V. Akimov⁹⁶, G.L. Alberghi^{20a,20b}, J. Albert¹⁶⁹, S. Albrand⁵⁵, M.J. Alconada Verzini⁷¹, M. Aleksa³⁰, I.N. Aleksandrov⁶⁵, C. Alexa^{26a}, G. Alexander¹⁵³, T. Alexopoulos¹⁰, M. Alhroob¹¹³, G. Alimonti^{91a}, L. Alio⁸⁵, J. Alison³¹, S.P. Alkire³⁵, B.M.M. Allbrooke¹⁴⁹, P.P. Allport⁷⁴, A. Aloisio^{104a,104b}, A. Alonso³⁶, F. Alonso⁷¹, C. Alpigiani⁷⁶, A. Altheimer³⁵, B. Alvarez Gonzalez³⁰, D. Álvarez Piqueras¹⁶⁷, M.G. Alviggi^{104a,104b}, B.T. Amadio¹⁵, K. Amako⁶⁶, Y. Amaral Coutinho^{24a}, C. Amelung²³, D. Amidei⁸⁹, S.P. Amor Dos Santos^{126a,126c}, A. Amorim^{126a,126b}, S. Amoroso⁴⁸, N. Amram¹⁵³, G. Amundsen²³, C. Anastopoulos¹³⁹, L.S. Ancu⁴⁹, N. Andari¹⁰⁸, T. Andeen³⁵, C.F. Anders^{58b}, G. Anders³⁰, J.K. Anders⁷⁴, K.J. Anderson³¹, A. Andreazza^{91a,91b}, V. Andrei^{58a}, S. Angelidakis⁹, I. Angelozzi¹⁰⁷, P. Anger⁴⁴, A. Angerami³⁵, F. Anghinolfi³⁰, A.V. Anisenkov^{109,c}, N. Anjos¹², A. Annovi^{124a,124b}, M. Antonelli⁴⁷, A. Antonov⁹⁸, J. Antos^{144b}, F. Anulli^{132a}, M. Aoki⁶⁶, L. Aperio Bella¹⁸, G. Arabidze⁹⁰, Y. Arai⁶⁶, J.P. Araque^{126a}, A.T.H. Arce⁴⁵, F.A. Arduh⁷¹, J-F. Arguin⁹⁵, S. Argyropoulos⁴², M. Arik^{19a}, A.J. Armbruster³⁰, O. Arnaez³⁰, V. Arnal⁸², H. Arnold⁴⁸, M. Arratia²⁸, O. Arslan²¹, A. Artamonov⁹⁷, G. Artoni²³, S. Asai¹⁵⁵, N. Asbah⁴², A. Ashkenazi¹⁵³, B. Åsman^{146a,146b}, L. Asquith¹⁴⁹, K. Assamagan²⁵, R. Astalos^{144a}, M. Atkinson¹⁶⁵, N.B. Atlay¹⁴¹, K. Augsten¹²⁸, M. Aurousseau^{145b}, G. Avolio³⁰, B. Axen¹⁵, M.K. Ayoub¹¹⁷, G. Azuelos^{95,d}, M.A. Baak³⁰, A.E. Baas^{58a}, M.J. Baca¹⁸, C. Bacci^{134a,134b}, H. Bachacou¹³⁶, K. Bachas¹⁵⁴, M. Backes³⁰, M. Backhaus³⁰, P. Bagiacchi^{132a,132b}, P. Bagnaia^{132a,132b}, Y. Bai^{33a}, T. Bain³⁵, J.T. Baines¹³¹, O.K. Baker¹⁷⁶, E.M. Baldin^{109,c}, P. Balek¹²⁹, T. Balestri¹⁴⁸, F. Balli⁸⁴, E. Banas³⁹, Sw. Banerjee¹⁷³, A.A.E. Bannoura¹⁷⁵, H.S. Bansil¹⁸, L. Barak³⁰, E.L. Barberio⁸⁸, D. Barberis^{50a,50b}, M. Barbero⁸⁵, T. Barillari¹⁰¹, M. Barisonzi^{164a,164b}, T. Barklow¹⁴³, N. Barlow²⁸, S.L. Barnes⁸⁴, B.M. Barnett¹³¹, R.M. Barnett¹⁵, Z. Barnovska⁵, A. Baroncelli^{134a}, G. Barone²³, A.J. Barr¹²⁰, F. Barreiro⁸², J. Barreiro Guimarães da Costa⁵⁷, R. Bartoldus¹⁴³, A.E. Barton⁷², P. Bartos^{144a}, A. Basalaev¹²³, A. Bassalat¹¹⁷, A. Basye¹⁶⁵, R.L. Bates⁵³, S.J. Batista¹⁵⁸, J.R. Batley²⁸, M. Battaglia¹³⁷, M. Bause^{132a,132b}, F. Bauer¹³⁶, H.S. Bawa^{143,e}, J.B. Beacham¹¹¹, M.D. Beattie⁷², T. Beau⁸⁰, P.H. Beauchemin¹⁶¹, R. Beccherle^{124a,124b}, P. Bechtel²¹, H.P. Beck^{17,f}, K. Becker¹²⁰, M. Becker⁸³, S. Becker¹⁰⁰, M. Beckingham¹⁷⁰, C. Becot¹¹⁷, A.J. Beddall^{19b}, A. Beddall^{19b}, V.A. Bednyakov⁶⁵, C.P. Bee¹⁴⁸, L.J. Beemster¹⁰⁷, T.A. Beermann¹⁷⁵, M. Begel²⁵, J.K. Behr¹²⁰, C. Belanger-Champagne⁸⁷, W.H. Bell⁴⁹, G. Bella¹⁵³, L. Bellagamba^{20a}, A. Bellerive²⁹, M. Bellomo⁸⁶, K. Belotskiy⁹⁸, O. Beltramello³⁰, O. Benary¹⁵³, D. Benchebkroun^{135a}, M. Bender¹⁰⁰, K. Bendtz^{146a,146b}, N. Benekos¹⁰, Y. Benhammou¹⁵³, E. Benhar Noccioli⁴⁹, J.A. Benitez Garcia^{159b}, D.P. Benjamin⁴⁵, J.R. Bensinger²³, S. Bentvelsen¹⁰⁷, L. Beresford¹²⁰, M. Beretta⁴⁷, D. Berge¹⁰⁷, E. Bergeas Kuutmann¹⁶⁶, N. Berger⁵, F. Berghaus¹⁶⁹, J. Beringer¹⁵, C. Bernard²², N.R. Bernard⁸⁶, C. Bernius¹¹⁰, F.U. Bernlochner²¹, T. Berry⁷⁷, P. Berta¹²⁹, C. Bertella⁸³, G. Bertoli^{146a,146b}, F. Bertolucci^{124a,124b}, C. Bertsche¹¹³, D. Bertsche¹¹³, M.I. Besana^{91a}, G.J. Besjes³⁶, O. Bessidskaia Bylund^{146a,146b}, M. Bessner⁴², N. Besson¹³⁶, C. Betancourt⁴⁸, S. Bethke¹⁰¹, A.J. Bevan⁷⁶, W. Bhimji¹⁵, R.M. Bianchi¹²⁵, L. Bianchini²³, M. Bianco³⁰, O. Biebel¹⁰⁰, D. Biedermann¹⁶, S.P. Bieniek⁷⁸, M. Biglietti^{134a}, J. Bilbao De Mendizabal⁴⁹, H. Bilokon⁴⁷, M. Bindi⁵⁴, S. Binet¹¹⁷, A. Bingul^{19b}, C. Bini^{132a,132b}, S. Biondi^{20a,20b}, C.W. Black¹⁵⁰, J.E. Black¹⁴³, K.M. Black²², D. Blackburn¹³⁸, R.E. Blair⁶, J.-B. Blanchard¹³⁶, J.E. Blanco⁷⁷, T. Blazek^{144a}, I. Bloch⁴², C. Blocker²³, W. Blum^{83,*}, U. Blumenschein⁵⁴, G.J. Bobbink¹⁰⁷, V.S. Bobrovnikov^{109,c}, S.S. Bocchetta⁸¹, A. Bocci⁴⁵,

C. Bock¹⁰⁰, M. Boehler⁴⁸, J.A. Bogaerts³⁰, D. Bogavac¹³, A.G. Bogdanchikov¹⁰⁹, C. Bohm^{146a}, V. Boisvert⁷⁷, T. Bold^{38a}, V. Boldea^{26a}, A.S. Boldyrev⁹⁹, M. Bomben⁸⁰, M. Bona⁷⁶, M. Boonekamp¹³⁶, A. Borisov¹³⁰, G. Borissov⁷², S. Borroni⁴², J. Bortfeldt¹⁰⁰, V. Bortolotto^{60a,60b,60c}, K. Bos¹⁰⁷, D. Boscherini^{20a}, M. Bosman¹², J. Boudreau¹²⁵, J. Bouffard², E.V. Bouhova-Thacker⁷², D. Boumediene³⁴, C. Bourdarios¹¹⁷, N. Bousson¹¹⁴, A. Boveia³⁰, J. Boyd³⁰, I.R. Boyko⁶⁵, I. Bozic¹³, J. Bracinik¹⁸, A. Brandt⁸, G. Brandt⁵⁴, O. Brandt^{58a}, U. Bratzler¹⁵⁶, B. Brau⁸⁶, J.E. Brau¹¹⁶, H.M. Braun^{175,*}, S.F. Brazzale^{164a,164c}, W.D. Breaden Madden⁵³, K. Brendlinger¹²², A.J. Brennan⁸⁸, L. Brenner¹⁰⁷, R. Brenner¹⁶⁶, S. Bressler¹⁷², K. Bristow^{145c}, T.M. Bristow⁴⁶, D. Britton⁵³, D. Britzger⁴², F.M. Brochu²⁸, I. Brock²¹, R. Brock⁹⁰, J. Bronner¹⁰¹, G. Brooijmans³⁵, T. Brooks⁷⁷, W.K. Brooks^{32b}, J. Brosamer¹⁵, E. Brost¹¹⁶, J. Brown⁵⁵, P.A. Bruckman de Renstrom³⁹, D. Bruncko^{144b}, R. Bruneliere⁴⁸, A. Bruni^{20a}, G. Bruni^{20a}, M. Bruschi^{20a}, N. Bruscino²¹, L. Bryngemark⁸¹, T. Buanes¹⁴, Q. Buat¹⁴², P. Buchholz¹⁴¹, A.G. Buckley⁵³, S.I. Buda^{26a}, I.A. Budagov⁶⁵, F. Buehrer⁴⁸, L. Bugge¹¹⁹, M.K. Bugge¹¹⁹, O. Bulekov⁹⁸, D. Bullock⁸, H. Burckhart³⁰, S. Burdin⁷⁴, C.D. Burgard⁴⁸, B. Burghgrave¹⁰⁸, S. Burke¹³¹, I. Burmeister⁴³, E. Busato³⁴, D. Büscher⁴⁸, V. Büscher⁸³, P. Bussey⁵³, J.M. Butler²², A.I. Butt³, C.M. Buttar⁵³, J.M. Butterworth⁷⁸, P. Butti¹⁰⁷, W. Buttinger²⁵, A. Buzatu⁵³, A.R. Buzykaev^{109,c}, S. Cabrera Urbán¹⁶⁷, D. Caforio¹²⁸, V.M. Cairo^{37a,37b}, O. Cakir^{4a}, N. Calace⁴⁹, P. Calafiura¹⁵, A. Calandri¹³⁶, G. Calderini⁸⁰, P. Calfayan¹⁰⁰, L.P. Caloba^{24a}, D. Calvet³⁴, S. Calvet³⁴, R. Camacho Toro³¹, S. Camarda⁴², P. Camarri^{133a,133b}, D. Cameron¹¹⁹, R. Caminal Armadans¹⁶⁵, S. Campana³⁰, M. Campanelli⁷⁸, A. Campoverde¹⁴⁸, V. Canale^{104a,104b}, A. Canepa^{159a}, M. Cano Bret^{33e}, J. Cantero⁸², R. Cantrill^{126a}, T. Cao⁴⁰, M.D.M. Capeans Garrido³⁰, I. Caprini^{26a}, M. Caprini^{26a}, M. Capua^{37a,37b}, R. Caputo⁸³, R. Cardarelli^{133a}, F. Cardillo⁴⁸, T. Carli³⁰, G. Carlino^{104a}, L. Carminati^{91a,91b}, S. Caron¹⁰⁶, E. Carquin^{32a}, G.D. Carrillo-Montoya³⁰, J.R. Carter²⁸, J. Carvalho^{126a,126c}, D. Casadei⁷⁸, M.P. Casado¹², M. Casolino¹², E. Castaneda-Miranda^{145b}, A. Castelli¹⁰⁷, V. Castillo Gimenez¹⁶⁷, N.F. Castro^{126a,g}, P. Catastini⁵⁷, A. Catinaccio³⁰, J.R. Catmore¹¹⁹, A. Cattai³⁰, J. Caudron⁸³, V. Cavaliere¹⁶⁵, D. Cavalli^{91a}, M. Cavalli-Sforza¹², V. Cavasinni^{124a,124b}, F. Ceradini^{134a,134b}, B.C. Cerio⁴⁵, K. Cerny¹²⁹, A.S. Cerqueira^{24b}, A. Cerri¹⁴⁹, L. Cerrito⁷⁶, F. Cerutti¹⁵, M. Cerv³⁰, A. Cervelli¹⁷, S.A. Cetin^{19c}, A. Chafaq^{135a}, D. Chakraborty¹⁰⁸, I. Chalupkova¹²⁹, P. Chang¹⁶⁵, J.D. Chapman²⁸, D.G. Charlton¹⁸, C.C. Chau¹⁵⁸, C.A. Chavez Barajas¹⁴⁹, S. Cheatham¹⁵², A. Chegwidan⁹⁰, S. Chekanov⁶, S.V. Chekulaev^{159a}, G.A. Chelkov^{65,h}, M.A. Chelstowska⁸⁹, C. Chen⁶⁴, H. Chen²⁵, K. Chen¹⁴⁸, L. Chen^{33d,i}, S. Chen^{33c}, X. Chen^{33f}, Y. Chen⁶⁷, H.C. Cheng⁸⁹, Y. Cheng³¹, A. Cheplakov⁶⁵, E. Cheremushkina¹³⁰, R. Cherkaoui El Moursli^{135e}, V. Chernyatin^{25,*}, E. Cheu⁷, L. Chevalier¹³⁶, V. Chiarella⁴⁷, G. Chiarelli^{124a,124b}, G. Chiodini^{73a}, A.S. Chisholm¹⁸, R.T. Chislett⁷⁸, A. Chitan^{26a}, M.V. Chizhov⁶⁵, K. Choi⁶¹, S. Chouridou⁹, B.K.B. Chow¹⁰⁰, V. Christodoulou⁷⁸, D. Chromek-Burckhart³⁰, J. Chudoba¹²⁷, A.J. Chuinard⁸⁷, J.J. Chwastowski³⁹, L. Chytka¹¹⁵, G. Ciapetti^{132a,132b}, A.K. Ciftci^{4a}, D. Cinca⁵³, V. Cindro⁷⁵, I.A. Cioara²¹, A. Ciocio¹⁵, F. Ciotto^{104a,104b}, Z.H. Citron¹⁷², M. Ciubancan^{26a}, A. Clark⁴⁹, B.L. Clark⁵⁷, P.J. Clark⁴⁶, R.N. Clarke¹⁵, W. Cleland¹²⁵, C. Clement^{146a,146b}, Y. Coadou⁸⁵, M. Cobal^{164a,164c}, A. Coccaro¹³⁸, J. Cochran⁶⁴, L. Coffey²³, J.G. Cogan¹⁴³, L. Colasurdo¹⁰⁶, B. Cole³⁵, S. Cole¹⁰⁸, A.P. Colijn¹⁰⁷, J. Collot⁵⁵, T. Colombo^{58c}, G. Compostella¹⁰¹, P. Conde Muino^{126a,126b}, E. Coniavitis⁴⁸, S.H. Connell^{145b}, I.A. Connelly⁷⁷, V. Consorti⁴⁸, S. Constantinescu^{26a}, C. Conta^{121a,121b}, G. Conti³⁰, F. Conventi^{104a,j}, M. Cooke¹⁵, B.D. Cooper⁷⁸, A.M. Cooper-Sarkar¹²⁰, T. Cornelissen¹⁷⁵, M. Corradi^{20a}, F. Corriveau^{87,k}, A. Corso-Radu¹⁶³, A. Cortes-Gonzalez¹², G. Cortiana¹⁰¹, G. Costa^{91a}, M.J. Costa¹⁶⁷, D. Costanzo¹³⁹, D. Côte⁸, G. Cottin²⁸, G. Cowan⁷⁷, B.E. Cox⁸⁴, K. Cranmer¹¹⁰, G. Cree²⁹, S. Crépe-Renaudin⁵⁵, F. Crescioli⁸⁰, W.A. Cribbs^{146a,146b}, M. Crispin Ortuzar¹²⁰, M. Cristinziani²¹, V. Croft¹⁰⁶, G. Crosetti^{37a,37b}, T. Cuhadar Donszelmann¹³⁹, J. Cummings¹⁷⁶, M. Curatolo⁴⁷, C. Cuthbert¹⁵⁰, H. Cziri¹⁴¹, P. Czodrowski³, S. D'Auria⁵³, M. D'Onofrio⁷⁴, M.J. Da Cunha Sargedas De Sousa^{126a,126b}, C. Da Via⁸⁴, W. Dabrowski^{38a}, A. Dafinca¹²⁰, T. Dai⁸⁹,

O. Dale¹⁴, F. Dallaire⁹⁵, C. Dallapiccola⁸⁶, M. Dam³⁶, J.R. Dandoy³¹, N.P. Dang⁴⁸, A.C. Daniells¹⁸, M. Danninger¹⁶⁸, M. Dano Hoffmann¹³⁶, V. Dao⁴⁸, G. Darbo^{50a}, S. Darmora⁸, J. Dassoulas³, A. Dattagupta⁶¹, W. Davey²¹, C. David¹⁶⁹, T. Davidek¹²⁹, E. Davies^{120,l}, M. Davies¹⁵³, P. Davison⁷⁸, Y. Davygora^{58a}, E. Dawe⁸⁸, I. Dawson¹³⁹, R.K. Daya-Ishmukhametova⁸⁶, K. De⁸, R. de Asmundis^{104a}, A. De Benedetti¹¹³, S. De Castro^{20a,20b}, S. De Cecco⁸⁰, N. De Groot¹⁰⁶, P. de Jong¹⁰⁷, H. De la Torre⁸², F. De Lorenzi⁶⁴, D. De Pedis^{132a}, A. De Salvo^{132a}, U. De Sanctis¹⁴⁹, A. De Santo¹⁴⁹, J.B. De Vivie De Regie¹¹⁷, W.J. Dearnaley⁷², R. Debbe²⁵, C. Debenedetti¹³⁷, D.V. Dedovich⁶⁵, I. Deigaard¹⁰⁷, J. Del Peso⁸², T. Del Prete^{124a,124b}, D. Delgove¹¹⁷, F. Deliot¹³⁶, C.M. Delitzsch⁴⁹, M. Deliyergiyev⁷⁵, A. Dell'Acqua³⁰, L. Dell'Asta²², M. Dell'Orso^{124a,124b}, M. Della Pietra^{104a,j}, D. della Volpe⁴⁹, M. Delmastro⁵, P.A. Delsart⁵⁵, C. Deluca¹⁰⁷, D.A. DeMarco¹⁵⁸, S. Demers¹⁷⁶, M. Demichev⁶⁵, A. Demilly⁸⁰, S.P. Denisov¹³⁰, D. Derendarz³⁹, J.E. Derkaoui^{135d}, F. Derue⁸⁰, P. Dervan⁷⁴, K. Desch²¹, C. Deterre⁴², P.O. Deviveiros³⁰, A. Dewhurst¹³¹, S. Dhaliwal²³, A. Di Ciaccio^{133a,133b}, L. Di Ciaccio⁵, A. Di Domenico^{132a,132b}, C. Di Donato^{104a,104b}, A. Di Girolamo³⁰, B. Di Girolamo³⁰, A. Di Mattia¹⁵², B. Di Micco^{134a,134b}, R. Di Nardo⁴⁷, A. Di Simone⁴⁸, R. Di Sipio¹⁵⁸, D. Di Valentino²⁹, C. Diaconu⁸⁵, M. Diamond¹⁵⁸, F.A. Dias⁴⁶, M.A. Diaz^{32a}, E.B. Diehl⁸⁹, J. Dietrich¹⁶, S. Diglio⁸⁵, A. Dimitrievska¹³, J. Dingfelder²¹, P. Dita^{26a}, S. Dita^{26a}, F. Dittus³⁰, F. Djama⁸⁵, T. Djobava^{51b}, J.I. Djuvsland^{58a}, M.A.B. do Vale^{24c}, D. Dobos³⁰, M. Dobre^{26a}, C. Doglioni⁸¹, T. Dohmae¹⁵⁵, J. Dolejsi¹²⁹, Z. Dolezal¹²⁹, B.A. Dolgoshein^{98,*}, M. Donadelli^{24d}, S. Donati^{124a,124b}, P. Dondero^{121a,121b}, J. Donini³⁴, J. Dopke¹³¹, A. Doria^{104a}, M.T. Dova⁷¹, A.T. Doyle⁵³, E. Drechsler⁵⁴, M. Dris¹⁰, E. Dubreuil³⁴, E. Duchovni¹⁷², G. Duckeck¹⁰⁰, O.A. Ducu^{26a,85}, D. Duda¹⁰⁷, A. Dudarev³⁰, L. Dufлот¹¹⁷, L. Duguid⁷⁷, M. Dührssen³⁰, M. Dunford^{58a}, H. Duran Yildiz^{4a}, M. Düren⁵², A. Durglishvili^{51b}, D. Duschinger⁴⁴, M. Dyndal^{38a}, C. Eckardt⁴², K.M. Ecker¹⁰¹, R.C. Edgar⁸⁹, W. Edson², N.C. Edwards⁴⁶, W. Ehrenfeld²¹, T. Eifert³⁰, G. Eigen¹⁴, K. Einsweiler¹⁵, T. Ekelof¹⁶⁶, M. El Kacimi^{135c}, M. Ellert¹⁶⁶, S. Elles⁵, F. Ellinghaus¹⁷⁵, A.A. Elliot¹⁶⁹, N. Ellis³⁰, J. Elmsheuser¹⁰⁰, M. Elsing³⁰, D. Emelianov¹³¹, Y. Enari¹⁵⁵, O.C. Endner⁸³, M. Endo¹¹⁸, J. Erdmann⁴³, A. Ereditato¹⁷, G. Ernis¹⁷⁵, J. Ernst², M. Ernst²⁵, S. Errede¹⁶⁵, E. Ertel⁸³, M. Escalier¹¹⁷, H. Esch⁴³, C. Escobar¹²⁵, B. Esposito⁴⁷, A.I. Etienvre¹³⁶, E. Etzion¹⁵³, H. Evans⁶¹, A. Ezhilov¹²³, L. Fabbri^{20a,20b}, G. Facini³¹, R.M. Fakhruddinov¹³⁰, S. Falciano^{132a}, R.J. Falla⁷⁸, J. Faltova¹²⁹, Y. Fang^{33a}, M. Fanti^{91a,91b}, A. Farbin⁸, A. Farilla^{134a}, T. Farooque¹², S. Farrell¹⁵, S.M. Farrington¹⁷⁰, P. Farthouat³⁰, F. Fassi^{135e}, P. Fassnacht³⁰, D. Fassouliotis⁹, M. Fauci Giannelli⁷⁷, A. Favareto^{50a,50b}, L. Fayard¹¹⁷, P. Federic^{144a}, O.L. Fedin^{123,m}, W. Fedorko¹⁶⁸, S. Feigl³⁰, L. Feligioni⁸⁵, C. Feng^{33d}, E.J. Feng⁶, H. Feng⁸⁹, A.B. Fenyuk¹³⁰, L. Feremenga⁸, P. Fernandez Martinez¹⁶⁷, S. Fernandez Perez³⁰, J. Ferrando⁵³, A. Ferrari¹⁶⁶, P. Ferrari¹⁰⁷, R. Ferrari^{121a}, D.E. Ferreira de Lima⁵³, A. Ferrer¹⁶⁷, D. Ferrere⁴⁹, C. Ferretti⁸⁹, A. Ferretto Parodi^{50a,50b}, M. Fiascaris³¹, F. Fiedler⁸³, A. Filipčič⁷⁵, M. Filipuzzi⁴², F. Filthaut¹⁰⁶, M. Fincke-Keeler¹⁶⁹, K.D. Finelli¹⁵⁰, M.C.N. Fiolhais^{126a,126c}, L. Fiorini¹⁶⁷, A. Firan⁴⁰, A. Fischer², C. Fischer¹², J. Fischer¹⁷⁵, W.C. Fisher⁹⁰, E.A. Fitzgerald²³, N. Flaschel⁴², I. Fleck¹⁴¹, P. Fleischmann⁸⁹, S. Fleischmann¹⁷⁵, G.T. Fletcher¹³⁹, G. Fletcher⁷⁶, R.R.M. Fletcher¹²², T. Flick¹⁷⁵, A. Floderus⁸¹, L.R. Flores Castillo^{60a}, M.J. Flowerdew¹⁰¹, A. Formica¹³⁶, A. Forti⁸⁴, D. Fournier¹¹⁷, H. Fox⁷², S. Fracchia¹², P. Francavilla⁸⁰, M. Franchini^{20a,20b}, D. Francis³⁰, L. Franconi¹¹⁹, M. Franklin⁵⁷, M. Frate¹⁶³, M. Fraternali^{121a,121b}, D. Freeborn⁷⁸, S.T. French²⁸, F. Friedrich⁴⁴, D. Froidevaux³⁰, J.A. Frost¹²⁰, C. Fukunaga¹⁵⁶, E. Fullana Torregrosa⁸³, B.G. Fulsom¹⁴³, T. Fusayasu¹⁰², J. Fuster¹⁶⁷, C. Gabaldon⁵⁵, O. Gabizon¹⁷⁵, A. Gabrielli^{20a,20b}, A. Gabrielli^{132a,132b}, G.P. Gach^{38a}, S. Gadatsch³⁰, S. Gadomski⁴⁹, G. Gagliardi^{50a,50b}, P. Gagnon⁶¹, C. Galea¹⁰⁶, B. Galhardo^{126a,126c}, E.J. Gallas¹²⁰, B.J. Gallop¹³¹, P. Gallus¹²⁸, G. Galster³⁶, K.K. Gan¹¹¹, J. Gao^{33b,85}, Y. Gao⁴⁶, Y.S. Gao^{143,e}, F.M. Garay Walls⁴⁶, F. Garbersen¹⁷⁶, C. García¹⁶⁷, J.E. García Navarro¹⁶⁷, M. Garcia-Sciveres¹⁵, R.W. Gardner³¹, N. Garelli¹⁴³, V. Garonne¹¹⁹, C. Gatti⁴⁷, A. Gaudiello^{50a,50b}, G. Gaudio^{121a}, B. Gaur¹⁴¹, L. Gauthier⁹⁵, P. Gauzzi^{132a,132b}, I.L. Gavrilenko⁹⁶,

C. Gay¹⁶⁸, G. Gaycken²¹, E.N. Gazis¹⁰, P. Ge^{33d}, Z. Gecse¹⁶⁸, C.N.P. Gee¹³¹, Ch. Geich-Gimbel²¹, M.P. Geisler^{58a}, C. Gemme^{50a}, M.H. Genest⁵⁵, S. Gentile^{132a,132b}, M. George⁵⁴, S. George⁷⁷, D. Gerbaudo¹⁶³, A. Gershon¹⁵³, S. Ghasemi¹⁴¹, H. Ghazlane^{135b}, B. Giacobbe^{20a}, S. Giagu^{132a,132b}, V. Giangiobbe¹², P. Giannetti^{124a,124b}, B. Gibbard²⁵, S.M. Gibson⁷⁷, M. Gilchriese¹⁵, T.P.S. Gillam²⁸, D. Gillberg³⁰, G. Gilles³⁴, D.M. Gingrich^{3,d}, N. Giokaris⁹, M.P. Giordani^{164a,164c}, F.M. Giorgi^{20a}, F.M. Giorgi¹⁶, P.F. Giraud¹³⁶, P. Giromini⁴⁷, D. Giugni^{91a}, C. Giuliani⁴⁸, M. Giulini^{58b}, B.K. Gjelsten¹¹⁹, S. Gkaitatzis¹⁵⁴, I. Gkialas¹⁵⁴, E.L. Gkoukousis¹¹⁷, L.K. Gladilin⁹⁹, C. Glasman⁸², J. Glatzer³⁰, P.C.F. Glaysher⁴⁶, A. Glazov⁴², M. Goblirsch-Kolb¹⁰¹, J.R. Goddard⁷⁶, J. Godlewski³⁹, S. Goldfarb⁸⁹, T. Golling⁴⁹, D. Golubkov¹³⁰, A. Gomes^{126a,126b,126d}, R. Gonçalves^{126a}, J. Goncalves Pinto Firmino Da Costa¹³⁶, L. Gonella²¹, S. González de la Hoz¹⁶⁷, G. Gonzalez Parra¹², S. Gonzalez-Sevilla⁴⁹, L. Goossens³⁰, P.A. Gorbounov⁹⁷, H.A. Gordon²⁵, I. Gorelov¹⁰⁵, B. Gorini³⁰, E. Gorini^{73a,73b}, A. Gorišek⁷⁵, E. Gornicki³⁹, A.T. Goshaw⁴⁵, C. Gössling⁴³, M.I. Gostkin⁶⁵, D. Goujdami^{135c}, A.G. Goussiou¹³⁸, N. Govender^{145b}, E. Gozani¹⁵², H.M.X. Grabas¹³⁷, L. Graber⁵⁴, I. Grabowska-Bold^{38a}, P.O.J. Gradin¹⁶⁶, P. Grafström^{20a,20b}, K-J. Grahn⁴², J. Gramling⁴⁹, E. Gramstad¹¹⁹, S. Grancagnolo¹⁶, V. Gratchev¹²³, H.M. Gray³⁰, E. Graziani^{134a}, Z.D. Greenwood^{79,n}, K. Gregersen⁷⁸, I.M. Gregor⁴², P. Grenier¹⁴³, J. Griffiths⁸, A.A. Grillo¹³⁷, K. Grimm⁷², S. Grinstein^{12,o}, Ph. Gris³⁴, J.-F. Grivaz¹¹⁷, J.P. Grohs⁴⁴, A. Grohsjean⁴², E. Gross¹⁷², J. Grosse-Knetter⁵⁴, G.C. Grossi⁷⁹, Z.J. Grout¹⁴⁹, L. Guan⁸⁹, J. Guenther¹²⁸, F. Guescini⁴⁹, D. Guest¹⁷⁶, O. Gueta¹⁵³, E. Guido^{50a,50b}, T. Guillemain¹¹⁷, S. Guindon², U. Gul⁵³, C. Gumpert⁴⁴, J. Guo^{33e}, Y. Guo^{33b}, S. Gupta¹²⁰, G. Gustavino^{132a,132b}, P. Gutierrez¹¹³, N.G. Gutierrez Ortiz⁷⁸, C. Gutsche⁴⁴, C. Guyot¹³⁶, C. Gwenlan¹²⁰, C.B. Gwilliam⁷⁴, A. Haas¹¹⁰, C. Haber¹⁵, H.K. Hadavand⁸, N. Haddad^{135e}, P. Haefner²¹, S. Hageböck²¹, Z. Hajduk³⁹, H. Hakobyan¹⁷⁷, M. Haleem⁴², J. Haley¹¹⁴, D. Hall¹²⁰, G. Halladjian⁹⁰, G.D. Hallewell⁸⁵, K. Hamacher¹⁷⁵, P. Hamal¹¹⁵, K. Hamano¹⁶⁹, A. Hamilton^{145a}, G.N. Hamity¹³⁹, P.G. Hamnett⁴², L. Han^{33b}, K. Hanagaki^{66,p}, K. Hanawa¹⁵⁵, M. Hance¹⁵, P. Hanke^{58a}, R. Hanna¹³⁶, J.B. Hansen³⁶, J.D. Hansen³⁶, M.C. Hansen²¹, P.H. Hansen³⁶, K. Hara¹⁶⁰, A.S. Hard¹⁷³, T. Harenberg¹⁷⁵, F. Hariri¹¹⁷, S. Harkusha⁹², R.D. Harrington⁴⁶, P.F. Harrison¹⁷⁰, F. Hartjes¹⁰⁷, M. Hasegawa⁶⁷, Y. Hasegawa¹⁴⁰, A. Hasib¹¹³, S. Hassani¹³⁶, S. Haug¹⁷, R. Hauser⁹⁰, L. Hauswald⁴⁴, M. Havranek¹²⁷, C.M. Hawkes¹⁸, R.J. Hawkins³⁰, A.D. Hawkins⁸¹, T. Hayashi¹⁶⁰, D. Hayden⁹⁰, C.P. Hays¹²⁰, J.M. Hays⁷⁶, H.S. Hayward⁷⁴, S.J. Haywood¹³¹, S.J. Head¹⁸, T. Heck⁸³, V. Hedberg⁸¹, L. Heelan⁸, S. Heim¹²², T. Heim¹⁷⁵, B. Heinemann¹⁵, L. Heinrich¹¹⁰, J. Hejbal¹²⁷, L. Helary²², S. Hellman^{146a,146b}, D. Hellmich²¹, C. Helsens¹², J. Henderson¹²⁰, R.C.W. Henderson⁷², Y. Heng¹⁷³, C. Hengler⁴², A. Henrichs¹⁷⁶, A.M. Henriques Correia³⁰, S. Henrot-Versille¹¹⁷, G.H. Herbert¹⁶, Y. Hernández Jiménez¹⁶⁷, R. Herrberg-Schubert¹⁶, G. Herten⁴⁸, R. Hertenberger¹⁰⁰, L. Hervas³⁰, G.G. Hesketh⁷⁸, N.P. Hessey¹⁰⁷, J.W. Hetherly⁴⁰, R. Hickling⁷⁶, E. Higón-Rodríguez¹⁶⁷, E. Hill¹⁶⁹, J.C. Hill²⁸, K.H. Hiller⁴², S.J. Hillier¹⁸, I. Hinchliffe¹⁵, E. Hines¹²², R.R. Hinman¹⁵, M. Hirose¹⁵⁷, D. Hirschbuehl¹⁷⁵, J. Hobbs¹⁴⁸, N. Hod¹⁰⁷, M.C. Hodgkinson¹³⁹, P. Hodgson¹³⁹, A. Hoecker³⁰, M.R. Hoefkamp¹⁰⁵, F. Hoenig¹⁰⁰, M. Hohlfeld⁸³, D. Hohn²¹, T.R. Holmes¹⁵, M. Homann⁴³, T.M. Hong¹²⁵, L. Hooft van Huysduynen¹¹⁰, W.H. Hopkins¹¹⁶, Y. Horii¹⁰³, A.J. Horton¹⁴², J.-Y. Hostachy⁵⁵, S. Hou¹⁵¹, A. Hoummada^{135a}, J. Howard¹²⁰, J. Howarth⁴², M. Hrabovsky¹¹⁵, I. Hristova¹⁶, J. Hrivnac¹¹⁷, T. Hryn'ova⁵, A. Hrynevich⁹³, C. Hsu^{145c}, P.J. Hsu^{151,q}, S.-C. Hsu¹³⁸, D. Hu³⁵, Q. Hu^{33b}, X. Hu⁸⁹, Y. Huang⁴², Z. Hubacek¹²⁸, F. Hubaut⁸⁵, F. Huegging²¹, T.B. Huffman¹²⁰, E.W. Hughes³⁵, G. Hughes⁷², M. Huhtinen³⁰, T.A. Hülsing⁸³, N. Huseynov^{65,b}, J. Huston⁹⁰, J. Huth⁵⁷, G. Iacobucci⁴⁹, G. Iakovidis²⁵, I. Ibragimov¹⁴¹, L. Iconomidou-Fayard¹¹⁷, E. Ideal¹⁷⁶, Z. Idrissi^{135e}, P. Iengo³⁰, O. Igonkina¹⁰⁷, T. Iizawa¹⁷¹, Y. Ikegami⁶⁶, K. Ikematsu¹⁴¹, M. Ikeno⁶⁶, Y. Ilchenko^{31,r}, D. Iliadis¹⁵⁴, N. Ilic¹⁴³, T. Ince¹⁰¹, G. Introzzi^{121a,121b}, P. Ioannou⁹, M. Iodice^{134a}, K. Iordanidou³⁵, V. Ippolito⁵⁷, A. Irles Quiles¹⁶⁷, C. Isaksson¹⁶⁶, M. Ishino⁶⁸, M. Ishitsuka¹⁵⁷, R. Ishmukhametov¹¹¹, C. Issever¹²⁰, S. Istin^{19a}, J.M. Iturbe Ponce⁸⁴, R. Iuppa^{133a,133b}, J. Ivarsson⁸¹, W. Iwanski³⁹,

H. Iwasaki⁶⁶, J.M. Izen⁴¹, V. Izzo^{104a}, S. Jabbar³, B. Jackson¹²², M. Jackson⁷⁴, P. Jackson¹, M.R. Jaekel³⁰, V. Jain², K. Jakobs⁴⁸, S. Jakobsen³⁰, T. Jakoubek¹²⁷, J. Jakubek¹²⁸, D.O. Jamin¹¹⁴, D.K. Jana⁷⁹, E. Jansen⁷⁸, R. Jansky⁶², J. Janssen²¹, M. Janus⁵⁴, G. Jarlskog⁸¹, N. Javadov^{65,b}, T. Javůrek⁴⁸, L. Jeanty¹⁵, J. Jejelava^{51a,s}, G.-Y. Jeng¹⁵⁰, D. Jennens⁸⁸, P. Jenni^{48,t}, J. Jentzsch⁴³, C. Jeske¹⁷⁰, S. Jézéquel⁵, H. Ji¹⁷³, J. Jia¹⁴⁸, Y. Jiang^{33b}, S. Jiggins⁷⁸, J. Jimenez Pena¹⁶⁷, S. Jin^{33a}, A. Jinaru^{26a}, O. Jinnouchi¹⁵⁷, M.D. Joergensen³⁶, P. Johansson¹³⁹, K.A. Johns⁷, K. Jon-And^{146a,146b}, G. Jones¹⁷⁰, R.W.L. Jones⁷², T.J. Jones⁷⁴, J. Jongmanns^{58a}, P.M. Jorge^{126a,126b}, K.D. Joshi⁸⁴, J. Jovicevic^{159a}, X. Ju¹⁷³, C.A. Jung⁴³, P. Jussel⁶², A. Juste Rozas^{12,o}, M. Kaci¹⁶⁷, A. Kaczmarek³⁹, M. Kado¹¹⁷, H. Kagan¹¹¹, M. Kagan¹⁴³, S.J. Kahn⁸⁵, E. Kajomovitz⁴⁵, C.W. Kalderon¹²⁰, S. Kama⁴⁰, A. Kamenshchikov¹³⁰, N. Kanaya¹⁵⁵, S. Kaneti²⁸, V.A. Kantserov⁹⁸, J. Kanzaki⁶⁶, B. Kaplan¹¹⁰, L.S. Kaplan¹⁷³, A. Kapliy³¹, D. Kar^{145c}, K. Karakostas¹⁰, A. Karamaoun³, N. Karastathis^{10,107}, M.J. Kareem⁵⁴, E. Karentzos¹⁰, M. Karnevskiy⁸³, S.N. Karpov⁶⁵, Z.M. Karpova⁶⁵, K. Karthik¹¹⁰, V. Kartvelishvili⁷², A.N. Karyukhin¹³⁰, L. Kashif¹⁷³, R.D. Kass¹¹¹, A. Kastanas¹⁴, Y. Kataoka¹⁵⁵, C. Kato¹⁵⁵, A. Katre⁴⁹, J. Katzy⁴², K. Kawagoe⁷⁰, T. Kawamoto¹⁵⁵, G. Kawamura⁵⁴, S. Kazama¹⁵⁵, V.F. Kazanin^{109,c}, R. Keeler¹⁶⁹, R. Kehoe⁴⁰, J.S. Keller⁴², J.J. Kempster⁷⁷, H. Keoshkerian⁸⁴, O. Kepka¹²⁷, B.P. Kerševan⁷⁵, S. Kersten¹⁷⁵, R.A. Keyes⁸⁷, F. Khalil-zada¹¹, H. Khandanyan^{146a,146b}, A. Khanov¹¹⁴, A.G. Kharlamov^{109,c}, T.J. Khoo²⁸, V. Khovanskiy⁹⁷, E. Khramov⁶⁵, J. Khubua^{51b,u}, S. Kido⁶⁷, H.Y. Kim⁸, S.H. Kim¹⁶⁰, Y.K. Kim³¹, N. Kimura¹⁵⁴, O.M. Kind¹⁶, B.T. King⁷⁴, M. King¹⁶⁷, S.B. King¹⁶⁸, J. Kirk¹³¹, A.E. Kiryunin¹⁰¹, T. Kishimoto⁶⁷, D. Kisielewska^{38a}, F. Kiss⁴⁸, K. Kiuchi¹⁶⁰, O. Kivernyk¹³⁶, E. Kladiva^{144b}, M.H. Klein³⁵, M. Klein⁷⁴, U. Klein⁷⁴, K. Kleinknecht⁸³, P. Klimek^{146a,146b}, A. Klimentov²⁵, R. Klingenberg⁴³, J.A. Klinger¹³⁹, T. Klioutchnikova³⁰, E.-E. Kluge^{58a}, P. Kluit¹⁰⁷, S. Kluth¹⁰¹, J. Knapik³⁹, E. Kneringer⁶², E.B.F.G. Knoops⁸⁵, A. Knue⁵³, A. Kobayashi¹⁵⁵, D. Kobayashi¹⁵⁷, T. Kobayashi¹⁵⁵, M. Kobel⁴⁴, M. Kocian¹⁴³, P. Kodys¹²⁹, T. Koffas²⁹, E. Koffeman¹⁰⁷, L.A. Kogan¹²⁰, S. Kohlmann¹⁷⁵, Z. Kohout¹²⁸, T. Kohriki⁶⁶, T. Koi¹⁴³, H. Kolanoski¹⁶, I. Koletsou⁵, A.A. Komar^{96,*}, Y. Komori¹⁵⁵, T. Kondo⁶⁶, N. Kondrashova⁴², K. Köneke⁴⁸, A.C. König¹⁰⁶, T. Kono⁶⁶, R. Konoplich^{110,v}, N. Konstantinidis⁷⁸, R. Kopeliansky¹⁵², S. Koperny^{38a}, L. Köpke⁸³, A.K. Kopp⁴⁸, K. Korcyl³⁹, K. Kordas¹⁵⁴, A. Korn⁷⁸, A.A. Korol^{109,c}, I. Korolkov¹², E.V. Korolkova¹³⁹, O. Kortner¹⁰¹, S. Kortner¹⁰¹, T. Kosek¹²⁹, V.V. Kostyukhin²¹, V.M. Kotov⁶⁵, A. Kotwal⁴⁵, A. Kourkoumeli-Charalampidi¹⁵⁴, C. Kourkoumelis⁹, V. Kouskoura²⁵, A. Koutsman^{159a}, R. Kowalewski¹⁶⁹, T.Z. Kowalski^{38a}, W. Kozanecki¹³⁶, A.S. Kozhin¹³⁰, V.A. Kramarenko⁹⁹, G. Kramberger⁷⁵, D. Krasnopevtsev⁹⁸, M.W. Krasny⁸⁰, A. Krasznahorkay³⁰, J.K. Kraus²¹, A. Kravchenko²⁵, S. Kreiss¹¹⁰, M. Kretz^{58c}, J. Kretzschmar⁷⁴, K. Kreutzfeldt⁵², P. Krieger¹⁵⁸, K. Krizka³¹, K. Kroeninger⁴³, H. Kroha¹⁰¹, J. Kroll¹²², J. Kroseberg²¹, J. Krstic¹³, U. Kruchonak⁶⁵, H. Krüger²¹, N. Krumnack⁶⁴, A. Kruse¹⁷³, M.C. Kruse⁴⁵, M. Kruskal²², T. Kubota⁸⁸, H. Kucuk⁷⁸, S. Kудay^{4b}, S. Kuehn⁴⁸, A. Kugel^{58c}, F. Kuger¹⁷⁴, A. Kuhl¹³⁷, T. Kuhl⁴², V. Kukhtin⁶⁵, Y. Kulchitsky⁹², S. Kuleshov^{32b}, M. Kuna^{132a,132b}, T. Kunigo⁶⁸, A. Kupco¹²⁷, H. Kurashige⁶⁷, Y.A. Kurochkin⁹², V. Kus¹²⁷, E.S. Kuwertz¹⁶⁹, M. Kuze¹⁵⁷, J. Kvita¹¹⁵, T. Kwan¹⁶⁹, D. Kyriazopoulos¹³⁹, A. La Rosa¹³⁷, J.L. La Rosa Navarro^{24d}, L. La Rotonda^{37a,37b}, C. Lacasta¹⁶⁷, F. Lacava^{132a,132b}, J. Lacey²⁹, H. Lacker¹⁶, D. Lacour⁸⁰, V.R. Lacuesta¹⁶⁷, E. Ladygin⁶⁵, R. Lafaye⁵, B. Laforge⁸⁰, T. Lagouri¹⁷⁶, S. Lai⁵⁴, L. Lambourne⁷⁸, S. Lammers⁶¹, C.L. Lampen⁷, W. Lampl⁷, E. Lançon¹³⁶, U. Landgraf⁴⁸, M.P.J. Landon⁷⁶, V.S. Lang^{58a}, J.C. Lange¹², A.J. Lankford¹⁶³, F. Lanni²⁵, K. Lantzsche³⁰, A. Lanza^{121a}, S. Laplace⁸⁰, C. Lapoire³⁰, J.F. Laporte¹³⁶, T. Lari^{91a}, F. Lasagni Manghi^{20a,20b}, M. Lassnig³⁰, P. Laurelli⁴⁷, W. Lavrijsen¹⁵, A.T. Law¹³⁷, P. Laycock⁷⁴, T. Lazovich⁵⁷, O. Le Dortz⁸⁰, E. Le Guirriec⁸⁵, E. Le Menedeu¹², M. LeBlanc¹⁶⁹, T. LeCompte⁶, F. Ledroit-Guillon⁵⁵, C.A. Lee^{145b}, S.C. Lee¹⁵¹, L. Lee¹, G. Lefebvre⁸⁰, M. Lefebvre¹⁶⁹, F. Legger¹⁰⁰, C. Leggett¹⁵, A. Lehan⁷⁴, G. Lehmann Miotto³⁰, X. Lei⁷, W.A. Leight²⁹, A. Leisos^{154,w}, A.G. Leister¹⁷⁶, M.A.L. Leite^{24d}, R. Leitner¹²⁹, D. Lellouch¹⁷², B. Lemmer⁵⁴, K.J.C. Leney⁷⁸, T. Lenz²¹, B. Lenzi³⁰, R. Leone⁷, S. Leone^{124a,124b}, C. Leonidopoulos⁴⁶,

S. Leontsinis¹⁰, C. Leroy⁹⁵, C.G. Lester²⁸, M. Levchenko¹²³, J. Levêque⁵, D. Levin⁸⁹, L.J. Levinson¹⁷², M. Levy¹⁸, A. Lewis¹²⁰, A.M. Leyko²¹, M. Leyton⁴¹, B. Li^{33b,x}, H. Li¹⁴⁸, H.L. Li³¹, L. Li⁴⁵, L. Li^{33e}, S. Li⁴⁵, X. Li⁸⁴, Y. Li^{33c,y}, Z. Liang¹³⁷, H. Liao³⁴, B. Liberti^{133a}, A. Liblong¹⁵⁸, P. Lichard³⁰, K. Lie¹⁶⁵, J. Liebal²¹, W. Liebig¹⁴, C. Limbach²¹, A. Limosani¹⁵⁰, S.C. Lin^{151,z}, T.H. Lin⁸³, F. Linde¹⁰⁷, B.E. Lindquist¹⁴⁸, J.T. Linnemann⁹⁰, E. Lipeles¹²², A. Lipniacka¹⁴, M. Lisovyi^{58b}, T.M. Liss¹⁶⁵, D. Lissauer²⁵, A. Lister¹⁶⁸, A.M. Litke¹³⁷, B. Liu^{151,aa}, D. Liu¹⁵¹, H. Liu⁸⁹, J. Liu⁸⁵, J.B. Liu^{33b}, K. Liu⁸⁵, L. Liu¹⁶⁵, M. Liu⁴⁵, M. Liu^{33b}, Y. Liu^{33b}, M. Livan^{121a,121b}, A. Lleres⁵⁵, J. Llorente Merino⁸², S.L. Lloyd⁷⁶, F. Lo Sterzo¹⁵¹, E. Lobodzinska⁴², P. Loch⁷, W.S. Lockman¹³⁷, F.K. Loebinger⁸⁴, A.E. Loevschall-Jensen³⁶, A. Loginov¹⁷⁶, T. Lohse¹⁶, K. Lohwasser⁴², M. Lokajicek¹²⁷, B.A. Long²², J.D. Long⁸⁹, R.E. Long⁷², K.A. Looper¹¹¹, L. Lopes^{126a}, D. Lopez Mateos⁵⁷, B. Lopez Paredes¹³⁹, I. Lopez Paz¹², J. Lorenz¹⁰⁰, N. Lorenzo Martinez⁶¹, M. Losada¹⁶², P. Loscutoff¹⁵, P.J. Lösel¹⁰⁰, X. Lou^{33a}, A. Lounis¹¹⁷, J. Love⁶, P.A. Love⁷², N. Lu⁸⁹, H.J. Lubatti¹³⁸, C. Luci^{132a,132b}, A. Lucotte⁵⁵, F. Luehring⁶¹, W. Lukas⁶², L. Luminari^{132a}, O. Lundberg^{146a,146b}, B. Lund-Jensen¹⁴⁷, D. Lynn²⁵, R. Lysak¹²⁷, E. Lytken⁸¹, H. Ma²⁵, L.L. Ma^{33d}, G. Maccarrone⁴⁷, A. Macchiolo¹⁰¹, C.M. Macdonald¹³⁹, B. Maček⁷⁵, J. Machado Miguens^{122,126b}, D. Macina³⁰, D. Madaffari⁸⁵, R. Madar³⁴, H.J. Maddocks⁷², W.F. Mader⁴⁴, A. Madsen¹⁶⁶, J. Maeda⁶⁷, S. Maeland¹⁴, T. Maeno²⁵, A. Maevskiy⁹⁹, E. Magradze⁵⁴, K. Mahboubi⁴⁸, J. Mahlstedt¹⁰⁷, C. Maiani¹³⁶, C. Maidantchik^{24a}, A.A. Maier¹⁰¹, T. Maier¹⁰⁰, A. Maio^{126a,126b,126d}, S. Majewski¹¹⁶, Y. Makida⁶⁶, N. Makovec¹¹⁷, B. Malaescu⁸⁰, Pa. Malecki³⁹, V.P. Maleev¹²³, F. Malek⁵⁵, U. Mallik⁶³, D. Malon⁶, C. Malone¹⁴³, S. Maltezos¹⁰, V.M. Malyshev¹⁰⁹, S. Malyukov³⁰, J. Mamuzic⁴², G. Mancini⁴⁷, B. Mandelli³⁰, L. Mandelli^{91a}, I. Mandić⁷⁵, R. Mandrysch⁶³, J. Maneira^{126a,126b}, A. Manfredini¹⁰¹, L. Manhaes de Andrade Filho^{24b}, J. Manjarres Ramos^{159b}, A. Mann¹⁰⁰, A. Manousakis-Katsikakis⁹, B. Mansoulie¹³⁶, R. Mantifel⁸⁷, M. Mantoani⁵⁴, L. Mapelli³⁰, L. March^{145c}, G. Marchiori⁸⁰, M. Marcisovsky¹²⁷, C.P. Marino¹⁶⁹, M. Marjanovic¹³, D.E. Marley⁸⁹, F. Marroquim^{24a}, S.P. Marsden⁸⁴, Z. Marshall¹⁵, L.F. Marti¹⁷, S. Marti-Garcia¹⁶⁷, B. Martin⁹⁰, T.A. Martin¹⁷⁰, V.J. Martin⁴⁶, B. Martin dit Latour¹⁴, M. Martinez^{12,o}, S. Martin-Haugh¹³¹, V.S. Martoiu^{26a}, A.C. Martyniuk⁷⁸, M. Marx¹³⁸, F. Marzano^{132a}, A. Marzin³⁰, L. Masetti⁸³, T. Mashimo¹⁵⁵, R. Mashinistov⁹⁶, J. Masik⁸⁴, A.L. Maslennikov^{109,c}, I. Massa^{20a,20b}, L. Massa^{20a,20b}, N. Massol⁵, P. Mastrandrea¹⁴⁸, A. Mastroberardino^{37a,37b}, T. Masubuchi¹⁵⁵, P. Mättig¹⁷⁵, J. Mattmann⁸³, J. Maurer^{26a}, S.J. Maxfield⁷⁴, D.A. Maximov^{109,c}, R. Mazini¹⁵¹, S.M. Mazza^{91a,91b}, L. Mazzaferro^{133a,133b}, G. Mc Goldrick¹⁵⁸, S.P. Mc Kee⁸⁹, A. McCarn⁸⁹, R.L. McCarthy¹⁴⁸, T.G. McCarthy²⁹, N.A. McCubbin¹³¹, K.W. McFarlane^{56,*}, J.A. Mcfayden⁷⁸, G. Mchedlidze⁵⁴, S.J. McMahon¹³¹, R.A. McPherson^{169,k}, M. Medinnis⁴², S. Meehan^{145a}, S. Mehlhase¹⁰⁰, A. Mehta⁷⁴, K. Meier^{58a}, C. Meineck¹⁰⁰, B. Meirose⁴¹, B.R. Mellado Garcia^{145c}, F. Meloni¹⁷, A. Mengarelli^{20a,20b}, S. Menke¹⁰¹, E. Meoni¹⁶¹, K.M. Mercurio⁵⁷, S. Mergelmeyer²¹, P. Mermod⁴⁹, L. Merola^{104a,104b}, C. Meroni^{91a}, F.S. Merritt³¹, A. Messina^{132a,132b}, J. Metcalfe²⁵, A.S. Mete¹⁶³, C. Meyer⁸³, C. Meyer¹²², J-P. Meyer¹³⁶, J. Meyer¹⁰⁷, H. Meyer Zu Theenhausen^{58a}, R.P. Middleton¹³¹, S. Miglioranzì^{164a,164c}, L. Mijović²¹, G. Mikenberg¹⁷², M. Mikestikova¹²⁷, M. Mikuž⁷⁵, M. Milesi⁸⁸, A. Milic³⁰, D.W. Miller³¹, C. Mills⁴⁶, A. Milov¹⁷², D.A. Milstead^{146a,146b}, A.A. Minaenko¹³⁰, Y. Minami¹⁵⁵, I.A. Minashvili⁶⁵, A.I. Mincer¹¹⁰, B. Mindur^{38a}, M. Mineev⁶⁵, Y. Ming¹⁷³, L.M. Mir¹², T. Mitani¹⁷¹, J. Mitrevski¹⁰⁰, V.A. Mitsou¹⁶⁷, A. Miucci⁴⁹, P.S. Miyagawa¹³⁹, J.U. Mjörnmark⁸¹, T. Moa^{146a,146b}, K. Mochizuki⁸⁵, S. Mohapatra³⁵, W. Mohr⁴⁸, S. Molander^{146a,146b}, R. Moles-Valls²¹, K. Mönig⁴², C. Monini⁵⁵, J. Monk³⁶, E. Monnier⁸⁵, J. Montejo Berlingen¹², F. Monticelli⁷¹, S. Monzani^{132a,132b}, R.W. Moore³, N. Morange¹¹⁷, D. Moreno¹⁶², M. Moreno Llácer⁵⁴, P. Morettini^{50a}, D. Mori¹⁴², M. Morii⁵⁷, M. Morinaga¹⁵⁵, V. Morisbak¹¹⁹, S. Moritz⁸³, A.K. Morley¹⁵⁰, G. Mornacchi³⁰, J.D. Morris⁷⁶, S.S. Mortensen³⁶, A. Morton⁵³, L. Morvaj¹⁰³, M. Mosidze^{51b}, J. Moss¹¹¹, K. Motohashi¹⁵⁷, R. Mount¹⁴³, E. Mountricha²⁵, S.V. Mouraviev^{96,*}, E.J.W. Moyse⁸⁶, S. Muanza⁸⁵, R.D. Mudd¹⁸, F. Mueller¹⁰¹, J. Mueller¹²⁵, R.S.P. Mueller¹⁰⁰, T. Mueller²⁸,

D. Muenstermann⁴⁹, P. Mullen⁵³, G.A. Mullier¹⁷, J.A. Murillo Quijada¹⁸, W.J. Murray^{170,131}, H. Musheghyan⁵⁴, E. Musto¹⁵², A.G. Myagkov^{130,ab}, M. Myska¹²⁸, B.P. Nachman¹⁴³, O. Nackenhorst⁵⁴, J. Nadal⁵⁴, K. Nagai¹²⁰, R. Nagai¹⁵⁷, Y. Nagai⁸⁵, K. Nagano⁶⁶, A. Nagarkar¹¹¹, Y. Nagasaka⁵⁹, K. Nagata¹⁶⁰, M. Nagel¹⁰¹, E. Nagy⁸⁵, A.M. Nairz³⁰, Y. Nakahama³⁰, K. Nakamura⁶⁶, T. Nakamura¹⁵⁵, I. Nakano¹¹², H. Namasivayam⁴¹, R.F. Naranjo Garcia⁴², R. Narayan³¹, D.I. Narrias Villar^{58a}, T. Naumann⁴², G. Navarro¹⁶², R. Nayyar⁷, H.A. Neal⁸⁹, P.Yu. Nechaeva⁹⁶, T.J. Neep⁸⁴, P.D. Nef¹⁴³, A. Negri^{121a,121b}, M. Negrini^{20a}, S. Nektarijevic¹⁰⁶, C. Nellist¹¹⁷, A. Nelson¹⁶³, S. Nemecek¹²⁷, P. Nemethy¹¹⁰, A.A. Nepomuceno^{24a}, M. Nessi^{30,ac}, M.S. Neubauer¹⁶⁵, M. Neumann¹⁷⁵, R.M. Neves¹¹⁰, P. Nevski²⁵, P.R. Newman¹⁸, D.H. Nguyen⁶, R.B. Nickerson¹²⁰, R. Nicolaidou¹³⁶, B. Nicquevert³⁰, J. Nielsen¹³⁷, N. Nikiforou³⁵, A. Nikiforov¹⁶, V. Nikolaenko^{130,ab}, I. Nikolic-Audit⁸⁰, K. Nikolopoulos¹⁸, J.K. Nilsen¹¹⁹, P. Nilsson²⁵, Y. Ninomiya¹⁵⁵, A. Nisati^{132a}, R. Nisius¹⁰¹, T. Nobe¹⁵⁵, M. Nomachi¹¹⁸, I. Nomidis²⁹, T. Nooney⁷⁶, S. Norberg¹¹³, M. Nordberg³⁰, O. Novgorodova⁴⁴, S. Nowak¹⁰¹, M. Nozaki⁶⁶, L. Nozka¹¹⁵, K. Ntekas¹⁰, G. Nunes Hanninger⁸⁸, T. Nunnemann¹⁰⁰, E. Nurse⁷⁸, F. Nuti⁸⁸, B.J. O'Brien⁴⁶, F. O'grady⁷, D.C. O'Neil¹⁴², V. O'Shea⁵³, F.G. Oakham^{29,d}, H. Oberlack¹⁰¹, T. Obermann²¹, J. Ocariz⁸⁰, A. Ochi⁶⁷, I. Ochoa⁷⁸, J.P. Ochoa-Ricoux^{32a}, S. Oda⁷⁰, S. Odaka⁶⁶, H. Ogren⁶¹, A. Oh⁸⁴, S.H. Oh⁴⁵, C.C. Ohm¹⁵, H. Ohman¹⁶⁶, H. Oide³⁰, W. Okamura¹¹⁸, H. Okawa¹⁶⁰, Y. Okumura³¹, T. Okuyama⁶⁶, A. Olariu^{26a}, S.A. Olivares Pino⁴⁶, D. Oliveira Damazio²⁵, E. Oliver Garcia¹⁶⁷, A. Olszewski³⁹, J. Olszowska³⁹, A. Onofre^{126a,126e}, P.U.E. Onyisi^{31,r}, C.J. Oram^{159a}, M.J. Oreglia³¹, Y. Oren¹⁵³, D. Orestano^{134a,134b}, N. Orlando¹⁵⁴, C. Oropeza Barrera⁵³, R.S. Orr¹⁵⁸, B. Osculati^{50a,50b}, R. Ospanov⁸⁴, G. Otero y Garzon²⁷, H. Otono⁷⁰, M. Ouchrif^{135d}, F. Ould-Saada¹¹⁹, A. Ouraou¹³⁶, K.P. Oussoren¹⁰⁷, Q. Ouyang^{33a}, A. Ovcharova¹⁵, M. Owen⁵³, R.E. Owen¹⁸, V.E. Ozcan^{19a}, N. Ozturk⁸, K. Pachal¹⁴², A. Pacheco Pages¹², C. Padilla Aranda¹², M. Pagáčová⁴⁸, S. Pagan Griso¹⁵, E. Paganis¹³⁹, F. Paige²⁵, P. Pais⁸⁶, K. Pajchel¹¹⁹, G. Palacino^{159b}, S. Palestini³⁰, M. Palka^{38b}, D. Pallin³⁴, A. Palma^{126a,126b}, Y.B. Pan¹⁷³, E. Panagiotopoulou¹⁰, C.E. Pandini⁸⁰, J.G. Panduro Vazquez⁷⁷, P. Pani^{146a,146b}, S. Panitkin²⁵, D. Pantea^{26a}, L. Paolozzi⁴⁹, Th.D. Papadopoulou¹⁰, K. Papageorgiou¹⁵⁴, A. Paramonov⁶, D. Paredes Hernandez¹⁵⁴, M.A. Parker²⁸, K.A. Parker¹³⁹, F. Parodi^{50a,50b}, J.A. Parsons³⁵, U. Parzefall⁴⁸, E. Pasqualucci^{132a}, S. Passaggio^{50a}, F. Pastore^{134a,134b,*}, Fr. Pastore⁷⁷, G. Pásztor²⁹, S. Patariaia¹⁷⁵, N.D. Patel¹⁵⁰, J.R. Pater⁸⁴, T. Pauly³⁰, J. Pearce¹⁶⁹, B. Pearson¹¹³, L.E. Pedersen³⁶, M. Pedersen¹¹⁹, S. Pedraza Lopez¹⁶⁷, R. Pedro^{126a,126b}, S.V. Peleganchuk^{109,c}, D. Pelikan¹⁶⁶, O. Penc¹²⁷, C. Peng^{33a}, H. Peng^{33b}, B. Penning³¹, J. Penwell⁶¹, D.V. Perepelitsa²⁵, E. Perez Codina^{159a}, M.T. Pérez García-Están¹⁶⁷, L. Perini^{91a,91b}, H. Pernegger³⁰, S. Perrella^{104a,104b}, R. Peschke⁴², V.D. Peshekhonov⁶⁵, K. Peters³⁰, R.F.Y. Peters⁸⁴, B.A. Petersen³⁰, T.C. Petersen³⁶, E. Petit⁴², A. Petridis¹, C. Petridou¹⁵⁴, P. Petroff¹¹⁷, E. Petrolo^{132a}, F. Petrucci^{134a,134b}, N.E. Pettersson¹⁵⁷, R. Pezoa^{32b}, P.W. Phillips¹³¹, G. Piacquadio¹⁴³, E. Pianori¹⁷⁰, A. Picazio⁴⁹, E. Piccaro⁷⁶, M. Piccinini^{20a,20b}, M.A. Pickering¹²⁰, R. Piegaia²⁷, D.T. Pignotti¹¹¹, J.E. Pilcher³¹, A.D. Pilkington⁸⁴, J. Pina^{126a,126b,126d}, M. Pinamonti^{164a,164c,ad}, J.L. Pinfold³, A. Pingel³⁶, S. Pires⁸⁰, H. Pirumov⁴², M. Pitt¹⁷², C. Pizio^{91a,91b}, L. Plazak^{144a}, M.-A. Pleier²⁵, V. Pleskot¹²⁹, E. Plotnikova⁶⁵, P. Plucinski^{146a,146b}, D. Pluth⁶⁴, R. Poettgen^{146a,146b}, L. Poggioli¹¹⁷, D. Pohl²¹, G. Polesello^{121a}, A. Poley⁴², A. Policicchio^{37a,37b}, R. Polifka¹⁵⁸, A. Polini^{20a}, C.S. Pollard⁵³, V. Polychronakos²⁵, K. Pommès³⁰, L. Pontecorvo^{132a}, B.G. Pope⁹⁰, G.A. Popeneciu^{26b}, D.S. Popovic¹³, A. Poppleton³⁰, S. Pospisil¹²⁸, K. Potamianos¹⁵, I.N. Potrap⁶⁵, C.J. Potter¹⁴⁹, C.T. Potter¹¹⁶, G. Poulard³⁰, J. Poveda³⁰, V. Pozdnyakov⁶⁵, P. Pralavorio⁸⁵, A. Pranko¹⁵, S. Prasad³⁰, S. Prell⁶⁴, D. Price⁸⁴, L.E. Price⁶, M. Primavera^{73a}, S. Prince⁸⁷, M. Proissl⁴⁶, K. Prokofiev^{60c}, F. Prokoshin^{32b}, E. Protopapadaki¹³⁶, S. Protopopescu²⁵, J. Proudfoot⁶, M. Przybycien^{38a}, E. Ptacek¹¹⁶, D. Puddu^{134a,134b}, E. Pueschel⁸⁶, D. Pulton¹⁴⁸, M. Purohit^{25,ae}, P. Puzo¹¹⁷, J. Qian⁸⁹, G. Qin⁵³, Y. Qin⁸⁴, A. Quadt⁵⁴, D.R. Quarrie¹⁵, W.B. Quayle^{164a,164b}, M. Queitsch-Maitland⁸⁴, D. Quilty⁵³, S. Raddum¹¹⁹, V. Radeka²⁵, V. Radescu⁴², S.K. Radhakrishnan¹⁴⁸, P. Radloff¹¹⁶, P. Rados⁸⁸, F. Ragusa^{91a,91b}, G. Rahal¹⁷⁸, S. Rajagopalan²⁵,

M. Rammensee³⁰, C. Rangel-Smith¹⁶⁶, F. Rauscher¹⁰⁰, S. Rave⁸³, T. Ravenscroft⁵³, M. Raymond³⁰, A.L. Read¹¹⁹, N.P. Readioff⁷⁴, D.M. Rebuzzi^{121a,121b}, A. Redelbach¹⁷⁴, G. Redlinger²⁵, R. Reece¹³⁷, K. Reeves⁴¹, L. Rehnisch¹⁶, J. Reichert¹²², H. Reisin²⁷, M. Relich¹⁶³, C. Rembser³⁰, H. Ren^{33a}, A. Renaud¹¹⁷, M. Rescigno^{132a}, S. Resconi^{91a}, O.L. Rezanova^{109,c}, P. Reznicek¹²⁹, R. Rezvani⁹⁵, R. Richter¹⁰¹, S. Richter⁷⁸, E. Richter-Was^{38b}, O. Ricken²¹, M. Ridel⁸⁰, P. Rieck¹⁶, C.J. Riegel¹⁷⁵, J. Rieger⁵⁴, M. Rijssenbeek¹⁴⁸, A. Rimoldi^{121a,121b}, L. Rinaldi^{20a}, B. Ristić⁴⁹, E. Ritsch³⁰, I. Riu¹², F. Rizatdinova¹¹⁴, E. Rizvi⁷⁶, S.H. Robertson^{87,k}, A. Robichaud-Veronneau⁸⁷, D. Robinson²⁸, J.E.M. Robinson⁴², A. Robson⁵³, C. Roda^{124a,124b}, S. Roe³⁰, O. Røhne¹¹⁹, S. Rolli¹⁶¹, A. Romanouk⁹⁸, M. Romano^{20a,20b}, S.M. Romano Saez³⁴, E. Romero Adam¹⁶⁷, N. Rompotis¹³⁸, M. Ronzani⁴⁸, L. Roos⁸⁰, E. Ros¹⁶⁷, S. Rosati^{132a}, K. Rosbach⁴⁸, P. Rose¹³⁷, P.L. Rosendahl¹⁴, O. Rosenthal¹⁴¹, V. Rossetti^{146a,146b}, E. Rossi^{104a,104b}, L.P. Rossi^{50a}, J.H.N. Rosten²⁸, R. Rosten¹³⁸, M. Rotaru^{26a}, I. Roth¹⁷², J. Rothberg¹³⁸, D. Rousseau¹¹⁷, C.R. Royon¹³⁶, A. Rozanov⁸⁵, Y. Rozen¹⁵², X. Ruan^{145c}, F. Rubbo¹⁴³, I. Rubinskiy⁴², V.I. Rud⁹⁹, C. Rudolph⁴⁴, M.S. Rudolph¹⁵⁸, F. Rühr⁴⁸, A. Ruiz-Martinez³⁰, Z. Rurikova⁴⁸, N.A. Rusakovich⁶⁵, A. Ruschke¹⁰⁰, H.L. Russell¹³⁸, J.P. Rutherford⁷, N. Ruthmann⁴⁸, Y.F. Ryabov¹²³, M. Rybar¹⁶⁵, G. Rybkin¹¹⁷, N.C. Ryder¹²⁰, A.F. Saavedra¹⁵⁰, G. Sabato¹⁰⁷, S. Sacerdoti²⁷, A. Saddique³, H.F.W. Sadrozinski¹³⁷, R. Sadykov⁶⁵, F. Safai Tehrani^{132a}, M. Sahinsoy^{58a}, M. Saimpert¹³⁶, T. Saito¹⁵⁵, H. Sakamoto¹⁵⁵, Y. Sakurai¹⁷¹, G. Salamanna^{134a,134b}, A. Salamon^{133a}, J.E. Salazar Loyola^{32b}, M. Saleem¹¹³, D. Salek¹⁰⁷, P.H. Sales De Bruin¹³⁸, D. Saliagic¹⁰¹, A. Salnikov¹⁴³, J. Salt¹⁶⁷, D. Salvatore^{37a,37b}, F. Salvatore¹⁴⁹, A. Salvucci^{60a}, A. Salzburger³⁰, D. Sammel⁴⁸, D. Sampsonidis¹⁵⁴, A. Sanchez^{104a,104b}, J. Sánchez¹⁶⁷, V. Sanchez Martinez¹⁶⁷, H. Sandaker¹¹⁹, R.L. Sandbach⁷⁶, H.G. Sander⁸³, M.P. Sanders¹⁰⁰, M. Sandhoff¹⁷⁵, C. Sandoval¹⁶², R. Sandstroem¹⁰¹, D.P.C. Sankey¹³¹, M. Sannino^{50a,50b}, A. Sansoni⁴⁷, C. Santoni³⁴, R. Santonico^{133a,133b}, H. Santos^{126a}, I. Santoyo Castillo¹⁴⁹, K. Sapp¹²⁵, A. Saponov⁶⁵, J.G. Saraiva^{126a,126d}, B. Sarrazin²¹, O. Sasaki⁶⁶, Y. Sasaki¹⁵⁵, K. Sato¹⁶⁰, G. Sauvage^{5,*}, E. Sauvan⁵, G. Savage⁷⁷, P. Savard^{158,d}, C. Sawyer¹³¹, L. Sawyer^{79,n}, J. Saxon³¹, C. Sbarra^{20a}, A. Sbrizzi^{20a,20b}, T. Scanlon⁷⁸, D.A. Scannicchio¹⁶³, M. Scarcella¹⁵⁰, V. Scarfone^{37a,37b}, J. Schaarschmidt¹⁷², P. Schacht¹⁰¹, D. Schaefer³⁰, R. Schaefer⁴², J. Schaeffer⁸³, S. Schaepe²¹, S. Schaetzel^{58b}, U. Schäfer⁸³, A.C. Schaffer¹¹⁷, D. Schaile¹⁰⁰, R.D. Schamberger¹⁴⁸, V. Scharf^{58a}, V.A. Schegelsky¹²³, D. Scheirich¹²⁹, M. Schernau¹⁶³, C. Schiavi^{50a,50b}, C. Schillo⁴⁸, M. Schioppa^{37a,37b}, S. Schlenker³⁰, K. Schmieden³⁰, C. Schmitt⁸³, S. Schmitt^{58b}, S. Schmitt⁴², B. Schneider^{159a}, Y.J. Schnellbach⁷⁴, U. Schnoor⁴⁴, L. Schoeffel¹³⁶, A. Schoening^{58b}, B.D. Schoenrock⁹⁰, E. Schopf²¹, A.L.S. Schorlemmer⁵⁴, M. Schott⁸³, D. Schouten^{159a}, J. Schovancova⁸, S. Schramm⁴⁹, M. Schreyer¹⁷⁴, C. Schroeder⁸³, N. Schuh⁸³, M.J. Schultens²¹, H.-C. Schultz-Coulon^{58a}, H. Schulz¹⁶, M. Schumacher⁴⁸, B.A. Schumm¹³⁷, Ph. Schune¹³⁶, C. Schwanenberger⁸⁴, A. Schwartzman¹⁴³, T.A. Schwarz⁸⁹, Ph. Schwegler¹⁰¹, H. Schweiger⁸⁴, Ph. Schwemling¹³⁶, R. Schwienhorst⁹⁰, J. Schwindling¹³⁶, T. Schwindt²¹, F.G. Sciacca¹⁷, E. Scifo¹¹⁷, G. Sciolla²³, F. Scuri^{124a,124b}, F. Scutti²¹, J. Searcy⁸⁹, G. Sedov⁴², E. Sedykh¹²³, P. Seema²¹, S.C. Seidel¹⁰⁵, A. Seiden¹³⁷, F. Seifert¹²⁸, J.M. Seixas^{24a}, G. Sekhniaidze^{104a}, K. Sekhon⁸⁹, S.J. Sekula⁴⁰, D.M. Seliverstov^{123,*}, N. Semprini-Cesari^{20a,20b}, C. Serfon³⁰, L. Serin¹¹⁷, L. Serkin^{164a,164b}, T. Serre⁸⁵, M. Sessa^{134a,134b}, R. Seuster^{159a}, H. Severini¹¹³, T. Sfiligoj⁷⁵, F. Sforza³⁰, A. Sfyrila³⁰, E. Shabalina⁵⁴, M. Shamim¹¹⁶, L.Y. Shan^{33a}, R. Shang¹⁶⁵, J.T. Shank²², M. Shapiro¹⁵, P.B. Shatalov⁹⁷, K. Shaw^{164a,164b}, S.M. Shaw⁸⁴, A. Shcherbakova^{146a,146b}, C.Y. Shehu¹⁴⁹, P. Sherwood⁷⁸, L. Shi^{151,af}, S. Shimizu⁶⁷, C.O. Shimmin¹⁶³, M. Shimojima¹⁰², M. Shiyakova⁶⁵, A. Shmeleva⁹⁶, D. Shoaleh Saadi⁹⁵, M.J. Shochet³¹, S. Shojai^{91a,91b}, S. Shrestha¹¹¹, E. Shulga⁹⁸, M.A. Shupe⁷, S. Shushkevich⁴², P. Sicho¹²⁷, P.E. Sidebo¹⁴⁷, O. Sidiropoulou¹⁷⁴, D. Sidorov¹¹⁴, A. Sidoti^{20a,20b}, F. Siegert⁴⁴, Dj. Sijacki¹³, J. Silva^{126a,126d}, Y. Silver¹⁵³, S.B. Silverstein^{146a}, V. Simak¹²⁸, O. Simard⁵, Lj. Simic¹³, S. Simion¹¹⁷, E. Simioni⁸³, B. Simmons⁷⁸, D. Simon³⁴, P. Sinervo¹⁵⁸, N.B. Sinev¹¹⁶, M. Sioli^{20a,20b}, G. Siragusa¹⁷⁴, A.N. Sisakyan^{65,*}, S.Yu. Sivoklov⁹⁹, J. Sjölin^{146a,146b}, T.B. Sjursen¹⁴,

M.B. Skinner⁷², H.P. Skottowe⁵⁷, P. Skubic¹¹³, M. Slater¹⁸, T. Slavicek¹²⁸, M. Slawinska¹⁰⁷, K. Sliwa¹⁶¹, V. Smakhtin¹⁷², B.H. Smart⁴⁶, L. Smestad¹⁴, S.Yu. Smirnov⁹⁸, Y. Smirnov⁹⁸, L.N. Smirnova^{99,ag}, O. Smirnova⁸¹, M.N.K. Smith³⁵, R.W. Smith³⁵, M. Smizanska⁷², K. Smolek¹²⁸, A.A. Snesarev⁹⁶, G. Snidero⁷⁶, S. Snyder²⁵, R. Sobie^{169,k}, F. Socher⁴⁴, A. Soffer¹⁵³, D.A. Soh^{151,af}, G. Sokhrannyi⁷⁵, C.A. Solans³⁰, M. Solar¹²⁸, J. Solc¹²⁸, E.Yu. Soldatov⁹⁸, U. Soldevila¹⁶⁷, A.A. Solodkov¹³⁰, A. Soloshenko⁶⁵, O.V. Solovyanov¹³⁰, V. Solovyev¹²³, P. Sommer⁴⁸, H.Y. Song^{33b}, N. Soni¹, A. Sood¹⁵, A. Sopczak¹²⁸, B. Sopko¹²⁸, V. Sopko¹²⁸, V. Sorin¹², D. Sosa^{58b}, M. Sosebee⁸, C.L. Sotiropoulou^{124a,124b}, R. Soualah^{164a,164c}, A.M. Soukharev^{109,c}, D. South⁴², B.C. Sowden⁷⁷, S. Spagnolo^{73a,73b}, M. Spalla^{124a,124b}, M. Spangenberg¹⁷⁰, F. Spanò⁷⁷, W.R. Spearman⁵⁷, D. Sperlich¹⁶, F. Spettel¹⁰¹, R. Spighi^{20a}, G. Spigo³⁰, L.A. Spiller⁸⁸, M. Spousta¹²⁹, T. Spreitzer¹⁵⁸, R.D. St. Denis^{53,*}, S. Staerz⁴⁴, J. Stahlman¹²², R. Stamen^{58a}, S. Stamm¹⁶, E. Stanecka³⁹, C. Stanescu^{134a}, M. Stanescu-Bellu⁴², M.M. Stanitzki⁴², S. Stapnes¹¹⁹, E.A. Starchenko¹³⁰, J. Stark⁵⁵, P. Staroba¹²⁷, P. Starovoitov^{58a}, R. Staszewski³⁹, P. Stavina^{144a,*}, P. Steinberg²⁵, B. Stelzer¹⁴², H.J. Stelzer³⁰, O. Stelzer-Chilton^{159a}, H. Stenzel⁵², G.A. Stewart⁵³, J.A. Stillings²¹, M.C. Stockton⁸⁷, M. Stoebe⁸⁷, G. Stoica^{26a}, P. Stolte⁵⁴, S. Stonjek¹⁰¹, A.R. Stradling⁸, A. Straessner⁴⁴, M.E. Stramaglia¹⁷, J. Strandberg¹⁴⁷, S. Strandberg^{146a,146b}, A. Strandlie¹¹⁹, E. Strauss¹⁴³, M. Strauss¹¹³, P. Strizenec^{144b}, R. Ströhmer¹⁷⁴, D.M. Strom¹¹⁶, R. Stroynowski⁴⁰, A. Strubig¹⁰⁶, S.A. Stucci¹⁷, B. Stugu¹⁴, N.A. Styles⁴², D. Su¹⁴³, J. Su¹²⁵, R. Subramaniam⁷⁹, A. Succurro¹², Y. Sugaya¹¹⁸, C. Suhr¹⁰⁸, M. Suk¹²⁸, V.V. Sulin⁹⁶, S. Sultansoy^{4c}, T. Sumida⁶⁸, S. Sun⁵⁷, X. Sun^{33a}, J.E. Sundermann⁴⁸, K. Suruliz¹⁴⁹, G. Susinno^{37a,37b}, M.R. Sutton¹⁴⁹, S. Suzuki⁶⁶, M. Svatos¹²⁷, M. Swiatlowski¹⁴³, I. Sykora^{144a}, T. Sykora¹²⁹, D. Ta⁹⁰, C. Taccini^{134a,134b}, K. Tackmann⁴², J. Taenzer¹⁵⁸, A. Taffard¹⁶³, R. Tafirout^{159a}, N. Taiblum¹⁵³, H. Takai²⁵, R. Takashima⁶⁹, H. Takeda⁶⁷, T. Takeshita¹⁴⁰, Y. Takubo⁶⁶, M. Talby⁸⁵, A.A. Talyshev^{109,c}, J.Y.C. Tam¹⁷⁴, K.G. Tan⁸⁸, J. Tanaka¹⁵⁵, R. Tanaka¹¹⁷, S. Tanaka⁶⁶, B.B. Tannenwald¹¹¹, N. Tannoury²¹, S. Tapprogge⁸³, S. Tarem¹⁵², F. Tarrade²⁹, G.F. Tartarelli^{91a}, P. Tas¹²⁹, M. Tasevsky¹²⁷, T. Tashiro⁶⁸, E. Tassi^{37a,37b}, A. Tavares Delgado^{126a,126b}, Y. Tayalati^{135d}, F.E. Taylor⁹⁴, G.N. Taylor⁸⁸, W. Taylor^{159b}, F.A. Teischinger³⁰, M. Teixeira Dias Castanheira⁷⁶, P. Teixeira-Dias⁷⁷, K.K. Temming⁴⁸, D. Temple¹⁴², H. Ten Kate³⁰, P.K. Teng¹⁵¹, J.J. Teoh¹¹⁸, F. Tepel¹⁷⁵, S. Terada⁶⁶, K. Terashi¹⁵⁵, J. Terron⁸², S. Terzo¹⁰¹, M. Testa⁴⁷, R.J. Teuscher^{158,k}, T. Theveneaux-Pelzer³⁴, J.P. Thomas¹⁸, J. Thomas-Wilsker⁷⁷, E.N. Thompson³⁵, P.D. Thompson¹⁸, R.J. Thompson⁸⁴, A.S. Thompson⁵³, L.A. Thomsen¹⁷⁶, E. Thomson¹²², M. Thomson²⁸, R.P. Thun^{89,*}, M.J. Tibbetts¹⁵, R.E. Ticse Torres⁸⁵, V.O. Tikhomirov^{96,ah}, Yu.A. Tikhonov^{109,c}, S. Timoshenko⁹⁸, E. Tiouchichine⁸⁵, P. Tipton¹⁷⁶, S. Tisserant⁸⁵, K. Todome¹⁵⁷, T. Todorov^{5,*}, S. Todorova-Nova¹²⁹, J. Tojo⁷⁰, S. Tokár^{144a}, K. Tokushuku⁶⁶, K. Tollefson⁹⁰, E. Tolley⁵⁷, L. Tomlinson⁸⁴, M. Tomoto¹⁰³, L. Tompkins^{143,ai}, K. Toms¹⁰⁵, E. Torrence¹¹⁶, H. Torres¹⁴², E. Torró Pastor¹³⁸, J. Toth^{85,aj}, F. Touchard⁸⁵, D.R. Tovey¹³⁹, T. Trefzger¹⁷⁴, L. Tremblet³⁰, A. Tricoli³⁰, I.M. Trigger^{159a}, S. Trincaz-Duvoid⁸⁰, M.F. Tripiana¹², W. Trischuk¹⁵⁸, B. Trocme⁵⁵, C. Troncon^{91a}, M. Trottier-McDonald¹⁵, M. Trovatelli¹⁶⁹, P. True⁹⁰, L. Truong^{164a,164c}, M. Trzebinski³⁹, A. Trzupek³⁹, C. Tsarouchas³⁰, J.C.-L. Tseng¹²⁰, P.V. Tsiarshka⁹², D. Tsionou¹⁵⁴, G. Tsipolitis¹⁰, N. Tsirintanis⁹, S. Tsiskaridze¹², V. Tsiskaridze⁴⁸, E.G. Tskhadadze^{51a}, I.I. Tsukerman⁹⁷, V. Tsulaia¹⁵, S. Tsuno⁶⁶, D. Tsybychev¹⁴⁸, A. Tudorache^{26a}, V. Tudorache^{26a}, A.N. Tuna¹²², S.A. Tupputi^{20a,20b}, S. Turchikhin^{99,ag}, D. Turecek¹²⁸, R. Turra^{91a,91b}, A.J. Turvey⁴⁰, P.M. Tuts³⁵, A. Tykhonov⁴⁹, M. Tylmad^{146a,146b}, M. Tyndel¹³¹, I. Ueda¹⁵⁵, R. Ueno²⁹, M. Ughetto^{146a,146b}, M. Uglan¹⁴, F. Ukegawa¹⁶⁰, G. Unal³⁰, A. Undrus²⁵, G. Unel¹⁶³, F.C. Ungaro⁴⁸, Y. Unno⁶⁶, C. Unverdorben¹⁰⁰, J. Urban^{144b}, P. Urquijo⁸⁸, P. Urrejola⁸³, G. Usai⁸, A. Usanova⁶², L. Vacavant⁸⁵, V. Vacek¹²⁸, B. Vachon⁸⁷, C. Valderanis⁸³, N. Valencic¹⁰⁷, S. Valentini^{20a,20b}, A. Valero¹⁶⁷, L. Valery¹², S. Valkar¹²⁹, E. Valladolid Gallego¹⁶⁷, S. Vallecorsa⁴⁹, J.A. Valls Ferrer¹⁶⁷, W. Van Den Wollenberg¹⁰⁷, P.C. Van Der Deijl¹⁰⁷, R. van der Geer¹⁰⁷, H. van der Graaf¹⁰⁷, N. van Eldik¹⁵², P. van Gemmeren⁶,

J. Van Nieuwkoop¹⁴², I. van Vulpen¹⁰⁷, M.C. van Woerden³⁰, M. Vanadia^{132a,132b}, W. Vandelli³⁰, R. Vanguri¹²², A. Vaniachine⁶, F. Vannucci⁸⁰, G. Vardanyan¹⁷⁷, R. Vari^{132a}, E.W. Varnes⁷, T. Varol⁴⁰, D. Varouchas⁸⁰, A. Vartapetian⁸, K.E. Varvell¹⁵⁰, F. Vazeille³⁴, T. Vazquez Schroeder⁸⁷, J. Veatch⁷, L.M. Veloce¹⁵⁸, F. Veloso^{126a,126c}, T. Velz²¹, S. Veneziano^{132a}, A. Ventura^{73a,73b}, D. Ventura⁸⁶, M. Venturi¹⁶⁹, N. Venturi¹⁵⁸, A. Venturini²³, V. Vercesi^{121a}, M. Verducci^{132a,132b}, W. Verkerke¹⁰⁷, J.C. Vermeulen¹⁰⁷, A. Vest⁴⁴, M.C. Vetterli^{142,d}, O. Viazlo⁸¹, I. Vichou¹⁶⁵, T. Vickey¹³⁹, O.E. Vickey Boeriu¹³⁹, G.H.A. Viehhauser¹²⁰, S. Viel¹⁵, R. Vigne⁶², M. Villa^{20a,20b}, M. Villaplana Perez^{91a,91b}, E. Vilucchi⁴⁷, M.G. Vinciter²⁹, V.B. Vinogradov⁶⁵, I. Vivarelli¹⁴⁹, F. Vives Vaque³, S. Vlachos¹⁰, D. Vladoiu¹⁰⁰, M. Vlasak¹²⁸, M. Vogel^{32a}, P. Vokac¹²⁸, G. Volpi^{124a,124b}, M. Volpi⁸⁸, H. von der Schmitt¹⁰¹, H. von Radziewski⁴⁸, E. von Toerne²¹, V. Vorobel¹²⁹, K. Vorobev⁹⁸, M. Vos¹⁶⁷, R. Voss³⁰, J.H. Vosseveld⁷⁴, N. Vranjes¹³, M. Vranjes Milosavljevic¹³, V. Vrba¹²⁷, M. Vreeswijk¹⁰⁷, R. Vuillermet³⁰, I. Vukotic³¹, Z. Vykydal¹²⁸, P. Wagner²¹, W. Wagner¹⁷⁵, H. Wahlberg⁷¹, S. Wahrmund⁴⁴, J. Wakabayashi¹⁰³, J. Walder⁷², R. Walker¹⁰⁰, W. Walkowiak¹⁴¹, C. Wang¹⁵¹, F. Wang¹⁷³, H. Wang¹⁵, H. Wang⁴⁰, J. Wang⁴², J. Wang^{33a}, K. Wang⁸⁷, R. Wang⁶, S.M. Wang¹⁵¹, T. Wang²¹, T. Wang³⁵, X. Wang¹⁷⁶, C. Wanotayaroj¹¹⁶, A. Warburton⁸⁷, C.P. Ward²⁸, D.R. Wardrope⁷⁸, A. Washbrook⁴⁶, C. Wasicki⁴², P.M. Watkins¹⁸, A.T. Watson¹⁸, I.J. Watson¹⁵⁰, M.F. Watson¹⁸, G. Watts¹³⁸, S. Watts⁸⁴, B.M. Waugh⁷⁸, S. Webb⁸⁴, M.S. Weber¹⁷, S.W. Weber¹⁷⁴, J.S. Webster³¹, A.R. Weidberg¹²⁰, B. Weinert⁶¹, J. Weingarten⁵⁴, C. Weiser⁴⁸, H. Weits¹⁰⁷, P.S. Wells³⁰, T. Wenaus²⁵, T. Wengler³⁰, S. Wenig³⁰, N. Wermes²¹, M. Werner⁴⁸, P. Werner³⁰, M. Wessels^{58a}, J. Wetter¹⁶¹, K. Whalen¹¹⁶, A.M. Wharton⁷², A. White⁸, M.J. White¹, R. White^{32b}, S. White^{124a,124b}, D. Whiteson¹⁶³, F.J. Wickens¹³¹, W. Wiedenmann¹⁷³, M. Wielers¹³¹, P. Wienemann²¹, C. Wigglesworth³⁶, L.A.M. Wiik-Fuchs²¹, A. Wildauer¹⁰¹, H.G. Wilkens³⁰, H.H. Williams¹²², S. Williams¹⁰⁷, C. Willis⁹⁰, S. Willocq⁸⁶, A. Wilson⁸⁹, J.A. Wilson¹⁸, I. Wingerter-Seez⁵, F. Winklmeier¹¹⁶, B.T. Winter²¹, M. Wittgen¹⁴³, J. Wittkowski¹⁰⁰, S.J. Wollstadt⁸³, M.W. Wolter³⁹, H. Wolters^{126a,126c}, B.K. Wosiek³⁹, J. Wotschack³⁰, M.J. Woudstra⁸⁴, K.W. Wozniak³⁹, M. Wu⁵⁵, M. Wu³¹, S.L. Wu¹⁷³, X. Wu⁴⁹, Y. Wu⁸⁹, T.R. Wyatt⁸⁴, B.M. Wynne⁴⁶, S. Xella³⁶, D. Xu^{33a}, L. Xu²⁵, B. Yabsley¹⁵⁰, S. Yacoub^{145a}, R. Yakabe⁶⁷, M. Yamada⁶⁶, D. Yamaguchi¹⁵⁷, Y. Yamaguchi¹¹⁸, A. Yamamoto⁶⁶, S. Yamamoto¹⁵⁵, T. Yamanaka¹⁵⁵, K. Yamauchi¹⁰³, Y. Yamazaki⁶⁷, Z. Yan²², H. Yang^{33e}, H. Yang¹⁷³, Y. Yang¹⁵¹, W.-M. Yao¹⁵, Y. Yasu⁶⁶, E. Yatsenko⁵, K.H. Yau Wong²¹, J. Ye⁴⁰, S. Ye²⁵, I. Yeletskikh⁶⁵, A.L. Yen⁵⁷, E. Yildirim⁴², K. Yorita¹⁷¹, R. Yoshida⁶, K. Yoshihara¹²², C. Young¹⁴³, C.J.S. Young³⁰, S. Youssef²², D.R. Yu¹⁵, J. Yu⁸, J.M. Yu⁸⁹, J. Yu¹¹⁴, L. Yuan⁶⁷, S.P.Y. Yuen²¹, A. Yurkewicz¹⁰⁸, I. Yusuff^{28,ak}, B. Zabinski³⁹, R. Zaidan⁶³, A.M. Zaitsev^{130,ab}, J. Zalieckas¹⁴, A. Zaman¹⁴⁸, S. Zambito⁵⁷, L. Zanello^{132a,132b}, D. Zanzi⁸⁸, C. Zeitnitz¹⁷⁵, M. Zeman¹²⁸, A. Zemla^{38a}, Q. Zeng¹⁴³, K. Zengel²³, O. Zenin¹³⁰, T. Ženiš^{144a}, D. Zerwas¹¹⁷, D. Zhang⁸⁹, F. Zhang¹⁷³, H. Zhang^{33c}, J. Zhang⁶, L. Zhang⁴⁸, R. Zhang^{33b}, X. Zhang^{33d}, Z. Zhang¹¹⁷, X. Zhao⁴⁰, Y. Zhao^{33d,117}, Z. Zhao^{33b}, A. Zhemchugov⁶⁵, J. Zhong¹²⁰, B. Zhou⁸⁹, C. Zhou⁴⁵, L. Zhou³⁵, L. Zhou⁴⁰, N. Zhou^{33f}, C.G. Zhu^{33d}, H. Zhu^{33a}, J. Zhu⁸⁹, Y. Zhu^{33b}, X. Zhuang^{33a}, K. Zhukov⁹⁶, A. Zibell¹⁷⁴, D. Zieminska⁶¹, N.I. Zimine⁶⁵, C. Zimmermann⁸³, S. Zimmermann⁴⁸, Z. Zinonos⁵⁴, M. Zinser⁸³, M. Ziolkowski¹⁴¹, L. Živković¹³, G. Zobernig¹⁷³, A. Zoccoli^{20a,20b}, M. zur Nedden¹⁶, G. Zurzolo^{104a,104b}, L. Zwalinski³⁰.

¹ Department of Physics, University of Adelaide, Adelaide, Australia

² Physics Department, SUNY Albany, Albany NY, United States of America

³ Department of Physics, University of Alberta, Edmonton AB, Canada

⁴ (a) Department of Physics, Ankara University, Ankara; (b) Istanbul Aydin University, Istanbul; (c)

Division of Physics, TOBB University of Economics and Technology, Ankara, Turkey

⁵ LAPP, CNRS/IN2P3 and Université Savoie Mont Blanc, Annecy-le-Vieux, France

⁶ High Energy Physics Division, Argonne National Laboratory, Argonne IL, United States of America

- ⁷ Department of Physics, University of Arizona, Tucson AZ, United States of America
- ⁸ Department of Physics, The University of Texas at Arlington, Arlington TX, United States of America
- ⁹ Physics Department, University of Athens, Athens, Greece
- ¹⁰ Physics Department, National Technical University of Athens, Zografou, Greece
- ¹¹ Institute of Physics, Azerbaijan Academy of Sciences, Baku, Azerbaijan
- ¹² Institut de Física d'Altes Energies and Departament de Física de la Universitat Autònoma de Barcelona, Barcelona, Spain
- ¹³ Institute of Physics, University of Belgrade, Belgrade, Serbia
- ¹⁴ Department for Physics and Technology, University of Bergen, Bergen, Norway
- ¹⁵ Physics Division, Lawrence Berkeley National Laboratory and University of California, Berkeley CA, United States of America
- ¹⁶ Department of Physics, Humboldt University, Berlin, Germany
- ¹⁷ Albert Einstein Center for Fundamental Physics and Laboratory for High Energy Physics, University of Bern, Bern, Switzerland
- ¹⁸ School of Physics and Astronomy, University of Birmingham, Birmingham, United Kingdom
- ¹⁹ ^(a) Department of Physics, Bogazici University, Istanbul; ^(b) Department of Physics Engineering, Gaziantep University, Gaziantep; ^(c) Department of Physics, Dogus University, Istanbul, Turkey
- ²⁰ ^(a) INFN Sezione di Bologna; ^(b) Dipartimento di Fisica e Astronomia, Università di Bologna, Bologna, Italy
- ²¹ Physikalisches Institut, University of Bonn, Bonn, Germany
- ²² Department of Physics, Boston University, Boston MA, United States of America
- ²³ Department of Physics, Brandeis University, Waltham MA, United States of America
- ²⁴ ^(a) Universidade Federal do Rio De Janeiro COPPE/EE/IF, Rio de Janeiro; ^(b) Electrical Circuits Department, Federal University of Juiz de Fora (UFJF), Juiz de Fora; ^(c) Federal University of Sao Joao del Rei (UFSJ), Sao Joao del Rei; ^(d) Instituto de Fisica, Universidade de Sao Paulo, Sao Paulo, Brazil
- ²⁵ Physics Department, Brookhaven National Laboratory, Upton NY, United States of America
- ²⁶ ^(a) National Institute of Physics and Nuclear Engineering, Bucharest; ^(b) National Institute for Research and Development of Isotopic and Molecular Technologies, Physics Department, Cluj Napoca; ^(c) University Politehnica Bucharest, Bucharest; ^(d) West University in Timisoara, Timisoara, Romania
- ²⁷ Departamento de Física, Universidad de Buenos Aires, Buenos Aires, Argentina
- ²⁸ Cavendish Laboratory, University of Cambridge, Cambridge, United Kingdom
- ²⁹ Department of Physics, Carleton University, Ottawa ON, Canada
- ³⁰ CERN, Geneva, Switzerland
- ³¹ Enrico Fermi Institute, University of Chicago, Chicago IL, United States of America
- ³² ^(a) Departamento de Física, Pontificia Universidad Católica de Chile, Santiago; ^(b) Departamento de Física, Universidad Técnica Federico Santa María, Valparaíso, Chile
- ³³ ^(a) Institute of High Energy Physics, Chinese Academy of Sciences, Beijing; ^(b) Department of Modern Physics, University of Science and Technology of China, Anhui; ^(c) Department of Physics, Nanjing University, Jiangsu; ^(d) School of Physics, Shandong University, Shandong; ^(e) Department of Physics and Astronomy, Shanghai Key Laboratory for Particle Physics and Cosmology, Shanghai Jiao Tong University, Shanghai; ^(f) Physics Department, Tsinghua University, Beijing 100084, China
- ³⁴ Laboratoire de Physique Corpusculaire, Clermont Université and Université Blaise Pascal and CNRS/IN2P3, Clermont-Ferrand, France
- ³⁵ Nevis Laboratory, Columbia University, Irvington NY, United States of America
- ³⁶ Niels Bohr Institute, University of Copenhagen, Kobenhavn, Denmark
- ³⁷ ^(a) INFN Gruppo Collegato di Cosenza, Laboratori Nazionali di Frascati; ^(b) Dipartimento di Fisica, Università della Calabria, Rende, Italy

- 38 ^(a) AGH University of Science and Technology, Faculty of Physics and Applied Computer Science, Krakow; ^(b) Marian Smoluchowski Institute of Physics, Jagiellonian University, Krakow, Poland
- 39 Institute of Nuclear Physics Polish Academy of Sciences, Krakow, Poland
- 40 Physics Department, Southern Methodist University, Dallas TX, United States of America
- 41 Physics Department, University of Texas at Dallas, Richardson TX, United States of America
- 42 DESY, Hamburg and Zeuthen, Germany
- 43 Institut für Experimentelle Physik IV, Technische Universität Dortmund, Dortmund, Germany
- 44 Institut für Kern- und Teilchenphysik, Technische Universität Dresden, Dresden, Germany
- 45 Department of Physics, Duke University, Durham NC, United States of America
- 46 SUPA - School of Physics and Astronomy, University of Edinburgh, Edinburgh, United Kingdom
- 47 INFN Laboratori Nazionali di Frascati, Frascati, Italy
- 48 Fakultät für Mathematik und Physik, Albert-Ludwigs-Universität, Freiburg, Germany
- 49 Section de Physique, Université de Genève, Geneva, Switzerland
- 50 ^(a) INFN Sezione di Genova; ^(b) Dipartimento di Fisica, Università di Genova, Genova, Italy
- 51 ^(a) E. Andronikashvili Institute of Physics, Iv. Javakhishvili Tbilisi State University, Tbilisi; ^(b) High Energy Physics Institute, Tbilisi State University, Tbilisi, Georgia
- 52 II Physikalisches Institut, Justus-Liebig-Universität Giessen, Giessen, Germany
- 53 SUPA - School of Physics and Astronomy, University of Glasgow, Glasgow, United Kingdom
- 54 II Physikalisches Institut, Georg-August-Universität, Göttingen, Germany
- 55 Laboratoire de Physique Subatomique et de Cosmologie, Université Grenoble-Alpes, CNRS/IN2P3, Grenoble, France
- 56 Department of Physics, Hampton University, Hampton VA, United States of America
- 57 Laboratory for Particle Physics and Cosmology, Harvard University, Cambridge MA, United States of America
- 58 ^(a) Kirchhoff-Institut für Physik, Ruprecht-Karls-Universität Heidelberg, Heidelberg; ^(b) Physikalisches Institut, Ruprecht-Karls-Universität Heidelberg, Heidelberg; ^(c) ZITI Institut für technische Informatik, Ruprecht-Karls-Universität Heidelberg, Mannheim, Germany
- 59 Faculty of Applied Information Science, Hiroshima Institute of Technology, Hiroshima, Japan
- 60 ^(a) Department of Physics, The Chinese University of Hong Kong, Shatin, N.T., Hong Kong; ^(b) Department of Physics, The University of Hong Kong, Hong Kong; ^(c) Department of Physics, The Hong Kong University of Science and Technology, Clear Water Bay, Kowloon, Hong Kong, China
- 61 Department of Physics, Indiana University, Bloomington IN, United States of America
- 62 Institut für Astro- und Teilchenphysik, Leopold-Franzens-Universität, Innsbruck, Austria
- 63 University of Iowa, Iowa City IA, United States of America
- 64 Department of Physics and Astronomy, Iowa State University, Ames IA, United States of America
- 65 Joint Institute for Nuclear Research, JINR Dubna, Dubna, Russia
- 66 KEK, High Energy Accelerator Research Organization, Tsukuba, Japan
- 67 Graduate School of Science, Kobe University, Kobe, Japan
- 68 Faculty of Science, Kyoto University, Kyoto, Japan
- 69 Kyoto University of Education, Kyoto, Japan
- 70 Department of Physics, Kyushu University, Fukuoka, Japan
- 71 Instituto de Física La Plata, Universidad Nacional de La Plata and CONICET, La Plata, Argentina
- 72 Physics Department, Lancaster University, Lancaster, United Kingdom
- 73 ^(a) INFN Sezione di Lecce; ^(b) Dipartimento di Matematica e Fisica, Università del Salento, Lecce, Italy
- 74 Oliver Lodge Laboratory, University of Liverpool, Liverpool, United Kingdom
- 75 Department of Physics, Jožef Stefan Institute and University of Ljubljana, Ljubljana, Slovenia

- ⁷⁶ School of Physics and Astronomy, Queen Mary University of London, London, United Kingdom
- ⁷⁷ Department of Physics, Royal Holloway University of London, Surrey, United Kingdom
- ⁷⁸ Department of Physics and Astronomy, University College London, London, United Kingdom
- ⁷⁹ Louisiana Tech University, Ruston LA, United States of America
- ⁸⁰ Laboratoire de Physique Nucléaire et de Hautes Energies, UPMC and Université Paris-Diderot and CNRS/IN2P3, Paris, France
- ⁸¹ Fysiska institutionen, Lunds universitet, Lund, Sweden
- ⁸² Departamento de Física Teórica C-15, Universidad Autónoma de Madrid, Madrid, Spain
- ⁸³ Institut für Physik, Universität Mainz, Mainz, Germany
- ⁸⁴ School of Physics and Astronomy, University of Manchester, Manchester, United Kingdom
- ⁸⁵ CPPM, Aix-Marseille Université and CNRS/IN2P3, Marseille, France
- ⁸⁶ Department of Physics, University of Massachusetts, Amherst MA, United States of America
- ⁸⁷ Department of Physics, McGill University, Montreal QC, Canada
- ⁸⁸ School of Physics, University of Melbourne, Victoria, Australia
- ⁸⁹ Department of Physics, The University of Michigan, Ann Arbor MI, United States of America
- ⁹⁰ Department of Physics and Astronomy, Michigan State University, East Lansing MI, United States of America
- ⁹¹ ^(a) INFN Sezione di Milano; ^(b) Dipartimento di Fisica, Università di Milano, Milano, Italy
- ⁹² B.I. Stepanov Institute of Physics, National Academy of Sciences of Belarus, Minsk, Republic of Belarus
- ⁹³ National Scientific and Educational Centre for Particle and High Energy Physics, Minsk, Republic of Belarus
- ⁹⁴ Department of Physics, Massachusetts Institute of Technology, Cambridge MA, United States of America
- ⁹⁵ Group of Particle Physics, University of Montreal, Montreal QC, Canada
- ⁹⁶ P.N. Lebedev Institute of Physics, Academy of Sciences, Moscow, Russia
- ⁹⁷ Institute for Theoretical and Experimental Physics (ITEP), Moscow, Russia
- ⁹⁸ National Research Nuclear University MEPhI, Moscow, Russia
- ⁹⁹ D.V. Skobeltsyn Institute of Nuclear Physics, M.V. Lomonosov Moscow State University, Moscow, Russia
- ¹⁰⁰ Fakultät für Physik, Ludwig-Maximilians-Universität München, München, Germany
- ¹⁰¹ Max-Planck-Institut für Physik (Werner-Heisenberg-Institut), München, Germany
- ¹⁰² Nagasaki Institute of Applied Science, Nagasaki, Japan
- ¹⁰³ Graduate School of Science and Kobayashi-Maskawa Institute, Nagoya University, Nagoya, Japan
- ¹⁰⁴ ^(a) INFN Sezione di Napoli; ^(b) Dipartimento di Fisica, Università di Napoli, Napoli, Italy
- ¹⁰⁵ Department of Physics and Astronomy, University of New Mexico, Albuquerque NM, United States of America
- ¹⁰⁶ Institute for Mathematics, Astrophysics and Particle Physics, Radboud University Nijmegen/Nikhef, Nijmegen, Netherlands
- ¹⁰⁷ Nikhef National Institute for Subatomic Physics and University of Amsterdam, Amsterdam, Netherlands
- ¹⁰⁸ Department of Physics, Northern Illinois University, DeKalb IL, United States of America
- ¹⁰⁹ Budker Institute of Nuclear Physics, SB RAS, Novosibirsk, Russia
- ¹¹⁰ Department of Physics, New York University, New York NY, United States of America
- ¹¹¹ Ohio State University, Columbus OH, United States of America
- ¹¹² Faculty of Science, Okayama University, Okayama, Japan
- ¹¹³ Homer L. Dodge Department of Physics and Astronomy, University of Oklahoma, Norman OK,

United States of America

¹¹⁴ Department of Physics, Oklahoma State University, Stillwater OK, United States of America

¹¹⁵ Palacký University, RCPTM, Olomouc, Czech Republic

¹¹⁶ Center for High Energy Physics, University of Oregon, Eugene OR, United States of America

¹¹⁷ LAL, Université Paris-Sud and CNRS/IN2P3, Orsay, France

¹¹⁸ Graduate School of Science, Osaka University, Osaka, Japan

¹¹⁹ Department of Physics, University of Oslo, Oslo, Norway

¹²⁰ Department of Physics, Oxford University, Oxford, United Kingdom

¹²¹ ^(a) INFN Sezione di Pavia; ^(b) Dipartimento di Fisica, Università di Pavia, Pavia, Italy

¹²² Department of Physics, University of Pennsylvania, Philadelphia PA, United States of America

¹²³ National Research Centre "Kurchatov Institute" B.P.Konstantinov Petersburg Nuclear Physics Institute, St. Petersburg, Russia

¹²⁴ ^(a) INFN Sezione di Pisa; ^(b) Dipartimento di Fisica E. Fermi, Università di Pisa, Pisa, Italy

¹²⁵ Department of Physics and Astronomy, University of Pittsburgh, Pittsburgh PA, United States of America

¹²⁶ ^(a) Laboratório de Instrumentação e Física Experimental de Partículas - LIP, Lisboa; ^(b) Faculdade de Ciências, Universidade de Lisboa, Lisboa; ^(c) Department of Physics, University of Coimbra, Coimbra; ^(d) Centro de Física Nuclear da Universidade de Lisboa, Lisboa; ^(e) Departamento de Física, Universidade do Minho, Braga; ^(f) Departamento de Física Teórica y del Cosmos and CAFPE, Universidad de Granada, Granada (Spain); ^(g) Dep Física and CEFITEC of Faculdade de Ciências e Tecnologia, Universidade Nova de Lisboa, Caparica, Portugal

¹²⁷ Institute of Physics, Academy of Sciences of the Czech Republic, Praha, Czech Republic

¹²⁸ Czech Technical University in Prague, Praha, Czech Republic

¹²⁹ Faculty of Mathematics and Physics, Charles University in Prague, Praha, Czech Republic

¹³⁰ State Research Center Institute for High Energy Physics, Protvino, Russia

¹³¹ Particle Physics Department, Rutherford Appleton Laboratory, Didcot, United Kingdom

¹³² ^(a) INFN Sezione di Roma; ^(b) Dipartimento di Fisica, Sapienza Università di Roma, Roma, Italy

¹³³ ^(a) INFN Sezione di Roma Tor Vergata; ^(b) Dipartimento di Fisica, Università di Roma Tor Vergata, Roma, Italy

¹³⁴ ^(a) INFN Sezione di Roma Tre; ^(b) Dipartimento di Matematica e Fisica, Università Roma Tre, Roma, Italy

¹³⁵ ^(a) Faculté des Sciences Ain Chock, Réseau Universitaire de Physique des Hautes Energies - Université Hassan II, Casablanca; ^(b) Centre National de l'Energie des Sciences Techniques Nucleaires, Rabat; ^(c) Faculté des Sciences Semlalia, Université Cadi Ayyad, LPHEA-Marrakech; ^(d) Faculté des Sciences, Université Mohamed Premier and LPTPM, Oujda; ^(e) Faculté des sciences, Université Mohammed V-Agdal, Rabat, Morocco

¹³⁶ DSM/IRFU (Institut de Recherches sur les Lois Fondamentales de l'Univers), CEA Saclay (Commissariat à l'Energie Atomique et aux Energies Alternatives), Gif-sur-Yvette, France

¹³⁷ Santa Cruz Institute for Particle Physics, University of California Santa Cruz, Santa Cruz CA, United States of America

¹³⁸ Department of Physics, University of Washington, Seattle WA, United States of America

¹³⁹ Department of Physics and Astronomy, University of Sheffield, Sheffield, United Kingdom

¹⁴⁰ Department of Physics, Shinshu University, Nagano, Japan

¹⁴¹ Fachbereich Physik, Universität Siegen, Siegen, Germany

¹⁴² Department of Physics, Simon Fraser University, Burnaby BC, Canada

¹⁴³ SLAC National Accelerator Laboratory, Stanford CA, United States of America

¹⁴⁴ ^(a) Faculty of Mathematics, Physics & Informatics, Comenius University, Bratislava; ^(b) Department

of Subnuclear Physics, Institute of Experimental Physics of the Slovak Academy of Sciences, Kosice, Slovak Republic

¹⁴⁵ ^(a) Department of Physics, University of Cape Town, Cape Town; ^(b) Department of Physics, University of Johannesburg, Johannesburg; ^(c) School of Physics, University of the Witwatersrand, Johannesburg, South Africa

¹⁴⁶ ^(a) Department of Physics, Stockholm University; ^(b) The Oskar Klein Centre, Stockholm, Sweden

¹⁴⁷ Physics Department, Royal Institute of Technology, Stockholm, Sweden

¹⁴⁸ Departments of Physics & Astronomy and Chemistry, Stony Brook University, Stony Brook NY, United States of America

¹⁴⁹ Department of Physics and Astronomy, University of Sussex, Brighton, United Kingdom

¹⁵⁰ School of Physics, University of Sydney, Sydney, Australia

¹⁵¹ Institute of Physics, Academia Sinica, Taipei, Taiwan

¹⁵² Department of Physics, Technion: Israel Institute of Technology, Haifa, Israel

¹⁵³ Raymond and Beverly Sackler School of Physics and Astronomy, Tel Aviv University, Tel Aviv, Israel

¹⁵⁴ Department of Physics, Aristotle University of Thessaloniki, Thessaloniki, Greece

¹⁵⁵ International Center for Elementary Particle Physics and Department of Physics, The University of Tokyo, Tokyo, Japan

¹⁵⁶ Graduate School of Science and Technology, Tokyo Metropolitan University, Tokyo, Japan

¹⁵⁷ Department of Physics, Tokyo Institute of Technology, Tokyo, Japan

¹⁵⁸ Department of Physics, University of Toronto, Toronto ON, Canada

¹⁵⁹ ^(a) TRIUMF, Vancouver BC; ^(b) Department of Physics and Astronomy, York University, Toronto ON, Canada

¹⁶⁰ Faculty of Pure and Applied Sciences, University of Tsukuba, Tsukuba, Japan

¹⁶¹ Department of Physics and Astronomy, Tufts University, Medford MA, United States of America

¹⁶² Centro de Investigaciones, Universidad Antonio Narino, Bogota, Colombia

¹⁶³ Department of Physics and Astronomy, University of California Irvine, Irvine CA, United States of America

¹⁶⁴ ^(a) INFN Gruppo Collegato di Udine, Sezione di Trieste, Udine; ^(b) ICTP, Trieste; ^(c) Dipartimento di Chimica, Fisica e Ambiente, Università di Udine, Udine, Italy

¹⁶⁵ Department of Physics, University of Illinois, Urbana IL, United States of America

¹⁶⁶ Department of Physics and Astronomy, University of Uppsala, Uppsala, Sweden

¹⁶⁷ Instituto de Física Corpuscular (IFIC) and Departamento de Física Atómica, Molecular y Nuclear and Departamento de Ingeniería Electrónica and Instituto de Microelectrónica de Barcelona (IMB-CNM), University of Valencia and CSIC, Valencia, Spain

¹⁶⁸ Department of Physics, University of British Columbia, Vancouver BC, Canada

¹⁶⁹ Department of Physics and Astronomy, University of Victoria, Victoria BC, Canada

¹⁷⁰ Department of Physics, University of Warwick, Coventry, United Kingdom

¹⁷¹ Waseda University, Tokyo, Japan

¹⁷² Department of Particle Physics, The Weizmann Institute of Science, Rehovot, Israel

¹⁷³ Department of Physics, University of Wisconsin, Madison WI, United States of America

¹⁷⁴ Fakultät für Physik und Astronomie, Julius-Maximilians-Universität, Würzburg, Germany

¹⁷⁵ Fachbereich C Physik, Bergische Universität Wuppertal, Wuppertal, Germany

¹⁷⁶ Department of Physics, Yale University, New Haven CT, United States of America

¹⁷⁷ Yerevan Physics Institute, Yerevan, Armenia

¹⁷⁸ Centre de Calcul de l'Institut National de Physique Nucléaire et de Physique des Particules (IN2P3), Villeurbanne, France

- ^a Also at Department of Physics, King's College London, London, United Kingdom
- ^b Also at Institute of Physics, Azerbaijan Academy of Sciences, Baku, Azerbaijan
- ^c Also at Novosibirsk State University, Novosibirsk, Russia
- ^d Also at TRIUMF, Vancouver BC, Canada
- ^e Also at Department of Physics, California State University, Fresno CA, United States of America
- ^f Also at Department of Physics, University of Fribourg, Fribourg, Switzerland
- ^g Also at Departamento de Fisica e Astronomia, Faculdade de Ciencias, Universidade do Porto, Portugal
- ^h Also at Tomsk State University, Tomsk, Russia
- ⁱ Also at CPPM, Aix-Marseille Université and CNRS/IN2P3, Marseille, France
- ^j Also at Università di Napoli Parthenope, Napoli, Italy
- ^k Also at Institute of Particle Physics (IPP), Canada
- ^l Also at Particle Physics Department, Rutherford Appleton Laboratory, Didcot, United Kingdom
- ^m Also at Department of Physics, St. Petersburg State Polytechnical University, St. Petersburg, Russia
- ⁿ Also at Louisiana Tech University, Ruston LA, United States of America
- ^o Also at Institucio Catalana de Recerca i Estudis Avancats, ICREA, Barcelona, Spain
- ^p Also at Graduate School of Science, Osaka University, Osaka, Japan
- ^q Also at Department of Physics, National Tsing Hua University, Taiwan
- ^r Also at Department of Physics, The University of Texas at Austin, Austin TX, United States of America
- ^s Also at Institute of Theoretical Physics, Ilia State University, Tbilisi, Georgia
- ^t Also at CERN, Geneva, Switzerland
- ^u Also at Georgian Technical University (GTU), Tbilisi, Georgia
- ^v Also at Manhattan College, New York NY, United States of America
- ^w Also at Hellenic Open University, Patras, Greece
- ^x Also at Institute of Physics, Academia Sinica, Taipei, Taiwan
- ^y Also at LAL, Université Paris-Sud and CNRS/IN2P3, Orsay, France
- ^z Also at Academia Sinica Grid Computing, Institute of Physics, Academia Sinica, Taipei, Taiwan
- ^{aa} Also at School of Physics, Shandong University, Shandong, China
- ^{ab} Also at Moscow Institute of Physics and Technology State University, Dolgoprudny, Russia
- ^{ac} Also at Section de Physique, Université de Genève, Geneva, Switzerland
- ^{ad} Also at International School for Advanced Studies (SISSA), Trieste, Italy
- ^{ae} Also at Department of Physics and Astronomy, University of South Carolina, Columbia SC, United States of America
- ^{af} Also at School of Physics and Engineering, Sun Yat-sen University, Guangzhou, China
- ^{ag} Also at Faculty of Physics, M.V.Lomonosov Moscow State University, Moscow, Russia
- ^{ah} Also at National Research Nuclear University MEPhI, Moscow, Russia
- ^{ai} Also at Department of Physics, Stanford University, Stanford CA, United States of America
- ^{aj} Also at Institute for Particle and Nuclear Physics, Wigner Research Centre for Physics, Budapest, Hungary
- ^{ak} Also at University of Malaya, Department of Physics, Kuala Lumpur, Malaysia
- * Deceased